

**A bone-anchored mechanoneural knee prosthesis
to enhance control and embodiment**

by
Tony Shu

S.M., Massachusetts Institute of Technology (2019)

B.Sc., Georgia Institute of Technology (2016)

Submitted to the Program in Media Arts and Sciences
School of Architecture and Planning
in partial fulfillment of the requirements for the degree of
Doctor of Philosophy in Media Arts and Sciences
at the

MASSACHUSETTS INSTITUTE OF TECHNOLOGY

May 2024

©2024 Tony Shu. All rights reserved.

*The author hereby grants to MIT a nonexclusive, worldwide,
irrevocable, royalty-free license to exercise any and all rights under
copyright, including to reproduce, preserve, distribute and publicly
display copies of the thesis, or release the thesis under an open-access
license.*

Author

Tony Shu

Program in Media Arts and Sciences

May 17, 2024

Certified by

Hugh Herr, Ph.D.

Professor of Media Arts and Sciences

Thesis Supervisor

Accepted by

Joseph Paradiso, Ph.D.

Academic Head, Program in Media Arts and Sciences

A bone-anchored mechanoneural knee prosthesis to enhance control and embodiment

by

Tony Shu

Submitted to the Program in Media Arts and Sciences,
School of Architecture and Planning
on May 17, 2024, in partial fulfillment of the
requirements for the degree of
Doctor of Philosophy in Media Arts and Sciences

Abstract

To maximally utilize the peripheral nervous system for prosthetic control, it is necessary to first understand the compounded errors induced by amputated physiology before developing the appropriate interfacing technologies to extract any latent movement information. Through this work, I develop a foundational approach to amputation interventions and artificial interfaces applied toward neurorobotic control at the transfemoral level.

The first part of this dissertation explores the neurophysiological and neuromechanical outcomes of a revisional transfemoral amputation that restores agonist-antagonist muscle dynamics. A within-subjects study is performed to investigate changes in muscular function and cortical activity as a result of the intervention. Through these data, I provide evidence that extant amputated musculature can be modified to restore functionality for the purpose of efferent neurorobotic control.

The second part of this dissertation explores a combined implementation of the revisional transfemoral amputation with a bone-anchored, or osseointegrated, transfemoral implant and chronically-implanted intramuscular electrodes. The clinical outcomes of the combined transfemoral platform are quantified through biophysical measurements and measurements of the stability of the implanted hardware to suggest the potential for bidirectional neurorobotic interfacing.

The third part of this dissertation compares cohorts of persons with amputation possessing varied muscle architectures and physical interfacing configurations on the ability to produce physiological neurorobotic knee dynamics. Two subjects with the novel transfemoral platform are compared to the other cohorts without individual aspects of the platform, demonstrating unprecedented agility and sustainment of prosthetic embodiment in the process.

Thesis Supervisor: Hugh Herr, Ph.D.

Title: Professor of Media Arts and Sciences

**A bone-anchored mechanoneural knee prosthesis to enhance
control and embodiment**

by

Tony Shu

The following people served as readers for this thesis:

Thesis Reader

Rickard Brånemark, MD, Ph.D.

Associate Professor

Department of Orthopaedics, Gothenburg University

Thesis Reader

Nidhi Seethapathi, Ph.D.

Frederick A. (1971) and Carole J. Middleton Career Development

Assistant Professor

Brain & Cognitive Sciences and

Electrical Engineering and Computer Science, MIT

Acknowledgments

To Professor Hugh Herr, you have provided the unwavering vision, the deft mentorship, and the incalculable resources for me to achieve something truly exciting in this great big world of bionics. I started at MIT with nary an idea of a muscle model, and now I am become the model-maker. Your guidance has bestowed upon me the conviction and strength necessary to navigate uncharted waters as I tell my own story. For this and more, please accept my deepest gratitude.

To Dr. Rickard Brånemark, thank you for making incredible contributions to your father's legacy. It is a labor that, quite literally, provides support for so many. Thank you for your wry humor that makes me believe I, too, could have a place in the academy. Most of all, thank you for your patience while I added my own grain of sand to the pile.

To Professor Nidhi Seethapathi, we need you. Our understanding of biomechanics and neural control of movement needs you. Thank you for your hard questions and your incredible support as I finished out my academic journey. I appreciated each small moment when you remained relatable despite my rush to meet every deadline. You remind me that at the end of the day, we are humans who do research, but humans nonetheless.

To the brave test pilots who put their bodies on the line, you are some of the most wonderful people I have had the privilege of meeting. To Terry and Tom, we laughed, we pushed, we did it one more time, together.

To Dr. Matthew Carty, Corey Sullivan, and everyone at Brigham that makes sure our patients get the best care possible, I have an immense respect for your dedication to the craft. It is grueling, difficult work that must be done, and it is my great privilege to be on the same team.

To Biomech, we know how to row, row, row our boat! Hyungeun, Seong Ho, Tsung-Han, the classic crew, most times were challenging, but some times were fun. Lindsey, thank you for everything you do to keep our heads above water. To Dan, Chandler, Ethan, Junqing, and John, we had to do the hard things, yet we did them

together. And to the rest of Biomech, this curmudgeon's shell is slightly softer thanks to you.

To the UROPs and undergrads who helped, I'm always going to appreciate your Gen Z proclivities that made the days go by faster. Sometimes you're the ones who teach us even if we don't say it enough.

To NH3 and my friends, your shenanigans were the fuel for my fire. Thanks to you, I'm one of the few people in the world who knows what it's like to be 20 and 40 simultaneously.

And finally, to my family, I know it wasn't always clear what I was up to in grad school, but you allowed me to push through to the end regardless. I dedicate this thesis to you and the sacrifices you made to get me here.



Contents

| | | |
|----------|---|-----------|
| 1 | Introduction | 17 |
| 1.1 | Motivation and Specific Aims | 18 |
| 1.2 | Mechanoneural Interfacing | 21 |
| 1.2.1 | Principles | 21 |
| 1.2.1.1 | Efferent and Afferent Signaling Modalities | 22 |
| 1.2.1.2 | Native Innervation and Reinnervation | 23 |
| 1.2.2 | Agonist-antagonist Myoneural Interface (AMI) | 25 |
| 1.3 | Osseointegration | 28 |
| 1.3.1 | Application as Limb Prosthesis Interface | 29 |
| 1.3.1.1 | Signal Conduit Through Osseointegrated Implants | 30 |
| 1.4 | Approaches to Transfemoral Prosthesis Control | 30 |
| 1.4.1 | Intrinsic Methodologies | 31 |
| 1.4.2 | Efferent Methodologies | 31 |
| 1.5 | Prosthetic Embodiment | 32 |
| 1.6 | Dissertation Summary | 34 |
| 2 | Clinical Revisional Implementation of the Agonist-antagonist Myoneural Interface | 35 |
| 2.1 | Rationale and Study Design | 36 |
| 2.2 | Methods | 38 |
| 2.2.1 | Phantom Range of Motion | 38 |
| 2.2.2 | Graded EMG and Ultrasound Measurement | 39 |
| 2.2.3 | fMRI Tasks and Imaging | 39 |

| | | |
|-----------|--|-----------|
| 2.2.4 | Task-space Motor Control with Visual Feedback | 41 |
| 2.3 | Results | 41 |
| 2.4 | Discussion | 46 |
| 3 | Combining Revisional AMI and Osseointegrated Structures as the Osseointegrated Mechanoneural Prosthesis (OMP) | 49 |
| 3.1 | Rationale and Study Design | 50 |
| 3.2 | Methods | 51 |
| 3.2.1 | Surgical and Clinical Procedures | 51 |
| 3.2.2 | Phantom Knee Range of Motion | 53 |
| 3.2.3 | Electrode Impedance Measurements | 53 |
| 3.2.4 | Signal-to-noise Ratio and Related Calculations | 53 |
| 3.2.5 | Functional Electrical Stimulation | 54 |
| 3.3 | Results | 55 |
| 3.4 | Discussion | 60 |
| 4 | The OMP: Unifying Knee Control and Embodiment | 63 |
| 4.1 | Rationale and Study Design | 64 |
| 4.2 | Methods | 65 |
| 4.2.1 | EMG Processing | 65 |
| 4.2.2 | Torque Computation | 67 |
| 4.2.3 | Mechatronics | 69 |
| 4.2.4 | Ultrasound | 70 |
| 4.2.5 | Experimental Tasks | 71 |
| 4.2.5.0.1 | Rhythmic Bandwidth | 71 |
| 4.2.5.0.2 | Freespace Reaching | 72 |
| 4.2.5.0.3 | Static Obstacle Drills | 74 |
| 4.2.5.0.4 | Sit to Stand | 75 |
| 4.2.5.0.5 | Level Ground Walking and Obstacle Avoidance | 76 |
| 4.2.5.0.6 | Stair Ascent and Descent | 78 |
| 4.2.5.0.7 | Embodiment Questionnaire | 78 |

| | |
|---|-----------|
| 4.3 Results | 78 |
| 4.4 Discussion | 90 |
| 5 Conclusion | 95 |
| Appendices | 97 |
| A Knee Torque Control Implementation | 99 |

List of Figures

| | | |
|-----|--|----|
| 1-1 | Principles of mechanoneural transduction and soft tissue reconstruction | 24 |
| 1-2 | Stages of osseointegration | 29 |
| 2-1 | Conventional transfemoral amputation and TF AMI architectures . . | 36 |
| 2-2 | Revisional TF AMI phantom range of motion | 42 |
| 2-3 | Revisional TF AMI agonist-antagonist neuromechanics | 42 |
| 2-4 | P1 average BOLD response during functional joint tasks at the end of the training week pre- and post-op | 43 |
| 2-5 | P2 average BOLD response during functional joint tasks at the end of the training week pre- and post-op | 44 |
| 2-6 | Revisional TF AMI control of intended knee movement direction . . . | 45 |
| 3-1 | Diagram of TF AMI and eOPRA hardware combined as the OMP . . | 52 |
| 3-2 | OMP operational and rehabilitation timeline | 52 |
| 3-3 | X-ray images following both OMP implementation stages | 55 |
| 3-4 | X-ray images showing reduced bone lucency in OMP2 after long-term osseointegration | 56 |
| 3-5 | Intramuscular electrode impedance and EMG SNR for OMP subjects | 57 |
| 3-6 | Signal power ratio of implanted intramuscular electrodes over surface electrodes | 58 |
| 3-7 | OMP phantom knee range of motion | 59 |
| 3-8 | OMP FES sensation maps and thresholds | 59 |
| 4-1 | BMI comparison across subjects | 65 |

| | | |
|------|---|----|
| 4-2 | EMG to muscle activation processing pipeline | 66 |
| 4-3 | OMP noise characteristics and filter configuration | 67 |
| 4-4 | Desired knee torque computation | 68 |
| 4-5 | Mechatronic knee system | 69 |
| 4-6 | Open loop torque control bandwidth for mechatronic knee | 70 |
| 4-7 | Closed loop torque controller for mechatronic knee | 71 |
| 4-8 | Complete control system for OMP subjects | 72 |
| 4-9 | Maximum phantom knee cycling bandwidth | 83 |
| 4-10 | Evaluation of volitional free space targeting ability | 84 |
| 4-11 | OMP level ground walking | 85 |
| 4-12 | Obstacle drill performance | 86 |
| 4-13 | Obstacle avoidance task | 87 |
| 4-14 | Sit to stand task performance | 88 |
| 4-15 | Stair ascent and descent | 89 |
| 4-16 | Prosthetic embodiment results | 89 |

List of Tables

| | | |
|-----|---|----|
| 2.1 | Revisional TF AMI subject biometrics | 38 |
| 2.2 | Revisional TF AMI fMRI functional data task run | 40 |
| 2.3 | Revisional TF AMI fMRI BOLD response summary values | 45 |
| 3.1 | Relevant OMP subject biometrics | 51 |
| 4.1 | Categorical differences between cohorts | 64 |
| 4.2 | Subject table | 81 |
| 4.3 | Obstacle avoidance scoring rubric | 82 |
| 4.4 | Embodiment questionnaire | 82 |

Chapter 1

Introduction

This chapter provides a relevant overview of human neuromusculoskeletal physiology in the context of limb amputation. Conceptual background is provided to explain how modern amputation paradigms are utilized toward the control of powered limb prostheses. In this exposition, limitations of the state-of-the-art are revealed along with potential avenues for further improvement.

1.1 Motivation and Specific Aims

The development of limb prostheses is straightforward from the perspective that the end goal is self-apparent: it is the ultimate accomplishment to enable physiological integration of artificial limbs equivalent in all ways to their biological counterparts. Such an achievement would sustain the abstract noumenon corresponding to full physiological integration referred to as embodiment [1]. However, despite a supposed requirement that a high degree of physiological integration and embodiment necessitates technological advancements in both artificial and biologic domains, development of these bionics has remained relatively understudied by scientists and medical professionals [2]. This is to say that the emergence of powerful actuators, energy storage technologies, and computer chips has far exceeded our ability to intuitively interact with them through neuromusculoskeletal interfacing.

Part of this disparity may be attributed to the greatly increased complexity of human biology compared to mechatronic systems. While a conventional mechanical or mechatronic prosthesis may be largely designed in isolation of biology, with the only requirement being that its functional performance is conducive toward restoring physiological organismal biomechanics with a standard-of-care attachment interface, a bionic prosthesis must restore organismal biomechanics with the additional stipulation that it does so without inducing secondary health comorbidities. Further, a bionic prosthesis should justify its physiological invasiveness with some degree of improved performance or rehabilitation over more conventional devices, independent of the aforementioned and immediate challenges to implementation.

Nonetheless, implementation difficulty is a poor standard by which to determine the *ultimate* utility of a given approach to problem-solving, and progress toward the best solutions is almost certainly not strictly monotonic despite being worthy of pursuit. In this context, it is widely accepted that some degree of direct detection of user intent is necessary for fluid limb control, and non-invasive interfacing is fundamentally limited in its ability to provide direct efferent control over a prosthetic limb [3, 4]. This negative sentiment on the utility of non-invasive interfacing is even

stronger in the case of referring afferent feedback to the prosthesis user; without invasive methodologies, it is wholly unclear how homologous and somatotopic sensations can be relayed to the central nervous system [2], yet these afferent signals are critical for full-bandwidth physiological control of joint dynamics [5].

The specific aims of this work are coordinated to demonstrate a step-function increase in rehabilitation from incorporating adapted soft tissues, hard tissues, and prosthetic implants within a unified prosthetic platform at the transfemoral level. These are undertaken to test the overarching hypothesis that furthering both artificial and biologic domains of bionics can restore physiological function and embodiment beyond levels afforded by attempted solutions that neglect one or both. Importantly, this paradigm represents a major departure from known conventional and experimental approaches to design of lower-extremity prostheses that primarily focus on cyclic gait and other patterned movements [4]. The aims are as follows:

Aim 1: Determine if and to what extent the AMI muscular construct recovers neuromechanics and neurophysiology in a revisional context. While the acute, natively innervated implementation of the AMI has been demonstrated to possess superior neuromechanics in a population of persons with transtibial amputation compared to one without [6], it is yet to be determined whether this advantage is conferred due to mechanical properties of the construct itself, or if it is due in part or in whole to other contributing factors related to the nature of the acute, transtibial implementation. In this aim, I explore the neuromechanical and neurophysiological outcomes of the AMI implemented as a surgical revision in two subjects with unilateral transfemoral amputation. In doing so, I investigate the causal ability of the AMI construct’s mechanical configuration to restore lost motor and cortical functionality in a more proximal amputation site. The study serves as a within-subjects pilot wherein longitudinal data are collected both before and after the surgical intervention.

Aim 2: Assess the clinical compatibility of the revisional AMI with a transfemoral bone-anchored implant and intramuscular electrodes. Though bone-anchored, or osseointegrated, implants alone have been demonstrated to provide effective mechanical attachment for prosthetic knees [7], and upper-extremity pros-

theses at both the transhumeral and transradial level have demonstrated successful chronic implantation of electrodes in non-antagonistic muscle tissues with leads routed through osseointegrated implants [8, 9, 10], there is no demonstration of successful transfemoral osseointegration with chronically implanted intramuscular electrodes, especially not concurrently with the AMI. In this aim, I explore the clinical compatibility of AMI, osseointegration, and implanted intramuscular electrodes combined as the unified osseointegrated mechanoneural prosthesis (OMP) platform. To determine the viability of each component's independent function and the platform's cumulative abilities, two subjects with preexisting unilateral transfemoral amputation are provided the OMP and assessed for successful integration.

Aim 3: Compare the relative advantages provided by the osseointegrated mechanoneural prosthesis (OMP) platform in a prosthetic control context. In this aim, an efferent knee control architecture is developed that deviates from typical approaches that emphasize intrinsic control or that utilize myoneural information only for selected portions of gait and movement. In contrast, this control architecture modulates prosthetic knee impedance from myoneural information in a continuous manner to more closely encapsulate the dynamics of intact physiology. The two OMP subjects are compared to the other amputee cohorts without individual aspects of the platform, demonstrating unprecedented agility and sustainment of prosthetic embodiment in the process.

The work within this dissertation demonstrates an invasive bionic interface at the transfemoral level that provides improved performance and embodiment over conventional approaches to prosthetic rehabilitation. In doing so, a mechanistic understanding of the principles underpinning these improvements are established to inform further work toward minimizing the gap a bionic limb reconstruction and intact physiology.

1.2 Mechanoneural Interfacing

As researchers develop their understanding of muscular physiology and neural regeneration, a new class of methodologies to extract movement intent from the peripheral nervous system emerges. These novel soft tissue constructs, known as mechanoneural interfaces (MIs), can be combined with artificial interfacing technologies to facilitate control and sensation of limb prostheses. By utilizing the body’s native afferent and efferent signalling pathways, MIs have demonstrated the capacity to enhance volitional prosthetic control, refer somatosensory sensation within proprioceptive and cutaneous modalities, and reduce post-amputation pain [2]. The following discussion is initially presented by Shu et al. and reproduced here [2].

1.2.1 Principles

Novel innervated soft tissue constructs have been developed that leverage advances in peripheral nerve regeneration and soft tissue reconstruction to increase the degree of restored human sensorimotor bandwidth. These surgically created soft tissue constructs are combined with artificial devices capable of sensing or stimulating to form mechanoneural interfaces (MIs) that facilitate prosthetic integration through the enhancement of efferent neural signals conveying motor commands outward from the peripheral nervous system (PNS), afferent neural signals conveying sensory information back from the external prosthesis to the central nervous system (CNS) or both. As its name suggests, an MI transduces neural commands to muscle actuation for use in efferent prosthetic control through muscle sensing or mechanical attachment, provides mechanical actuation to cause an afferent neural signal through biological mechanoreceptors, or enables both efferent and afferent modalities. For improved efferent signalling, contemporary MIs often increase the number of neuromuscular control sites along with their specificity. For improved afferent signalling, MIs typically utilize mechanoreceptors in muscle and cutaneous tissue to provide the user with somatosensory information. Additionally, free nerve-ending modalities, including chemical nociception and thermoreception, are also available to provide auxiliary

afferent signalling.

1.2.1.1 Efferent and Afferent Signaling Modalities

MIIs can be classified based on their efferent and afferent functional modalities. An MI with efferent control is able to directly actuate a prosthesis as an effort source, indirectly actuate a prosthesis by providing reference signals for mechatronic control or potentially operate under both modalities. When operating as an effort source, as in cineplastic techniques, efferent MIIs activate motor units in which alpha motor neuron action potential spikes elicit actin and myosin cross-bridge interactions, resulting in a muscle force that is propagated through a mechanical transmission to the prosthesis. When operating as a reference signal source, motor units are activated in the same manner, but instead of directly transmitting force to the prosthesis, measurements of resultant muscle state are used to inform a mechatronic controller responsible for prosthetic actuation. Candidate state signals include correlates of muscle activation measurements using for example EMG and physiological measurements, such as fascicle length [11]. Mechanoneural transduction and the corresponding biophysical amplification involving the motor units within neuromuscular soft tissues occurs whether an efferent MI operates as an effort source or a reference signal source.

An MI with afferent capabilities provides somatosensory feedback through mechanoreception, a phenomenon fundamental to the execution of organismal biomechanics. Two classes of mechanoreceptive afferents present as most relevant to the realization of movement: cutaneous and proprioceptive (Fig. 1-1). Broadly, cutaneous mechanoreceptive afferents convey sensations related to interfacial contact with the environment. These perceived sensations include, but are not limited to, touch, pressure, roughness and skin stretch [12] (Fig. 1-1e). Proprioceptive afferents convey sensations of internal bodily state that also provide indirect information about external environmental forces — muscle spindles convey muscle fascicle length and velocity, and Golgi tendon organs convey tendon and ligament force (Fig. 1-1c). Other proprioceptive afferents such as those from joint capsules also contribute towards perception of bodily movement, but their importance for proprioception is understood to be lower

than that of muscle spindles and Golgi tendons [13]. Most typically, an MI capable of cutaneous feedback possesses cutaneous sensory nerves and cutaneous end organs, and an MI capable of proprioceptive feedback possesses neuromuscular tissues (which may also be used for efferent control).

The roles of cutaneous and proprioceptive feedback have been ascertained in humans primarily through studies on their absence or disruption. In the upper extremities, it is believed that cutaneous feedback facilitates discrimination of contact points, texture, slippage and gross shape [14, 15, 16]. Proprioceptive feedback is thought to contribute to hand and finger positioning in support of efficient reaching [17] and to augment discrimination of specific shape, weight and impedance [18, 19]. The absence of either modality has been shown to diminish performance in functional tasks, suggesting that both cutaneous and proprioceptive feedback are necessary for the restoration of physiological performance [20, 21, 22]. In the lower extremities, plantar cutaneous feedback (that is, from the sole of the foot) plays a crucial role in adapting stance posture and recognizing ground contact events during gait [22, 23, 24, 25], and proprioceptive feedback is essential for maintaining gait stability and for responding to terrain irregularities [26]. Both modalities of feedback serve as input into spinal reflexive circuits that sustain the rhythmic bipedal gait cycle under a wide range of dynamic perturbations [27].

1.2.1.2 Native Innervation and Reinnervation

Modern MIs depend on soft tissue constructs that are surgically assembled with special consideration given to their spatial, vascularization and innervation constraints. Although successful implementation of all three aspects determines a construct's post-operative viability, it can be argued that the quality of innervation is the parameter that most strongly determines its functional efficacy. Bearing this in mind, MIs can also be divided into two types based on their innervation: native and regenerative [28]. Native MIs retain the original efferent and afferent nerve-to-muscle fibre or nerve-to-end organ innervations, preserving all motor and somatosensory pathways. However, in scenarios in which these native pathways no longer exist, perhaps due to traumatic

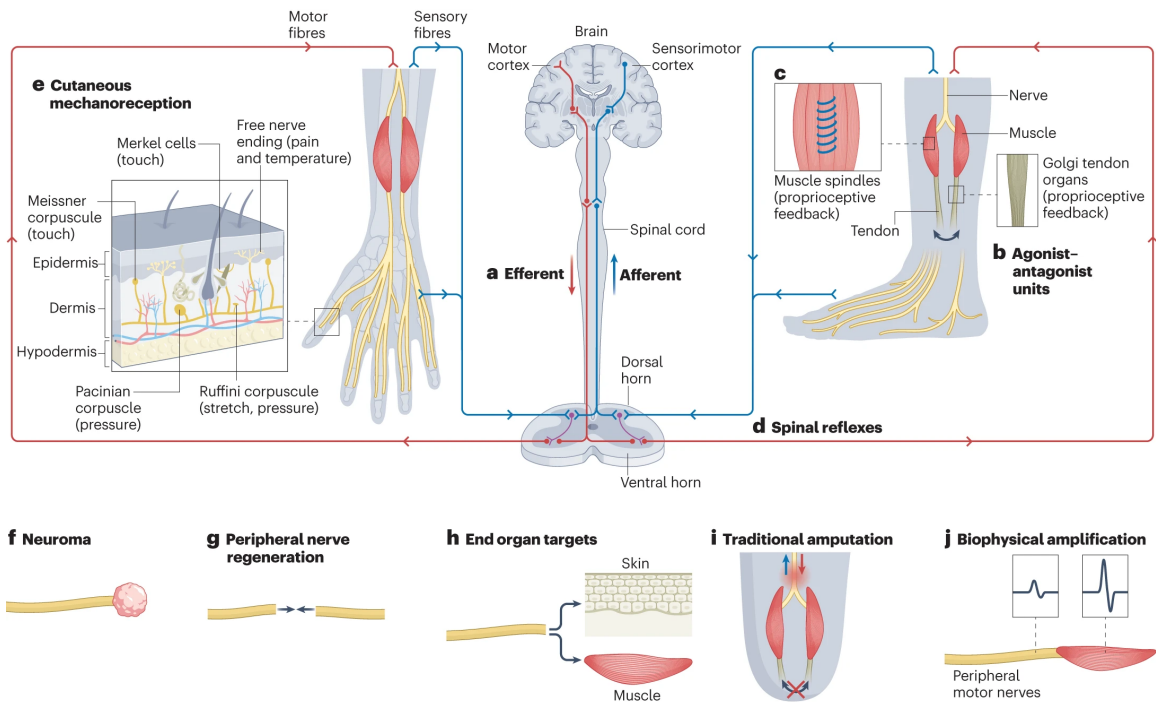


Figure 1-1: Principles of mechanoneural transduction and soft tissue reconstruction. **a**, Schematic of efferent signalling from and afferent signalling to the brain. Signals ultimately responsible for movement originate in the motor cortex and propagate impulse trains down to motor neurons located in the ventral horn of the spinal cord, before being conveyed to motor units that contract a particular muscle. **b**, Muscles in physiological agonist–antagonist pairs transfer force to the bone through tendons. Contraction of one muscle produces a corresponding stretch in its antagonist during non-isometric movements. **c**, Mechanoreceptors such as muscle spindles and Golgi tendon organs provide proprioceptive information that propagates back through the spinal cord to the sensory region of the sensorimotor cortex. **d**, Somatosensory afferents can also trigger motor neurons to amplify or suppress muscle activation through spinal reflexive circuits, without involvement of the sensorimotor cortex. Reflexes function to avoid injury or to quickly compensate for sudden dynamic perturbations, among other purposes. **e**, Cutaneous mechanoreceptors, such as free nerve endings, Merkel cells, Pacinian corpuscles, Meissner corpuscles and Ruffini corpuscles, provide cutaneous sensory information to the cortex through the spinal cord. **f**, Neuromas form when transected nerves cannot find appropriate end organs and become entangled with non-neural soft tissue. Symptomatic neuromas generate nociceptive afferents and contribute to residual limb pain and phantom limb pain. **g**, Peripheral nerves have remarkable regenerative capabilities across lesions, so long as the distal portion remains unaffected. **h**, End organ targets for reinnervation are found in muscle and dermal tissue. **i**, Traditional amputation, with extant but pathological signal transmission through residual nerves and pathological muscle coupling (no agonist–antagonist coupling), can lead to phantom limb pain and residual limb pain. **j**, Muscles act as biophysical amplifiers that increase the magnitude of action potential spikes received from peripheral motor nerves by an order of magnitude. Reproduced with permission from Springer Nature.

loss of soft tissues or a previous surgery, a regenerative MI can be pursued, in which a transected nerve is introduced into the target tissue containing denervated muscle fibres or end organs to attempt to restore functionality through axonal reinnervation.

Mammalian peripheral axons possess a remarkable capacity to regenerate free nerve endings and regenerate into denervated targets through biomolecular mechanisms, such as the upregulation of neurotrophic factors and the formation of bands of Büngner from specialized Schwann cells that provide directional guidance [29, 30]. In most cases, following PNS injury, there is a tendency for the majority of proximal motor axons to eventually reinnervate motor pathways, a phenomenon known as preferential motor reinnervation, which is hypothesized by several studies to be the result of collateral axonal pruning [31, 32, 33]. Another perspective presented by the same authors claims that, in addition to preferential motor reinnervation, sensory axons exhibit a preference for sensory pathways and their specificity is further preserved in that they preferentially target proprioceptors or cutaneous mechanoreceptors, depending on their origin [34]. However, these preferences are rather weak, and the authors note that the magnitude of specificity is low for all the reinnervations they observed in rodent models: only 53.88% for motor neurons, 60.44% for proprioceptors and 60.97% for cutaneous mechanoreceptors. In practical terms, an increased proportion of misdirected axons results in decreased functional recovery following peripheral nerve injury [35]. Considered together, these findings indicate the need for enhanced comprehension and refinement of peripheral nerve regeneration processes to reduce end organ cross-innervation and improve signalling quality.

1.2.2 Agonist-antagonist Myoneural Interface (AMI)

The AMI is an MI whose soft tissue construct consists of the surgical coaptation of physiologically paired agonist and antagonist muscles to enable bidirectional efferent prosthetic control with afferent proprioceptive signalling [36, 37, 38, 39, 40, 41]. By preserving natural mechanical coupling at the interface between both muscles, mechanoreceptors such as spindle fibres and Golgi tendon organs are stretched to provide relevant proprioceptive feedback, when forces are generated by contraction

of either muscle in the pair. The soft tissue architecture of the AMI primarily specifies a mechanical configuration agnostic to the nature of its individual agonist and antagonist muscles, and in humans, it is composed using natively innervated and vascularized muscles, referred to as a native AMI.

Early investigations of the AMI’s mechanical structure yielded a theoretical basis for determining desired joint position, impedance and torque signals for prosthetic control applications [42]. As a result, in the case of lower-extremity AMIs, one or more AMI pairs are implemented in the residuum for each intended prosthetic degree of freedom to be controlled [38]. The first two AMI pairs for ankle and subtalar control were implemented in a person with transtibial amputation by coapting the distal ends of natively innervated and vascularized residual muscles: tibialis anterior to lateral gastrocnemius and peroneus longus to tibialis posterior [37, 36]. By utilizing surface EMG recorded from all four relevant muscles, this individual was able to demonstrate independent control of ankle and subtalar degrees of freedom within an ankle-foot prosthesis. The individual could also reflexively position the prosthesis in free space to navigate obstacles and stairs in a more physiological manner than four individuals controlling the prosthesis with conventional transtibial amputation [36]. In a demonstration of the potential of the AMI to convey environmental interaction dynamics for proprioceptive closed-loop torque control, functional electrical stimulation (FES) of the individual’s residual tibialis anterior muscle in proportion to the displacement of an underlying force-resistive foot pedal allowed them to more precisely control the plantarflexion torque generated, thus enabling them to flex their foot in a controlled manner [36]. In a separate study, another individual with transtibial amputation possessing two AMI pairs was able to demonstrate modulation of prosthetic plantarflexion torque and adaptive energetic work loops during stance while walking over level ground at various speeds [43].

In population studies conducted to characterize the AMI, individuals with AMI constructs have demonstrated reduced pain, enhanced phantom joint range of motion, increased muscle fascicle strain, preserved motor control and increased physiological functional neuroimaging compared with individuals with conventional amputations

[44, 6, 45]. In a study including 15 patients with transtibial AMI constructs, patients with AMI constructs reported less pain than patients with conventional amputation, as well as a significant reduction in pain compared with their pre-operative baseline [45]. In a pair of studies including 15 and seven patients with transtibial AMI constructs, respectively [6, 45], persons with AMI constructs demonstrated improved phantom ankle and subtalar joint controllability in free space with respect to persons with conventional amputation, as the former were able to produce more selective efferent control signals, greater precision of movement and greater perceived range of motion [6, 45]. This improvement can be mechanistically explained by the positive correlation between residual limb agonist–antagonist muscle strains and sensorimotor responses, which suggests that the degree of preserved agonist–antagonist muscle strain is the neuromechanical determinant of person-specific preservation of motor control and proprioception [6]. In a functional neuroimaging study on activity in brain areas associated with proprioception, 12 patients with AMI constructs demonstrated activity at levels similar to those of persons in the control without amputation during movements in free space. This is in contrast to persons with conventional amputations, whose activation in the mentioned brain areas was significantly reduced [44]. The AMI architecture has also been implemented in three patients at the transfemoral level by coapting the biceps femoris to the rectus femoris and constructing native transtibial AMI pairs in the transfemoral compartment [45]. These patients have demonstrated significant measures of preserved function and perception of distal phantom joints.

With regard to structural limitations related to the AMI architecture, any proprioceptive feedback methodology that requires the use of an AMI muscle as an actuator, such as in an FES-based approach, is unable to homologously represent all environmental interactions. This is because closed-loop control of the antagonist muscle to refer forces to the agonist results in the user experiencing a contraction in the artificially stimulated antagonist superimposed with a physiological stretch response in the agonist. The described sensation is in direct contrast to intact limbs that can experience external forces, for example, those caused by ground reaction forces and in-

ertia, as a pure physiological stretch of musculotendinous tissue without an induced contraction in the agonist muscle [46]. A second limitation of the AMI is that its construct can only approximate physiological muscle redundancy and spatial configurations: its mechanical transmission defined at surgery may not capture the nonlinear state-dependent leverage and biarticular nature of muscles in physiological limbs. Regarding implementation, the AMI architecture in proximal transradial amputations may require careful surgical planning around volumetric and pathing constraints to successfully construct the multiple agonist–antagonist couplings responsible for wrist and hand motions[47]. Finally, no scientific assessments of the AMI’s influence on prosthetic embodiment have been reported yet.

1.3 Osseointegration

Osseointegration is a structural configuration whereby a load-bearing implant is mechanically bonded to living bone. The mechanism of such integration was first observed by Bothe, Beaton, and Davenport in 1940 [48]. The term osseointegration itself was coined by Per-Ingvar Brånemark, who developed the techniques so that they could be applied in bone-anchored titanium dental implants [49]. The typical osseointegrated implant is composed of surgical titanium and requires two surgical stages to fully implement [49]. In the first stage, the bone anchorage site is drilled and mechanically tapped to host corresponding threads on the mating implant fixture. The fixture is screwed into the hole and soft tissues over the implant are restored to seal off the assembly and minimize mechanical disturbances that may cause failure to osseointegrate. In the months following this first stage, the titanium-bone interface hosts callus formation in the interstitial volumes that produces mineralized bone tissues, fixing the implant in place by way of mechanical interlocking. In the second stage, the soft tissues over the fixture are removed and a mechanical abutment is installed into the fixture which serves as the attachment point for subsequent prosthetic components. Soft tissues surrounding form a stabilized stoma around the abutment with a continuous transition from external to internal soft tissue environments. Sub-

sequent mechanical loading of the prosthetic components transmit load directly to the bone, and over the course of years, these cyclic loading patterns strengthen the surrounding hard tissues to increase the mechanical strength of the interface [49].

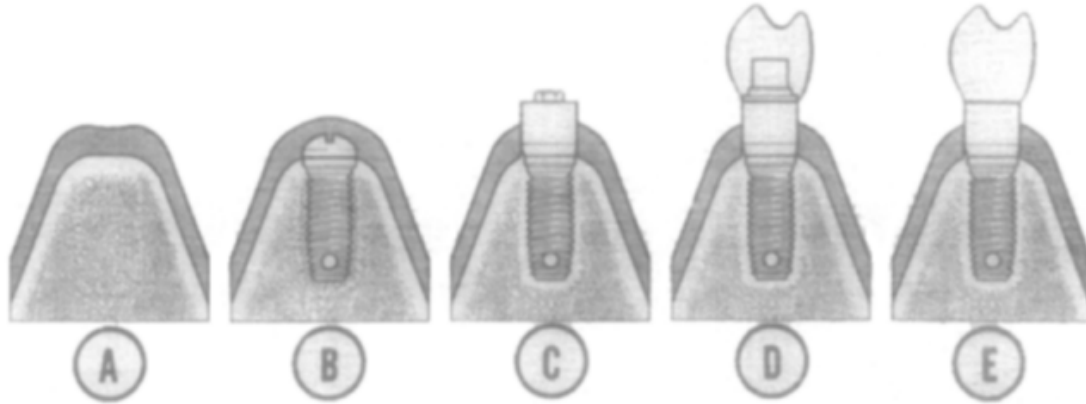


Figure 1-2: Stages of osseointegration. Diagrammatic representation of main steps and procedures for anchorage of a prosthesis to osseointegrated jaw bone fixtures. **A**, Preoperative situation. **B**, First stage with fixture installed and covered by mucoperiosteal tissues. **C**, Second stage with abutment connected to fixture after a healing period. **D** and **E**, Prosthesis attached to abutment. Reproduced with permission from Elsevier.

1.3.1 Application as Limb Prosthesis Interface

Since the widespread use of osseointegration in the application context of dental implants, it has also become clinically relevant for providing skeletal bone-anchoring of limb prostheses at most amputation levels [7]. The advantages of limb osseointegration are many, including:

1. Elimination of skin irritation and perspiration issues related to prosthetic socket usage, accommodation of weight loss and residuum volume changes, and increased comfort during sitting [50]
2. Enhanced awareness of limb position in space, increased sensation of the prosthesis through osseoperception [51]
3. Increased ease of donning and doffing the prosthesis [52]

4. Increased range of motion, limb strength, wear time, steps taken, force production in the residuum at the lower-extremity level [53]

However, bone-anchored implants for lower extremity prosthetic attachment must respect maximum load limits imposed at the titanium-bone interface to prevent fracture of the hard tissues and bending of the abutment [54, 55]. Further, the unphysiological loading patterns at the site of the implant typically limit maximum body mass to 100 kg in the transfemoral case to prevent patient and implant damage during more strenuous activities of daily living [56]. This fundamental mechanical limitation of direct bone fixation may set a ceiling on dynamic performance with powered prosthetic joints, representing a design tradeoff compared to prosthetic sockets which are known to allow participation in high impact sports.

1.3.1.1 Signal Conduit Through Osseointegrated Implants

More recently, osseointegrated implants and abutments have been adapted to provide a conduit for leads from permanently implanted electrodes, enabling chronic signal and stimulation transmission for control and sensation of neurobotic limb prostheses. In particular, the eOPRA system (Integrum, AB) has been implemented at the transhumeral and transradial levels, demonstrating improved signal-to-noise ratio (SNR) of efferent myoneural control signals and improved measures of prosthetic embodiment [8, 9, 10]. Thus far, implementation of the eOPRA system, or similar osseointegrated systems with peripheral signal transmission, have not been implemented at the lower extremity level.

1.4 Approaches to Transfemoral Prosthesis Control

In the domain of powered transfemoral prostheses, or those with the capabilities of actuation and production of positive power, there are two dominant classes of controllers that determine their behaviors: intrinsic and efferent. These are not mutually

exclusive, but are rather typically used in conjunction, especially in more experimental devices that seek to incorporate user volition while still promoting stable, expected cyclic dynamics [4].

1.4.1 Intrinsic Methodologies

Intrinsic methodologies rely upon sensors on-board or around the prosthesis to estimate the intended movement and dynamics desired by the user. These sensors include but are not limited to inertial measurement units, joint encoders, cameras and time of flight sensors, and force measurement devices [4]. From these data, various computational processes including impedance-based finite state machine (FSM) control [57] and gait phase-based variable approaches [58] can be used to predict desired dynamics and execute them at the prosthetic joint. The dynamics of interest may vary between kinematic trajectories, torque trajectories, or intermediate phase trajectories. Oftentimes, intrinsic methodologies may also seek to guarantee stability of joint dynamics under certain operating conditions [59]. The shared limitation of all intrinsic methodologies is that they are inherently responsive, requiring some dynamics-based input from the user and device to predict current or future dynamics at the joint. Hence, the realizable manifold of joint dynamics produced in this manner is limited due to coupled movements that would otherwise be independently realizable in physiology, e.g., movements of the hip that produce corresponding prosthetic actuation at the knee cannot be performed separately.

1.4.2 Efferent Methodologies

In contrast, efferent methodologies use myoneural or neural signals measured from the user to enact or volitionally control joint dynamics [4]. This structure parallels the physiological function of joints wherein mechanical actuation is propagated from neural communications in the information-domain through soft tissues including muscle. Thus, these methodologies largely decouple body dynamics from prosthetic joint dynamics and have the potential to increase the manifold of allowable com-

bined movements. While efferent control methodologies present themselves as the most “natural” and biomimetic, serious impediments to their practical implementation exist that encourage compensation by intrinsic methodologies. Control signals, such as EMG read through surface electrodes in a prosthetic socket, currently require extensive filtering, expert sensor placement, and intensive tuning before being usable for practical control applications [60, 61]. Additionally, errors in efferent muscle activation that stem from pathologies related to amputation itself may limit the effectiveness and accuracy of myoneural control signals that may otherwise be perfectly detected [37]. These challenges must be addressed before practical implementation of efferent control methodologies even if their theoretical performance ceiling can be understood to be higher than intrinsic methodologies.

1.5 Prosthetic Embodiment

The design of experimental limb prostheses is rooted in guiding principles derived from the human motor control theory established in the 20th century. These principles emphasize the simultaneous observation, generation and correction of limb dynamics in the task space by integrating afferent signals and efferent motor commands [62, 63] (Fig. 1-1). Within this framework, an optimal prosthetic interface allows the user to perceive all sensory modalities as they would with an intact limb, as the prosthesis concurrently generates the dynamics expected from the user’s internal mental representation of their limb. The resulting perceptual experience of this idealized closed-loop control is referred to as embodiment.

The definition of prosthetic embodiment is a subject of active debate among academics and researchers focused on clinical realization. Some undertake efforts to redefine the phenomenon while, simultaneously, others evaluate the current working definition in clinical settings. Although the scope of this Review cannot encompass all opinions on embodiment, we give a concise overview of the most prominent perspectives to provide a contextual framework on motivations for bionic limb reconstruction.

Prosthetic embodiment is often conceptualized as being composed of at least two

aspects, which have previously been defined as: i) ‘agency’, or the understanding that we are the initiator of the action and in control of the movement (volition); and ii) ‘ownership’, or the sense that parts of our own body belong to ourselves [64, 65]. Critically, these studies argue that embodiment is a continuous perceptual state that is relatively agnostic to the nature of the substrates involved, whether artificial or biological. For instance, studies have demonstrated that the overall shape of a hand is crucial for fostering a sense of ownership in upper-extremity amputees [66], but skin colour and material composition of the limb itself do not hinder it [67, 68]. To underscore this idea, some academics have summarized key studies to propose alternative time-dependent and visceral principles that sustain the perception of ownership and agency, particularly in the context of the upper extremities [69]: to facilitate ownership, sensory information should be synchronously integrated from an anatomically relevant appendage with spatial and tactile congruence [70, 71]. To facilitate agency, it is essential to establish a causal link between movement intent and the corresponding spatial and temporal outcomes [72, 73, 74]. As a corollary, the degree of agency is significantly reduced as a multivariate function of the magnitudes of spatial and temporal discrepancies [73, 75].

An additional third aspect, ‘body representation’, is proposed by a different study and defined to be the “knowledge, beliefs, and experiences we have of the physical structure of our bodies, and the cognitive and neural mechanisms by which we dynamically interact with our physical bodies” [1]. The authors posit that body representation can be divided into subcomponents that constitute the conscious body image and subconscious body schema. The body image encompasses the subjective experience of factors such as size, shape, structure, function and even beliefs held of the body [76, 77]. By contrast, the body schema encompasses the internalized forward and reverse models updated by somatosensory feedback that facilitate real-time control of the body and its environmental interactions [78]. To elaborate, the qualitative experience of a phantom limb is a phenomenon that can be cleanly classified under body representation, and a prosthesis that is represented within the body schema in a similar manner to an intact limb can be said to be ‘incorporated’ [79].

1.6 Dissertation Summary

The objective of this thesis work is to develop and characterize the soft and hard tissue interventions required for high fidelity control of prosthetic knee dynamics under a largely efferent control methodology.

Chapter 2 investigates the rehabilitative potential of implementing a knee AMI in the revisional case. Evidence is presented that suggests persons with existing transfemoral amputation can recover neuromechanics and neurophysiology for applications related to subsequent neurorobotic control.

Chapter 3 investigates the clinical and functional compatibility of integrating transfemoral osseointegration, revisional transfemoral AMI, and implanted intramuscular electrodes. Evidence is presented that suggests persons possessing all these interventions, integrated as the osseointegrated mechanoneural prosthesis (OMP) platform, successfully attain the advantages of each for applications related to subsequent neurorobotic control.

Chapter 4 investigates the ability of those with the transfemoral OMP to achieve agile neurorobotic knee dynamics compared to those with socket-based AMI interfaces and those with socket-based conventional transfemoral amputation. Evidence is presented that suggests OMP subjects demonstrate outsized improvements to neurorobotic knee agility and prosthetic agency relative to their physical fitness due at least in part to the advantages bestowed by the OMP platform.

Chapter 2

Clinical Revisional Implementation of the Agonist-antagonist Myoneural Interface

In this chapter, I present work that indicates the efficacy of the AMI in the context of a revisional transfemoral amputation to a degree comparable to that of the native implementation. Two individuals with preexisting unilateral transfemoral amputation were evaluated in a week-long study period before and after an intervention wherein extant soft tissues were revised into AMI muscle constructs intended for knee control, namely the rectus femoris (RF) for knee extension and biceps femoris (BF) for knee flexion. Post intervention, both subjects demonstrated significantly increased secondary muscle spindle firing rate graded with agonist contraction. In a functional brain imaging experiment, both subjects demonstrated quantifiably greater cortical activity in regions associated with lower-extremity joint movement and proprioception. In a virtual control task involving efferent electromyographic (EMG) control with visual feedback, both subjects demonstrated improved grading and targeted activation of muscles corresponding to intended movement. The data suggest that the revisional TF AMI can homogenize and recover motor functionality associated with knee joint control in populations with extant transfemoral amputation.

2.1 Rationale and Study Design

Intact human physiology depends on afferent feedback generated by proprioceptive mechanoreceptors experiencing agonist-antagonist muscle-tendon dynamics to produce stable and specific joint dynamics. However, in the case of a limb amputation, these interactive muscle-tendon dynamics are disrupted by transection of soft and hard tissues resulting in pathological anatomical configurations that no longer serve their original purpose of joint control. The AMI was developed to provide a first-order approximation of these lost agonist-antagonist interactions, and in doing so, restore a more physiological sense of proprioception to the user for improved prosthesis control. A diagram of conventional transfemoral amputation architecture compared to a transfemoral implementation of the AMI can be seen in Fig. 2-1.

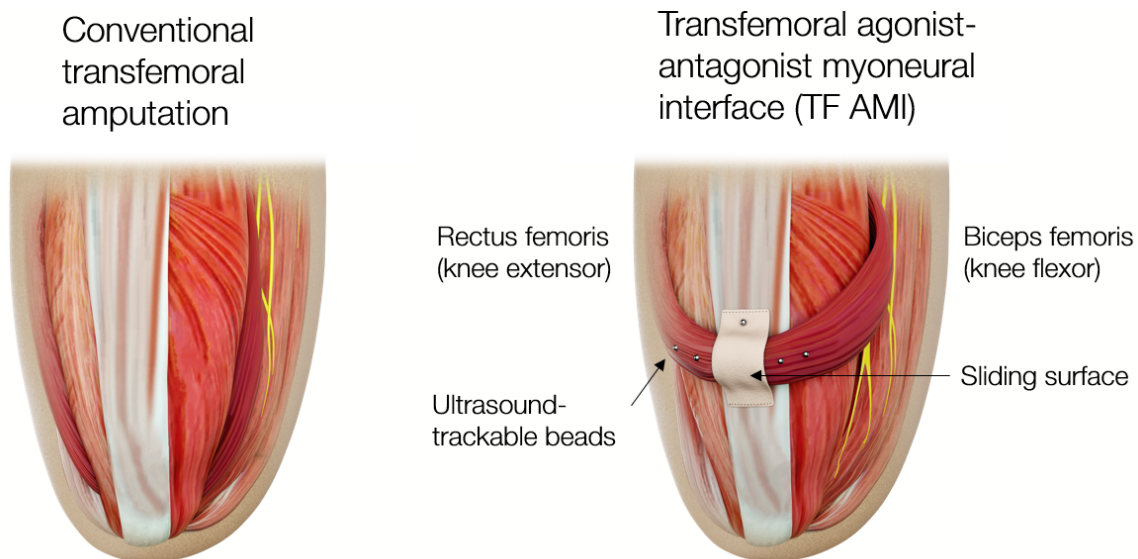


Figure 2-1: Conventional transfemoral amputation and TF AMI architectures.

While the AMI has been successfully implemented in the acute case for both transtibial and transfemoral amputation, with suggested improvements to proprioception and neuromechanical control metrics, its efficacy has yet to be demonstrated in a revisional capacity. As there exists an overwhelmingly greater number of persons with amputation without the AMI, it is clinically imperative to understand whether this population may benefit similarly from the rehabilitative advantages offered by

the interface.

Broadly, I hypothesize that the TF AMI will recover relevant cortical function associated with motor areas and augment neurobotic control. Specifically, I hypothesize the following:

1. Instantiation of the revision TF AMI will promote increased vividness of phantom imagery and fidelity of neuromuscular control towards enhanced control of task space objectives.
2. The mechanical configuration of the TF AMI increases proprioceptive afferents regardless of the native or revisional nature of its instantiation.
3. There will be observable expansion of the sensorimotor brain areas associated with control and sensation of the affected limb, implicating restoration of essential cortical structures.

By quantifying neuromechanical and neurophysiological measurements related to these hypotheses over a training period wherein subjects are exposed to neurobotic control repeated before and after the intervention, I intend to distinguish between changes due to the surgical intervention itself as opposed to changes induced by feedback and interaction with a neurobotic limb.

Pre-operative and post-operative investigations (6 months post procedure) will take place consisting of a 5-day training paradigm where subjects will be exposed to activities related to efferent joint control. Within the training paradigm, experiments will be conducted that assess:

1. Proprioceptive sensation (phantom range of motion)
2. Peripheral neuromuscular function (neuromechanics)
3. Central reorganization (functional neuroimaging)
4. Task-space motor control (game performance)

The experimental design is longitudinal. Each subject will serve as their own control in three ways, depending on the specific experiment: i) Pre-training versus post-training, ii) Affected limb versus unaffected limb, and iii) Pre-operatively and post-operatively.

2.2 Methods

Two subjects were recruited for an initial pilot study of this experimental protocol with informed consent for the operation at Brigham and Women’s Hospital (BWH)(Boston, MA) under the approval of the Partner’s Health System Institutional Review Board. Functional magnetic resonance imaging (fMRI) experiments were performed at BWH under the approval of the Partner’s Health System Institutional Review Board. All other experiments were carried out with informed consent at the MIT Media Lab (Cambridge, MA), under the approval of the MIT Committee on the Use of Humans as Experimental Subjects (MIT COUHES). Relevant subject biometrics are provided in Table 2.1.

| Subject ID | Activity level | Age (years) | Time since original TF amputation (years) | Biological sex | Height (m) | Weight (kg) | Prescribed device | Cause |
|------------|----------------|-------------|---|----------------|------------|-------------|-------------------|----------------|
| P1 | K4 | 59 | 4 | Male | 1.78 | 75 | Variable damper | Chondrosarcoma |
| P2 | K3 | 55 | 22 | Male | 1.83 | 86 | Powered | Trauma |

Table 2.1: Revisional TF AMI subject biometrics

2.2.1 Phantom Range of Motion

A wireless goniometer (Biometrics Ltd) was placed on the posterior side of the unaffected limb to measure mirrored ankle and subtalar joint movements. Separately, another wireless goniometer was placed spanning the knee joint of the unaffected limb to measure mirrored knee movements. Subjects were blindfolded and asked to repeatedly use their unaffected joints to mirror their subjective maximum perceived range of motion (ROM) of the phantom joints for each degree of freedom. These movements were repeated unilaterally on the unaffected side to measure the actual

capability of the unaffected joints used to normalize the prior measurements. This experiment was performed at the beginning and end of each training week, both pre- and post-operatively.

2.2.2 Graded EMG and Ultrasound Measurement

Muscle state movies were collected via ultrasound (US) probe as each patient volitionally contracted their the muscles involved in the TF AMI construction at preset levels of perceived effort on the affected side (phantom limb). Ultrasound measurements from both flexor and extensor muscles were processed to quantify fascicle strain using UltraTrack fascicle measurement software [80]. Separately, EMG was recorded from each muscle using surface electrodes as patients contracted each muscle at preset levels of perceived effort. Fascicle strains and EMG at each level of perceived effort were paired to produce a measure of secondary spindle firing rate through the following equation adapted from Formento et al., using their methodology to scale the constants appropriately for the knee muscles [81]:

$$\text{Type II firing rate} = 5.944 + 1.003 \cdot \text{strain}_{mm} + 1.486 \cdot \text{EMG}_{env} \quad (2.1)$$

Averaged values for strain and EMG were taken in the middle portion of each movement when muscles were strained, but static in length. This experiment was performed once per week pre- and post-operatively.

2.2.3 fMRI Tasks and Imaging

Neuroimaging was performed on a 7T scanner located at BWH to acquire fMRI and resting state MRI volumes. Subjects were positioned in a supine position with a pillow placed under their thighs. Head motion was restricted by foam padding inside the array coil. During the task-based fMRI, subjects were directed to alternately move their phantom limb and unaffected limb through visually prescribed movement patterns that encompass the plantarflexion and dorsiflexion ankle range of motion and flexion and extension knee range of motion. Subjects practiced the directed move-

ments prior to scanning to promote repeatable and accurate performance across task conditions. As a note, the subjects performed neuromuscular phantom movements, i.e., contraction of the appropriate muscles, rather than imagined movements in a manner according to Makin et al. [82].

The following experiments and associated task conditions were performed in the scanner at three equally spaced intervals per training week:

1. **Anatomical data:** Acquisition of magnetization-prepared rapid acquisition gradient echo sequence (MP2RAGE) [83]. 6:55 minutes. Manual shim prior to the MP2RAGE.
2. **Resting state data:** Closed eyes for 10 minutes.
3. **Functional data:** The following task run shown in Table 2.2 was performed by subjects twice on both left and right sides.

TASK, single run (2:30) :

| | | |
|--------------------------------------|------------|---|
| Rest | 20 seconds | Rest Now |
| Prep | 10 seconds | Prepare for: (Left/Right) Knee EXTEND FLEX |
| Knee Flexion Extension | 20 seconds | Flex (2 s), Extend (1 s) |
| Rest | 20 seconds | Rest |
| Prep | 10 seconds | Prepare for: (Left/Right) Foot UP DOWN |
| Ankle Dorsiflexion Plantarflexion | 20 seconds | Up (1 s) , Down (1 s) |

Table 2.2: Revisional TF AMI fMRI functional data task run

From anatomical images, cortical and surface representations of the AMI in the sensory (S1), motor (M1), and supplementary motor areas (SMA) were analyzed. From functional images, analyses were performed of the blood-oxygen-level-dependent (BOLD) response obtained during individual joint movements and, in conjunction with the regions identified from anatomical images, averaged to provide an overall activity level for a given region for a given movement.

2.2.4 Task-space Motor Control with Visual Feedback

A graphical user interface (GUI) was developed to provide visual feedback representing the user's EMG processed as intensities within intended movement directions using the Nonlinear Orthogonal Decomposition (NOD) algorithm [84]. Target activation levels at 25%, 50%, and 75% were overlaid over bar graphs representing intensity per movement direction of the knee, i.e., flexion and extension. Subjects were instrumented with surface electrodes over their residuum and asked to repeatedly activate their residual muscles to control a bar representing intensity of a specific movement direction to the targeted levels in a pattern of 3 seconds of activation between 3 seconds of rest. EMG and corresponding NOD decompositions were recorded during the entire sequence.

2.3 Results

For each degree of freedom per testing day, 8 repeated maximum ROM trials were averaged to produce an estimate of the true maximum for both mirrored affected and unaffected sides. Figure 2-2 shows phantom range of motion normalized against intact range of motion for all degrees of freedom per testing day.

Figure 2-3 shows improved secondary afferent firing rates as a result of the intervention for both affected side knee flexor and extensor muscles. A total of three movements were recorded per muscle per subject per direction of movement to provide a mean value for each level of activation.

Average BOLD responses during knee and ankle functional tasks both pre- and post-op are presented in Fig. 2-4 for P1 and Fig. 2-5 for P2. These data are taken from scans performed at the end of each training week. Summary BOLD values are provided in Table 2.3, demonstrating an increase in BOLD response during both tasks for both subjects in the post-op condition.

Figure 2-6 demonstrates subject performance in a freespace reaching task related to phantom knee extension and flexion. It can be seen through individual trials and summary metrics that the revisional TF AMI improves grading of efferent neuromus-

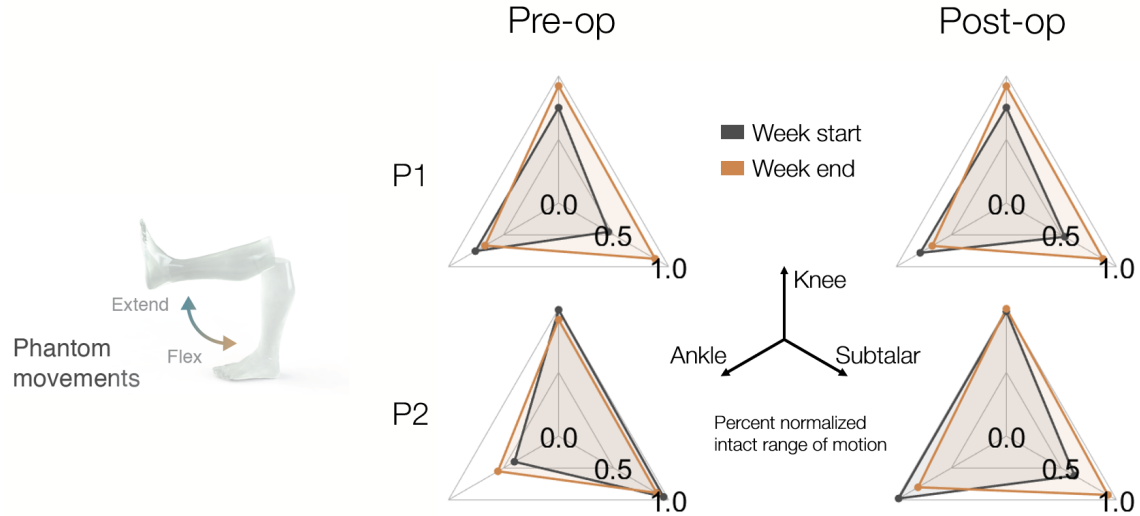


Figure 2-2: Revisional TF AMI subject phantom range of motion. Phantom range of motion for each degree of freedom is represented as a normalized value relative to physiological range of motion measured on the unaffected side. Phantom ranges of motion were confirmed by subjects to not exceed unaffected ranges of motion.

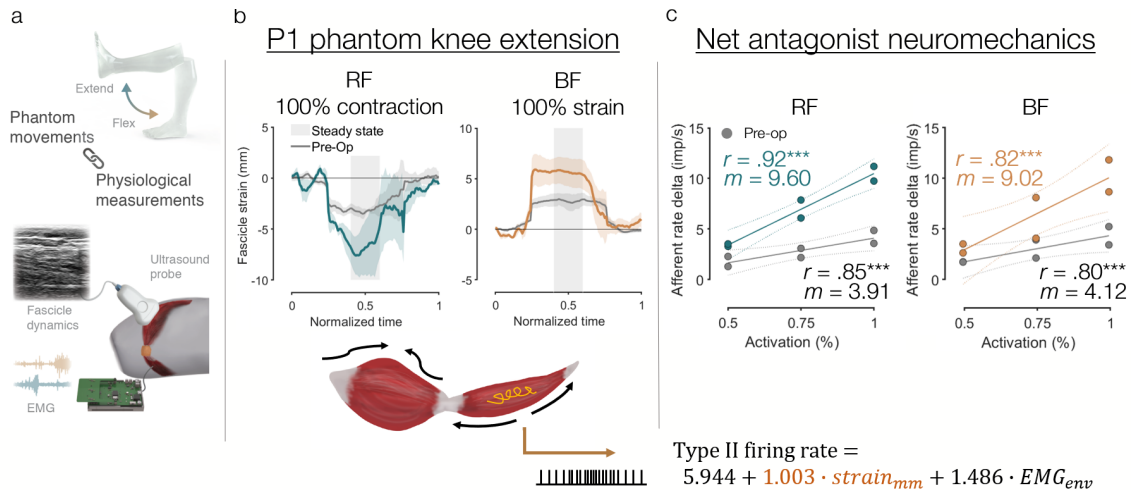
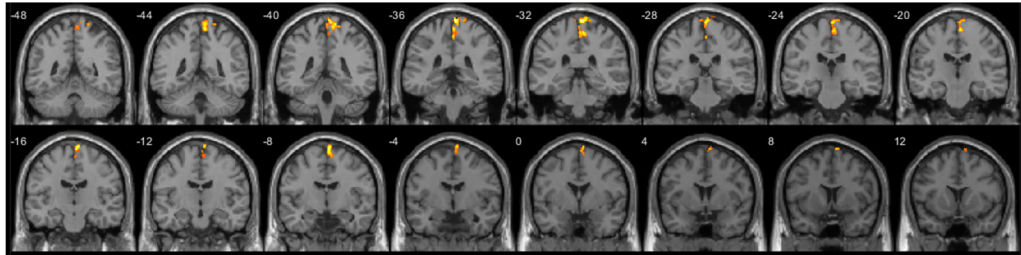


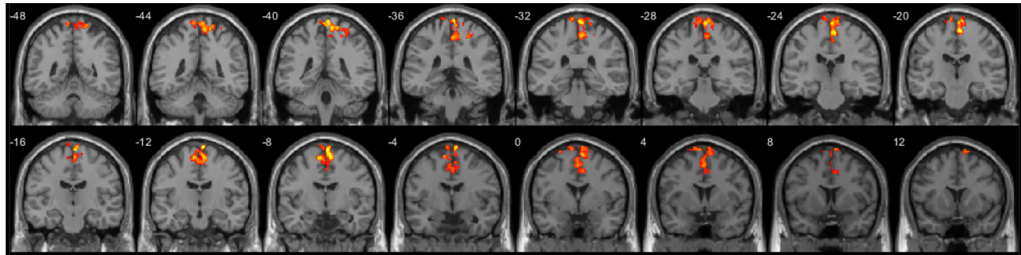
Figure 2-3: Revisional TF AMI subject neuromechanics. a) Experimental setup. b) Representative BF strain resulting from RF contraction for P1. Colored traces indicate post-op values. c) Net antagonist firing rate values (antagonist firing rate less agonist firing rate) for both subjects. Colored markers and linear regression trendlines indicate post-op values (** $P < 0.001$). Pearson correlation (r) and slopes (m) are reported inline).

cular control signals.

P1: PRE; Day 3; Left knee task

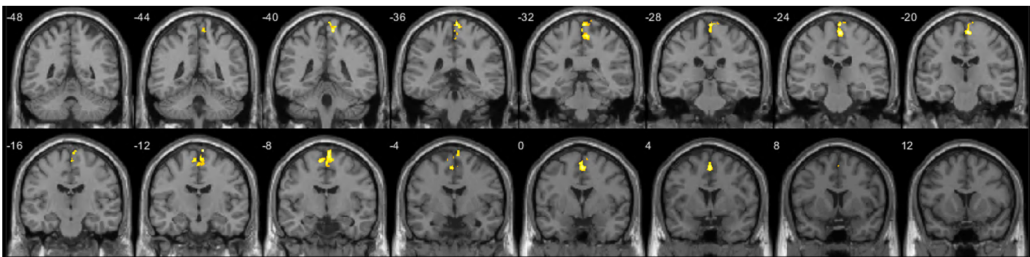


P1: POST; Day 3; Left knee task

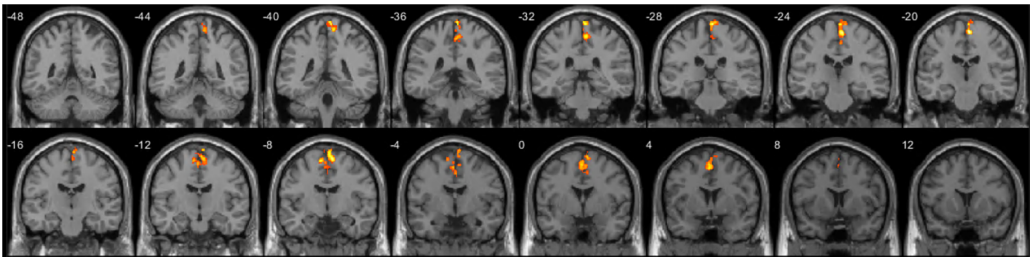


(a) Coronal slices with average BOLD response during phantom knee task. Top row, pre-op. Bottom row, post-op. Peak $t = 19.08$ in red.

P1: PRE; Day 3; Left foot task



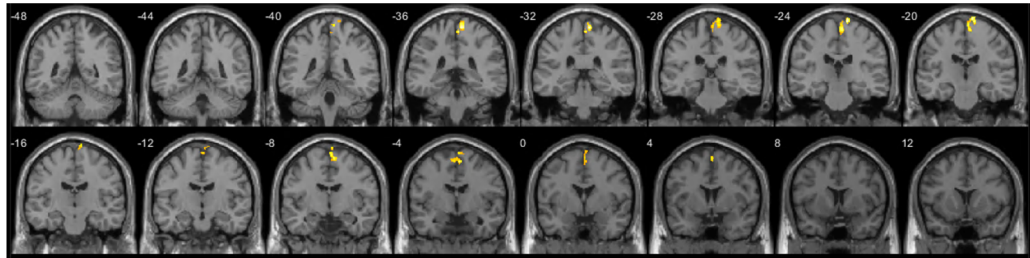
P1: POST; Day 3; Left foot task



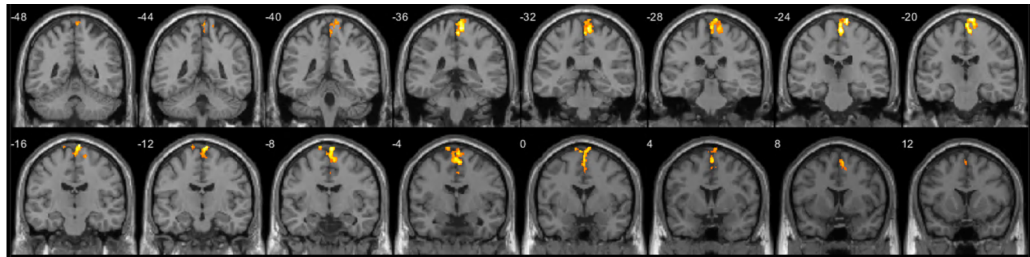
(b) Coronal slices with average BOLD response during phantom ankle task. Top row, pre-op. Bottom row, post-op. Peak $t = 11.82$ in red.

Figure 2-4: P1 average BOLD response during functional joint tasks at the end of the training week pre- and post-op.

P2: PRE; Day 3; Left knee task

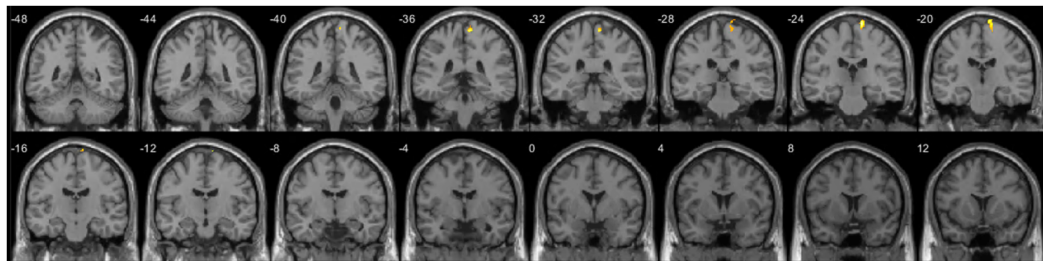


P2: POST; Day 3; Left knee task

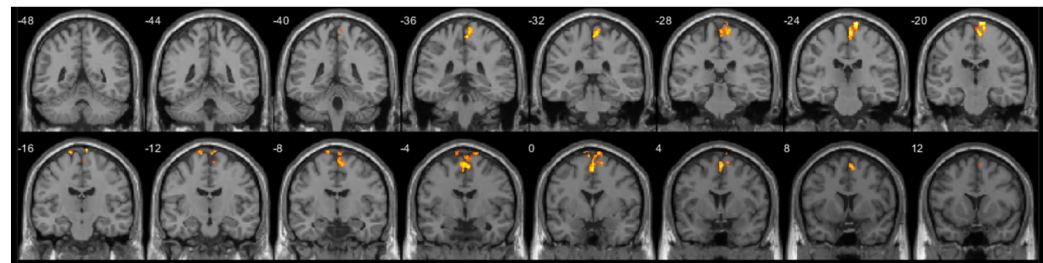


(a) Coronal slices with average BOLD response during phantom knee task. Top row, pre-op. Bottom row, post-op. Peak $t = 12.08$ in red.

P2: PRE; Day 3; Left foot task (lenient t threshold)



P2: POST; Day 3; Left foot task (lenient t threshold)



(b) Coronal slices with average BOLD response during phantom ankle task. Top row, pre-op. Bottom row, post-op. Peak $t = 7.66$ in red.

Figure 2-5: P2 average BOLD response during functional joint tasks at the end of the training week pre- and post-op.

| P1 | LEFT KNEE (number of voxels) | | | | Peak t | LEFT FOOT (number of voxels) | | | | Peak t |
|-------------|------------------------------|------------------|-------------------|------|--------|------------------------------|------------------|-------------------|-----|--------|
| ROI (Right) | Paracentral lobule | Precentral gyrus | Postcentral gyrus | SMA | | Paracentral lobule | Precentral gyrus | Postcentral gyrus | SMA | |
| PRE Day 3 | 839 | 8 | 197 | 517 | 11.13 | 504 | 6 | 59 | 603 | 7.48 |
| POST Day 3 | 1121 | 72 | 557 | 1621 | 19.08 | 765 | 9 | 52 | 930 | 11.82 |

| P2 | LEFT KNEE (number of voxels) | | | | Peak t | LEFT FOOT (number of voxels) | | | | Peak t |
|-------------|------------------------------|------------------|-------------------|-----|--------|------------------------------|------------------|-------------------|-----|--------|
| ROI (Right) | Paracentral lobule | Precentral gyrus | Postcentral gyrus | SMA | | Paracentral lobule | Precentral gyrus | Postcentral gyrus | SMA | |
| PRE Day 3 | 454 | 90 | 48 | 410 | 9.71 | 110 | 96 | 20 | 1 | 5.41 |
| POST Day 3 | 945 | 175 | 156 | 954 | 12.08 | 578 | 134 | 20 | 790 | 7.66 |

Table 2.3: Revisional TF AMI fMRI BOLD response summary values for both subjects during knee and ankle movement functional tasks at the end of each training week. SMA: supplementary motor area

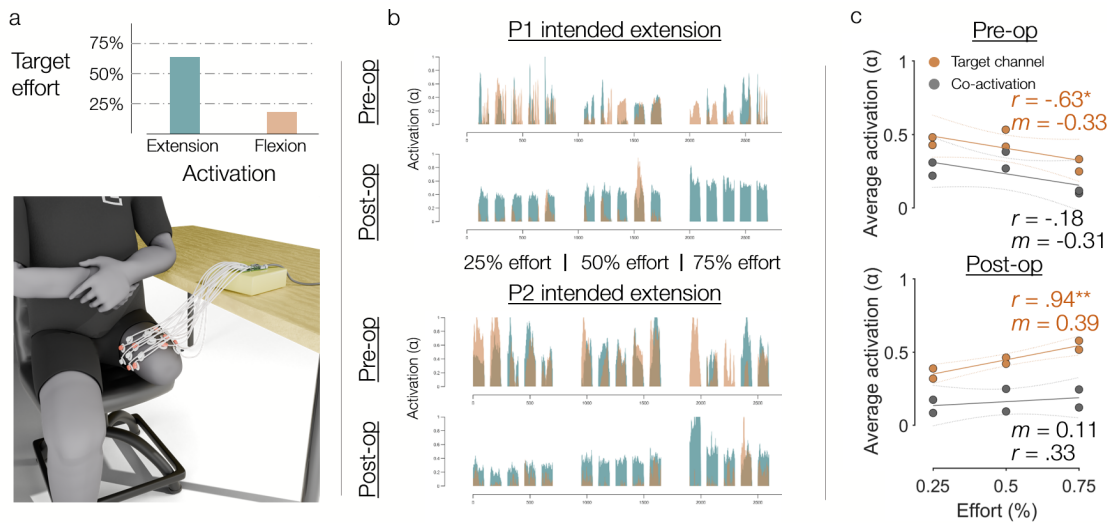


Figure 2-6: Revisional TF AMI control of intended knee movement direction. a) Experimental setup showing recording of EMG used for control of time-varying bar graphs representing intended knee movement direction and degree. Target levels of activation are indicated by dashed horizontal lines. b) Individual trials for intended knee extension of both subjects. More unintentional activation can be seen in the pre-op condition. Graded activation in the intended direction of movement develops post-op. c) Mean target direction activation for both subjects averaged from extension and flexion. Intended channel activation is positively graded according to target levels of activation. Linear regression trendlines are calculated for both target channel and off-target channel (co-activation) (* $P < 0.05$, ** $P < 0.01$. Pearson correlation (p) and slopes (m) are reported inline).

2.4 Discussion

As shown in Fig. 2-2, clear trends in changes to perceived phantom range of motion are not established as a result of the TF AMI revision or training between the two subjects. Qualitatively, P1 demonstrates a positive response to training at both the knee and subtalar joints in the pre-op training week that resets after the six-month recovery period. This observation yields two interesting implications. First, it would seem that the positive benefits of training are lost upon ceasing the training, as evidenced by the similar range of motion spider plot for P1 at the start of the post-op training week compared to the start of the pre-op training week. Second, despite no proper construction of a subtalar AMI for P1, training increases the perceived range of motion in that phantom joint both pre- and post-operatively. The first implication indicates that the effects of training may not be negligible in establishing perceived phantom range of motion. It is unknown if this is a fundamental property of amputation or if it would also apply to a hypothetical scenario wherein physiologically intact joints remain fixed in place for six months before being moved in range of motion test. The second implication suggests that the notion of muscle synergies may be exercised and improved even in the case of amputated physiology, with AMI constructs or not, i.e., training of the knee joint may have awakened a central response related to more distal phantom joints. Both of these implications would be possible to pursue in a greater population study of both non-amputated and amputated individuals.

In the case of P2, it is noteworthy that phantom knee range of motion matched that of the unaffected side in all conditions. A previous study on a cohort of persons possessing acute unilateral transtibial AMI constructs found that phantom ankle and subtalar ranges of motion were increased over a comparison population of unilateral transtibial amputation [6]. In that study, the increase in phantom range of motion was found to correlate with a moderate level of some antagonist strain in the AMI population compared to negligible strain in the control population. Similarly, in this study, both subjects possessed some non-negligible amount of net positive antagonist afferents even in the pre-op condition, as seen in Fig. 2-3c. Assuming that

neuromechanics of the lower-extremity between ankle, subtalar, and knee joints are uniformly centralized, then it may be the case that the central nervous system is also capable of sufficient plasticity to remap a relatively minor amount of proprioceptive knee afferents (relative to physiological levels) to near-physiological ranges of motion. Additionally, unlike P1, P2 demonstrates an improvement in ankle range of motion as a result of the intervention alone, and this improvement is relatively invariant with training. The cause of this difference is unclear, but may be related to a secondary procedure the patient received to transect their sciatic neuroma. The proximal transected end of their sciatic nerve underwent a fascicular split before implantation into adjacent vascularized, denervated muscle targets for reinnervation. Supposing that two adjacent reinnervated targets received efferent motor nerves responsible for dorsiflexion and plantarflexion, then it is possible that an ad-hoc revision AMI for the ankle was created in the process, though this is highly speculative.

More uniform is the improvement in afferent neuromechanics bestowed as a direct result of the intervention. As seen in Fig. 2-3c, both subjects gain approximately twice their original net afferent firing rate as a result of the increased ability of the antagonist muscle to strain from agonist contraction, even without training. These improvements are correlated with the increased peak t values and activated volume of central motor regions for both subjects, as seen in Table 2.3. The table also provides evidence of recovery of distal phantom joint neurophysiology despite no explicit intervention to do so, as the revisional TF AMI constructs were targeted toward improvements related to knee control. Further study should be performed on a larger interventional TF AMI population to understand if recovery of distal phantom joint function is caused by the revision. As an aside, P2 demonstrates overall lower peak t values in all tested fMRI conditions, even requiring a lenient t threshold in the left foot task 2-5b. This may be due to P2's longer time since original amputation compared to P1 (22 versus 4 years), as seen in Table 2.1, or the fact that P2 was originally amputated due to a traumatic incident which may have caused relatively increased soft tissue damage.

Finally, both subjects demonstrate a significant improvement in directional joint

activation after the intervention, as seen in Fig. 2-6c. Their intended channel activations are positively correlated with targeted effort percentage while off target co-activation remains relatively low and consistent. It can be understood that the relatively consistent improvement in muscle control and relatively inconsistent changes to phantom joint range of motion given the same post-op increase in proprioceptive afferents matches the findings within Song et al.'s previous study on persons with transtibial AMIs [6], within which improvements to muscle control were more readily attainable for a given amount of antagonist stretch compared to improvements to phantom range of motion.

Overall, both subjects demonstrate improvements in domains which may be more relevant to subsequent control of neurorobotics, e.g., muscle control. The fact that a peripheral soft tissue revision caused positive recovery of central neurophysiology also provides evidence that the revisional TF AMI may be of clinical benefit to persons with preexisting TF amputation, especially if commercial knees that can make use of EMG information become more prevalent.

Chapter 3

Combining Revisional AMI and Osseointegrated Structures as the Osseointegrated Mechanoneural Prosthesis (OMP)

Building from the results of Chapter 2, which indicate a potential gain in neuromuscular control and recovery of neurophysiology upon bestowment of the revisional TF AMI, this chapter describes the combined mechanical advantages of transfemoral osseointegration with the neuromuscular control advantages of the TF AMI toward a bionic knee platform designated as the osseointegrated mechanoneural prosthesis (OMP). The OMP unites these soft and hard tissue modifications, along with their corresponding advantages, while also providing a conduit through a titanium abutment wherein intramuscular electrodes may chronically conduct EMG from within the residuum outward to downstream processing electronics. In a pilot study, two additional subjects with preexisting unilateral transfemoral amputation were screened and provided a two-stage surgical intervention wherein extant soft tissues were revised into TF AMI muscle constructs, the residual femur was tapped and implanted with a titanium helical screw to host the permanently-exposed abutment, and intramuscu-

lar electrodes were implanted into the TF AMI muscles along with other regenerative muscle grafts with leads routed through the abutment. Both subjects demonstrated successful osseointegration and acceptance of the intramuscular electrodes in a manner that did not impede excursion and function of the revisional TF AMI. The data suggest that these soft and hard tissue modifications can be successfully combined in the transfemoral case for subsequent, chronic neurorobotic interactions.

3.1 Rationale and Study Design

The conventional procedure for transfemoral amputation is an approach that disregards physiological neuromuscular function in favor of plastic arrangements that are more conducive toward ensuring comfortable dynamic interactions with a prosthetic socket during weight-bearing activities. However, osseointegrated transdermal titanium implants, which can eliminate the need for sockets by directly transmitting mechanical loads from the prosthesis to the skeletal system, exhibit the clear potential for human-machine integration. By removing the need for a prosthetic socket and providing the physical architecture necessary for chronic signal conduction, soft tissue constructs such as the AMI can be implemented without physical and interfacing impediments.

Broadly, I hypothesize that the revisional TF AMI may be implemented without complication in addition to transfemoral osseointegration and implanted intramuscular electrodes to retain the independent functionality of all components. Specifically, I hypothesize the following:

1. The TF OMP successfully osseointegrates in the presence of AMI and implanted electrodes.
2. The TF OMP increases EMG signal-to-noise (SNR) ratio with stable electrode impedance values.
3. The TF OMP enables the facilitation of afferent feedback to revisional TF AMI musculature through functional electrical stimulation.

By indicating the above hypotheses in the positive, I intend to establish the viability of the OMP as a highly-integrated solution for limb rehabilitation that offers the potential for increased movement agility and prosthetic embodiment.

3.2 Methods

Above-knee revision amputations to implement the OMP were performed in two subjects in an elective setting at BWH in a time period spanning August 2019 and September 2022. A summary of subject biometrics is provided in Table 3.1.

| Subject ID | Amputation type (activity level) | Age (years) | Time since amputation (years) | Biological sex | Height (m) | Weight (kg) | Cause of amputation |
|-------------------|---|--------------------|--------------------------------------|-----------------------|-------------------|--------------------|----------------------------|
| OMP 1 | e-OPRA, AMI (K3) | 64 | 13.7 | Female | 1.63 | 96.6 | Cancer |
| OMP 2 | e-OPRA, AMI (K3) | 61 | 23.0 | Male | 1.78 | 93.4 | Cancer |

Table 3.1: Relevant OMP subject biometrics. e-OPRA: electronic osseointegrated prostheses for the rehabilitation of amputees (Integrum AB).

3.2.1 Surgical and Clinical Procedures

With respect to soft tissues, a revisional TF AMI was constructed in each subject to improve phantom limb proprioception for subsequent high-fidelity control of a prosthetic knee joint. Additionally, a fascicular split was performed on the sciatic nerve with distal ends introduced to autologous muscle grafts. This latter procedure was performed to promote peripheral nerve regeneration, attempt prophylactic prevention of symptomatic neuromas, and provide muscular targets for intramuscular electrodes for subsequent feedback through functional electrical stimulation (FES). With respect to hard tissue, the distal end of the residual femur was shortened approximately 1 cm through transection. The eOPRA BioHelix fixture (Integrum AB) was introduced into the medullary cavity. After a recovery period, a subsequent second surgical operation was performed wherein a titanium abutment was mated to

the fixture and intramuscular electrodes were implanted into the revisional TF AMI muscle constructs and autologous muscle grafts with leads routed through a femoral cortical window to the abutment. A total of 16 electrodes in 8 bipolar pairs were implanted into the residuum with redundancy on the two muscles of the TF AMI construct. The diagram presented in Fig. 3-1 demonstrates the final result of this implementation.

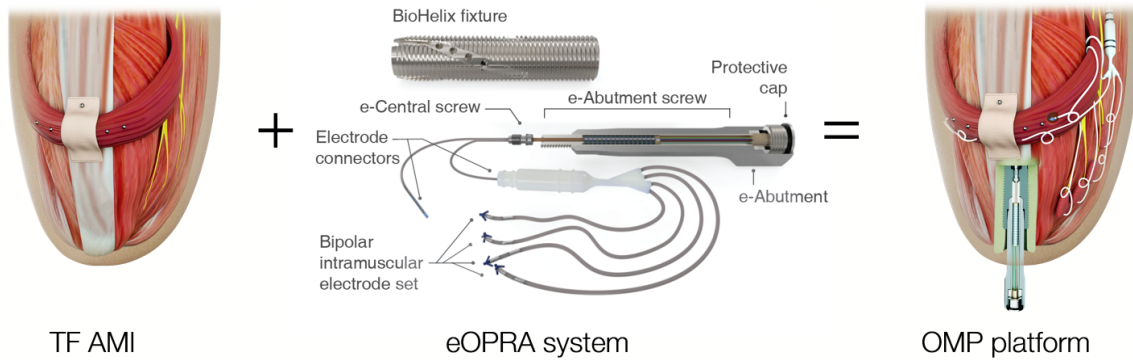


Figure 3-1: Diagram of TF AMI and eOPRA hardware combined as the OMP.

The exact timeline of events involved in the implementation of the OMP, including the major steps performed at each of two surgical stages are presented in Fig. 3-2 along with recovery and rehabilitation procedures.

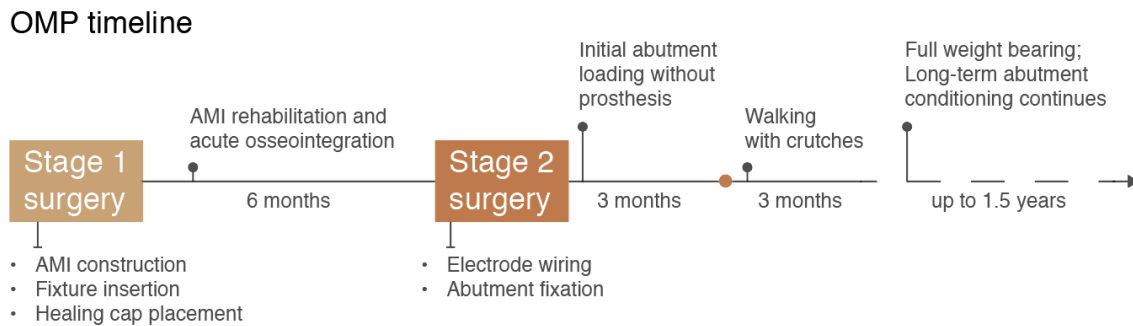


Figure 3-2: OMP operational and rehabilitation timeline.

Clinical data was collected in the preoperative, intraoperative, and perioperative periods, and included patient demographics, surgical time, x-rays, fluoroscopy movies, input/output, and pain control regimen and changes to such. Mean subject age at the time of the first stage was 60.10 ± 0.87 years and 60.97 ± 0.18 years at the second

stage. Mean operative time for stage one was 482.50 ± 61.52 minutes and 773.00 ± 65.05 minutes for stage two. Intravenous fluid requirements, estimated blood loss, and urine output were all within safe margins. Average length of post-operative stay was 3.50 ± 0.71 days for stage one and 5.00 ± 0.00 days for stage two. No complications were noted in the postoperative period [85]. Other clinical data are not reported here.

3.2.2 Phantom Knee Range of Motion

A wireless goniometer (Biometrics Ltd) was placed spanning the knee joint of the unaffected limb to measure mirrored knee movements. Subjects were blindfolded and asked to repeatedly use their unaffected knee to mirror their subjective maximum perceived ROM of the phantom knee as it was moved throughout its range of motion using residual muscle contraction.

3.2.3 Electrode Impedance Measurements

Impedance was measured using an analog ohmmeter for each intramuscular electrode in a monopolar configuration with the titanium abutment serving as an electrical ground. An AC carrier current at 1 kHz was used to avoid the high DC impedance of soft tissue. Electrode impedance was measured twice for each subject, with the last measurement up to 192 weeks post-implantation.

3.2.4 Signal-to-noise Ratio and Related Calculations

Average signal-to-noise ratio (SNR) for the RF and BF muscles in the TF AMI were measured by recording EMG from bipolar pairs in each muscle during maximum volitional contraction (MVC). EMG were processed into a normalized activation using the technique described by Yeon et al. [60]. SNR was calculated using Eq. 3.1 and reported in decibels.

$$SNR_{dB} = 10 \log_{10} \frac{EMG_{Max, Movement}^2}{EMG_{Max, Rest}^2} \quad (3.1)$$

Separately, a repeated measures test was conducted on the RF muscle at MVC while intramuscular EMG and surface EMG were recorded simultaneously to provide an estimate of the increased signal power available from intramuscular electrodes. A signal power ratio was defined according to Eq. 3.2.

$$\text{Signal power ratio} = \frac{EMG_{Implanted, Movement_i}^2 - EMG_{Implanted, Rest}^2}{EMG_{Surface, Movement_i}^2 - EMG_{Surface, Rest}^2} \quad (3.2)$$

3.2.5 Functional Electrical Stimulation

To test the potential of the OMP for providing sensory feedback, functional electrical stimulation (FES) was applied to each electrode in a unipolar manner at a 50 Hz stimulation frequency with 200 μs positive pulse time and 2,000 μs negative pulse time at $\frac{1}{10}$ the positive pulse current amplitude. The Digitimer DS5 (Digitimer Ltd.) unit was used to generate the stimulation pulses. Positive pulse current amplitude was modulated from threshold levels to a maximum of 10 mA or pain, whichever was lower. Subjects were asked to draw on a diagram of a leg to indicate the phantom anatomical centers of stimulus perception.

A just-noticeable difference test was applied to the RF to determine the subjects' discrimination threshold of the fixed FES pattern used to develop the sensation map. A reference current amplitude was selected as 2 mA above threshold values. In a repeated measures test, subjects were presented the reference stimulation for 2 s followed by a brief pause before being presented with a stimulation current either lower or higher than the reference stimulation. Subjects were asked to report whether the stimulation was higher or lower than the reference. Correct and incorrect responses were recorded. A test current range of 4 mA centered around the reference was tested with intervals of 0.05 mA near the center, expanding to 0.2 mA at the extreme ends. For each test current level, 10 trials were performed. Trials were administered in a predetermined, pseudorandom order.

3.3 Results

X-ray images taken during clinical followup of both OMP operative stages are shown in Fig. 3-3.

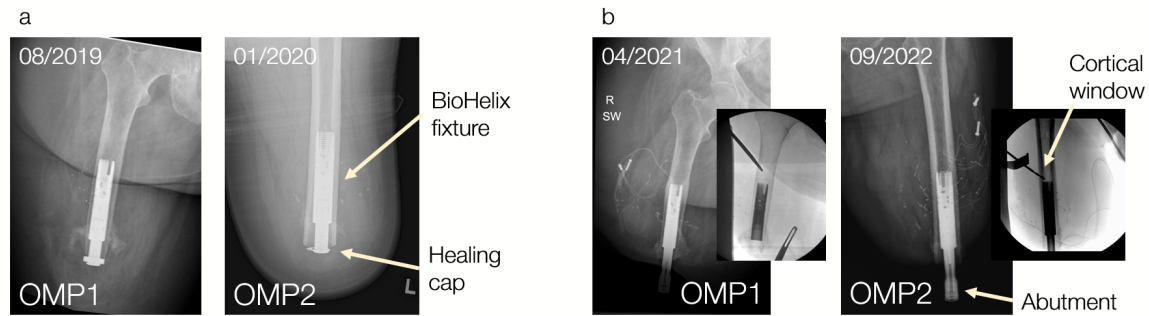


Figure 3-3: X-ray images following both OMP implementation stages. a) Post stage one with healing cap during acute osseointegration period. b) Post stage two with intramuscular electrodes routed to the titanium abutment through a cortical window. Small round occlusions are tantalum beads placed for muscle position tracking. Longer anisotropic occlusions are surgical staples.

Fig. 3-4 demonstrates the appearance of successful osseointegration around the helical threads of the BioHelix fixture in OMP2. Darker areas surrounding the fixture indicate greater hard tissue density from bone remodeling.

Monopolar electrode impedance was measured over a period of up to 192 weeks for each subject. As a note, both subjects experienced intermittent contact in two of the most proximal electrode rings within the abutment central screw. These are excluded from measurement. The remaining impedances are reported with revisional TF AMI SNR in Fig. 3-5.

Fig. 3-6 demonstrates the relative improvements in EMG signal power from intramuscular electrodes compared to surface electrodes along with accompanying physical measurements of muscle depth.

Range of motion of the phantom measured through contralateral mirroring for both OMP subjects is reported in Fig. 3-7.

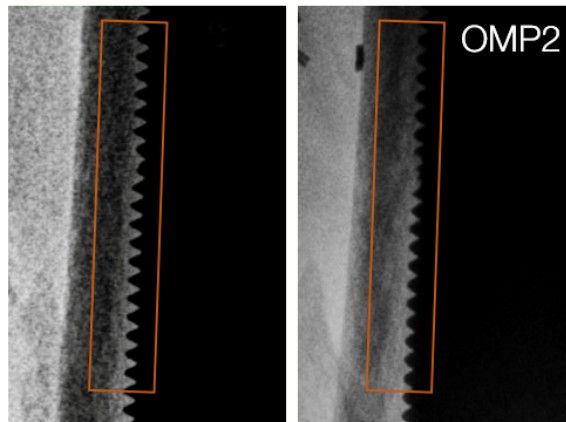
FES characteristics for both OMP subjects are reported Fig. 3-8.

BioHelix fixture



Loading
-23 months

Loading
+3 months



reduced lucency;
bone remodeling

Figure 3-4: X-ray images showing reduced bone lucency in OMP2 after long-term osseointegration.

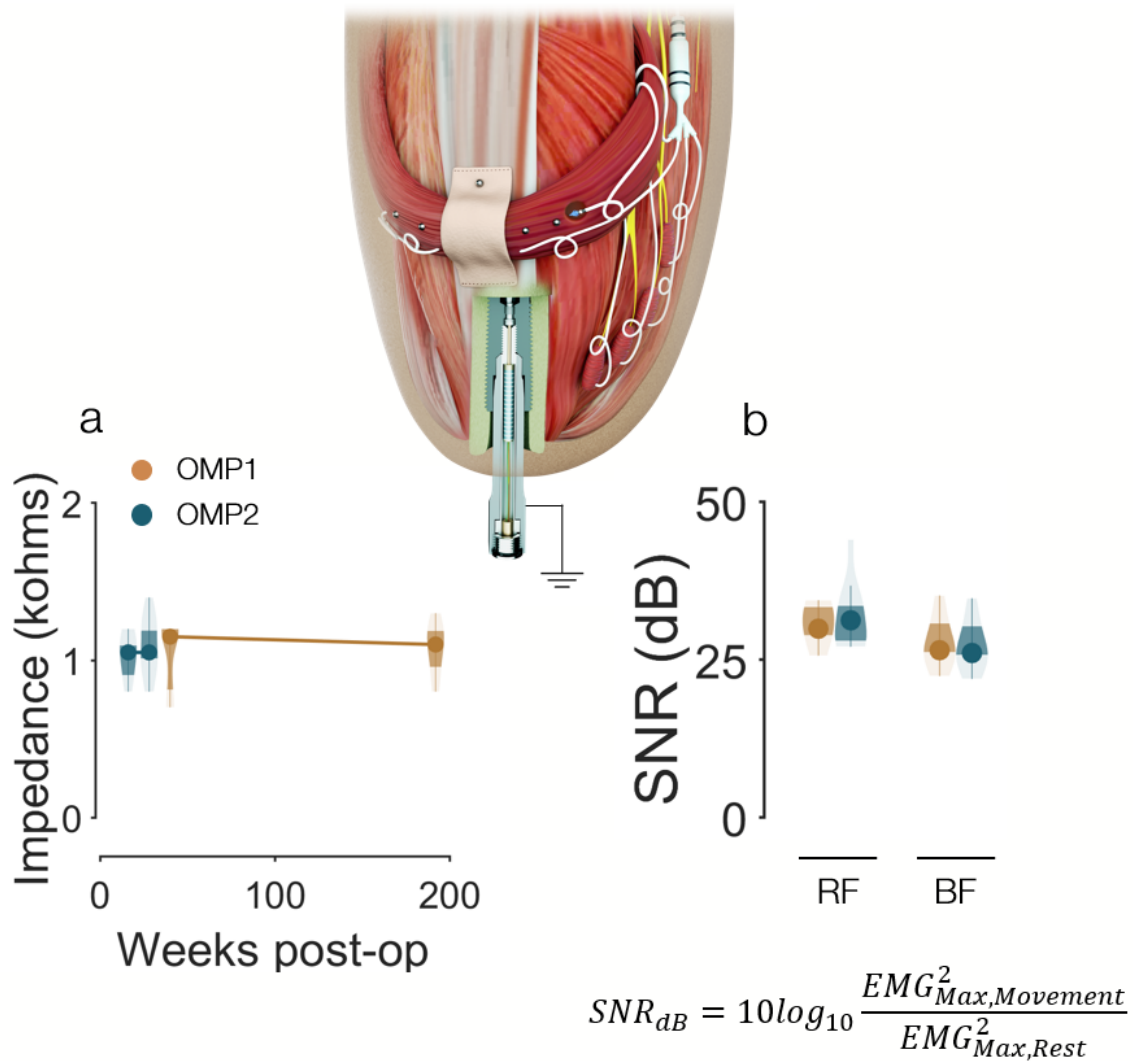
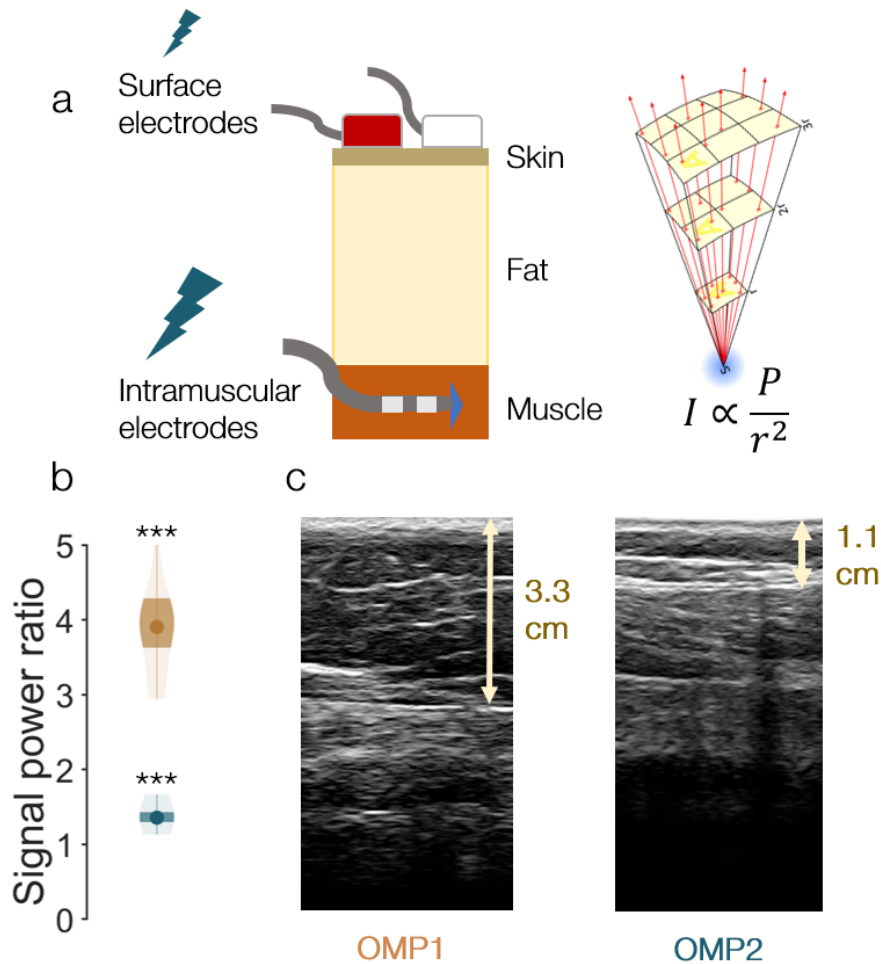


Figure 3-5: Monopolar intramuscular electrode impedance and bipolar EMG SNR for OMP subjects. a) Impedances of all functioning intramuscular leads over time. b) SNR of RF and BF intramuscular electrodes measured at MVC of each muscle.



$$\text{Signal power ratio} = \frac{EMG_{Implanted, Movement_i}^2 - EMG_{Implanted, Rest}^2}{EMG_{Surface, Movement_i}^2 - EMG_{Surface, Rest}^2}$$

Figure 3-6: Signal power ratio of implanted intramuscular electrodes over surface electrodes. a) Diagram of placement of surface electrodes relative to intramuscular electrodes. Signal power for a given source intensity follows the inverse square law, putting surface electrodes at a relative disadvantage for signal quality. b) Signal power ratio values for RF bipolar intramuscular electrodes compared to a bipolar surface pair. Intramuscular electrodes detect significantly greater signal power compared to surface electrodes (n=10 repetitions, ***P<0.001, paired t-test) c) Ultrasound images with RF muscle depth indicated for both subjects. OMP1 demonstrates both deeper muscle placement and greater signal power ratio compared to OMP2.

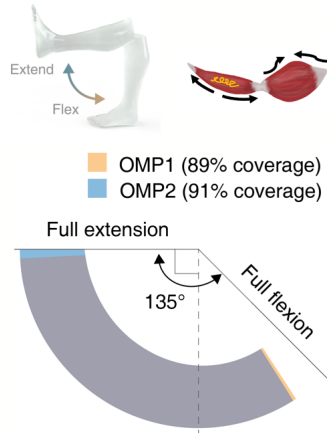


Figure 3-7: OMP phantom knee range of motion. Both subjects demonstrate near physiological perceived range of motion as a result of volitional muscle activation.

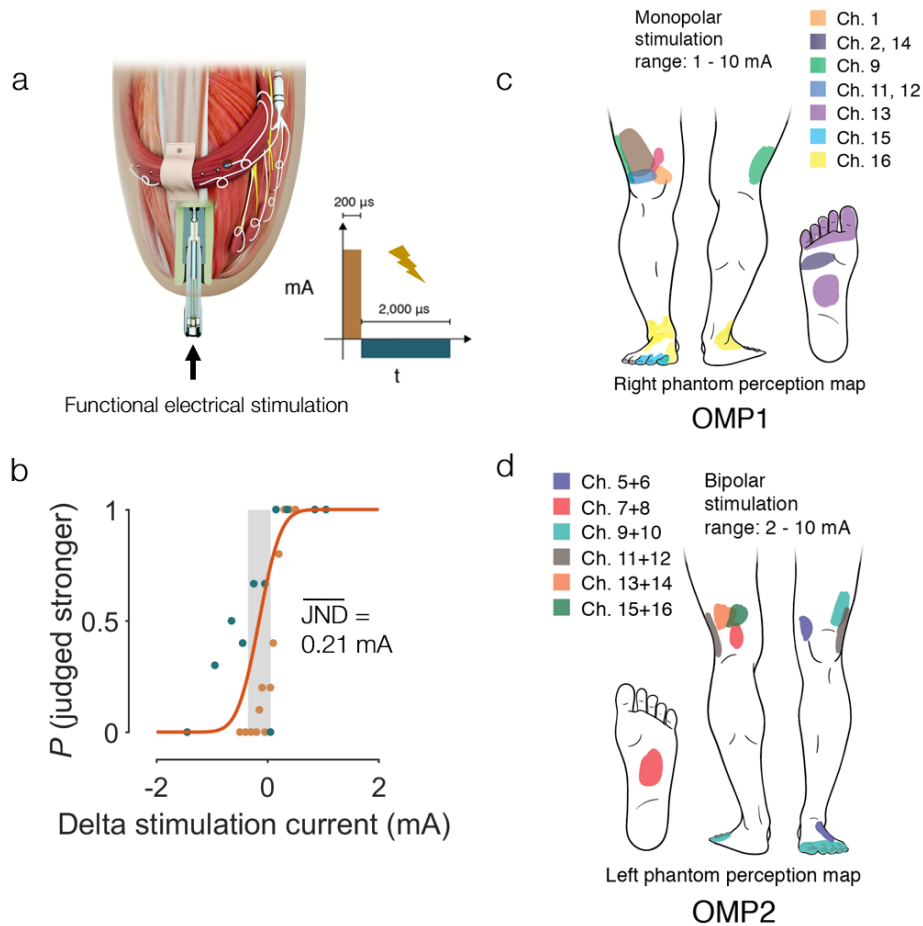


Figure 3-8: OMP FES sensation maps and thresholds. a) Stimulation pattern used for all subsequent testing. b) Just-noticeable difference (JND) at the RF. OMP1: orange markers, OMP2: blue markers. Mean JND of both OMP subjects reported. c) Resultant stimulation map for OMP1 using monopolar channels. d) Resultant stimulation map for OMP2 using bipolar pairs.

3.4 Discussion

Both OMP subjects successfully completed all stages of the operative and rehabilitation procedures indicated in Fig. 3-2. While OMP1 did not indicate any femoral loading sensitivity, OMP2 remained somewhat sensitive to levels of axial force and torque applied in the sagittal plane experienced during normal level-ground walking for the duration of testing period, reported at level 2 out of 10 on a numeric pain scale. However, upon questioning, it was reported by Integrum AB that some patients of the standard TF OPRA procedure remain sensitive for up to two years following their second stage surgery. Additionally, the subject had a previous diagnosis of osteopenia determined through DEXA imaging at the femoral neck on the affected side. Thus, the subject's sensitivity was noted but deemed nominal given their medical history. Bone remodeling, and hence not rejection of the fixture, is supported by the X-ray shown in Fig. 3-4.

OMP subjects demonstrate long-term stability of electrode impedance in their consistently contacting electrodes, as observed in Fig. 3-5a. Two of the electrodes in each subject, the ones most proximal within the e-central screw of the abutment, experienced intermittent contact depending on abutment loading conditions. After discussion with the manufacturer, the cause was determined to likely be related to tolerance stacking of the axially-aligned contact rings with the most proximal contacts becoming fully open circuits due to loading hysteresis. These contact issues have not been reported in upper-extremity implementations of the eOPRA system, perhaps due to lack of body-weight loading. However, upper-extremity recipients of the eOPRA system have also reported failure to osseointegrate for unknown reasons [10], possibly indicating that body-weight loading may be a variable that influences these two outcomes in opposite ways. For bipolar pairs in the RF muscles of both OMP subjects, SNR was demonstrated to be on par with values measured from intramuscular electrodes implanted in natively vascularized and innervated muscles in upper-extremity eOPRA subjects [9].

As seen in Fig. 3-6, bipolar intramuscular pairs in the RF muscle of both subjects

demonstrated a signal power ratio greater than one, suggesting the increased effectiveness of intramuscular electrodes over surface electrodes for future efferent control applications. Importantly, it can be suggested that muscle depth in the residuum may correlate to the reduced signal power measured by surface electrodes according to the inverse square law. This is evidenced by OMP1’s greater signal power ratio compared to OMP2’s signal power ratio despite both subjects’ SNR values of the same bipolar pair in the same muscle being nearly identical, as seen in Fig. 3-5b.

Both subjects demonstrated approximately physiological perceived phantom knee ROM to suggest no major issues with the function of the revisional TF AMI. Both subjects also anecdotally reported increased “vividness” of phantom knee movement after the TF AMI revision.

Notably, both subjects reported a range of sensations from parasthetic vibration to proprioceptive muscle-tendon stretch during the FES sensation mapping task in Fig. 3-8c and d. Only monopolar stimulation was provided to OMP1 and bipolar stimulation to OMP2 due to subject time constraints in both testing periods. Monopolar and bipolar FES methods were investigated to determine if drastic differences between sensations elicited from stimulation types were apparent, but none presented themselves as obvious to the researchers. The space of possible stimulation patterns was not explored thoroughly so data are presented only to qualitatively demonstrate the variety of phantom anatomical centers of stimulus perception. An average just-noticeable difference (JND) of 0.21 mA for the OMP subjects, as seen in Fig. 3-8b is higher than that reported in a case study on a single subject with acute transtibial AMI [36], though more data would be required to determine if this higher JND has any influence on practical performance during feedback-based tasks.

Overall, the lack of serious adverse events, the successful osseointegration and resulting ambulatory status of both subjects, and the clinical indications of revisional TF AMI function suggest compatibility of the soft and hard tissue modifications proposed in the OMP. Further, the stable electrode characteristics and sensation maps requiring use of the implanted intramuscular electrodes suggest serviceable signal input-output for subsequent applications in neurorobotic integration.


Chapter 4

The OMP: Unifying Knee Control and Embodiment

With preliminary work performed to characterize individual aspects of the OMP in isolation, it is now appropriate to test the potential of the platform for its intended purpose of bionic interfacing. In this chapter, I recruit two experimental cohorts consisting of persons with unilateral TF amputation without the AMI (n=7) and persons with unilateral TF with the AMI (n=6), both of which depend on prosthetic sockets for mechanical attachment. These two cohorts are compared against each other and the two OMP subjects in terms of neuromechanical function, neurorobotic task performance across a set of demanding conditions, and perceived embodiment of the neurorobotic device. Despite possessing the greatest physical disadvantages in terms of age, time since original amputation, rehabilitation potential K-level, and body-mass index (BMI), the OMP subjects achieve scores in these experiments that consistently exceed expectations, in several cases placing first among all cohorts. These results demonstrate the advantages of a new paradigm of transfemoral rehabilitation that leverages a highly integrated bionic platform to enable continuous user input for agile behaviors.

4.1 Rationale and Study Design

As discussed in the Introduction, increased invasiveness of a rehabilitative solution must be justified by a corresponding increase in rehabilitation. This study was designed to investigate the relative contributions of individual aspects of the OMP platform to neurorobotic control so that researchers can make maximally-informed decisions toward providing persons with transfemoral amputation optimal clinical benefit. The categorical differences between all three cohorts are provided in Table 4.1.



| | CTL | AMI | OMP |
|--|---------|---------|------------------|
| Electrode interface | Surface | Surface | Intramuscular |
| Mechanical interface | Socket | Socket | Osseointegration |
| Intentional agonist-antagonist muscle physiology | No | Yes | Yes |

Table 4.1: Categorical differences between cohorts

Relevant individual subject data on the study participants are presented in Table 4.2. It is notable that OMP subjects do not possess any obvious physical advantages that would benefit their performance over other participants besides those potentially provided by the platform itself. Fig. 4-1 emphasizes this notion by graphically demonstrating a distance metric based upon time since original amputation and BMI, increasing values of which imply increased muscular atrophy and decreased physical fitness, respectively.

Broadly, I hypothesize that the advantages bestowed by the OMP platform will provide outsized ability to restore neuromechanics, facilitate efferent control, and

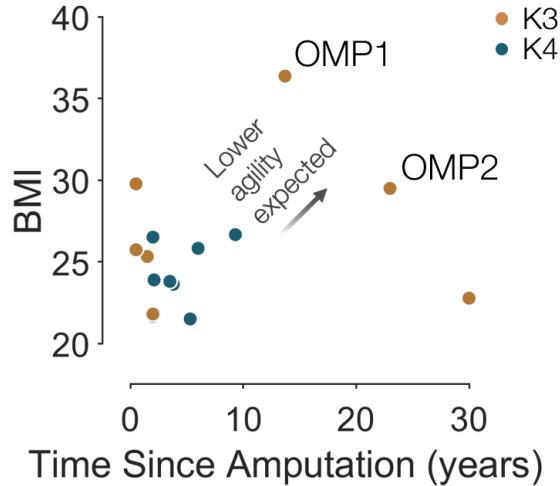


Figure 4-1: BMI comparison across subjects

sustain prosthetic embodiment. Specifically, I hypothesize the following:

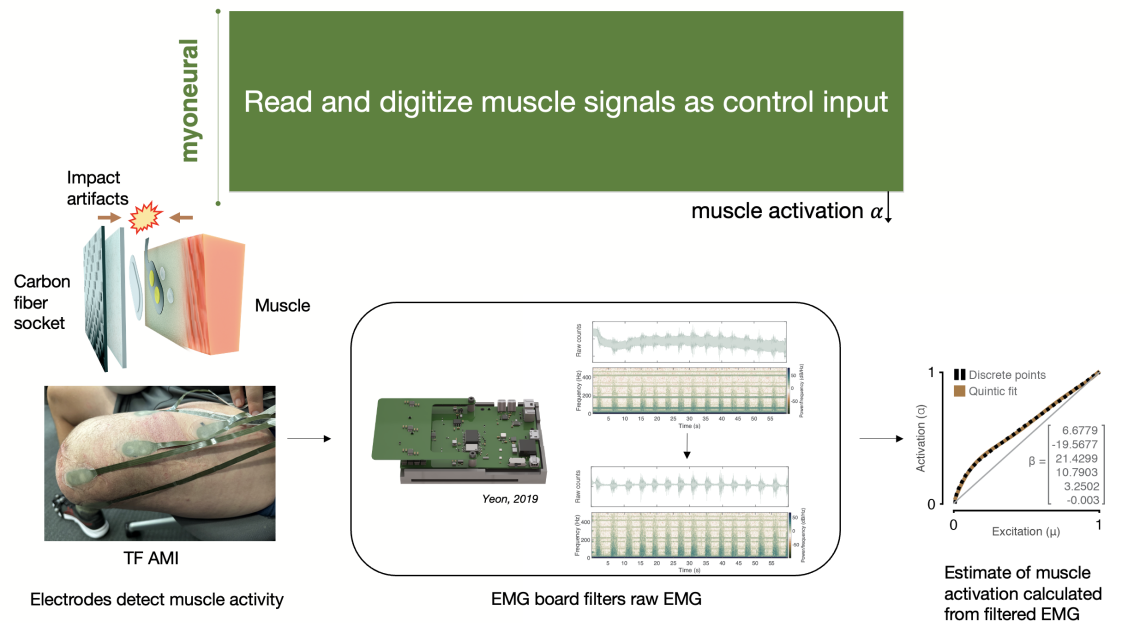
1. OMP subjects demonstrate increased control of peripheral neuromusculature, both with and without visual feedback, compared to AMI and CTL cohorts.
2. OMP subjects demonstrate greater accuracy and speed in agility-based knee control tasks compared to AMI and CTL cohorts.
3. OMP subjects demonstrate increased prosthetic embodiment with use of an efferently-controlled prosthesis over their prescribed passive devices as measured by a repeatedly-administered embodiment questionnaire after task-based experiments.

4.2 Methods

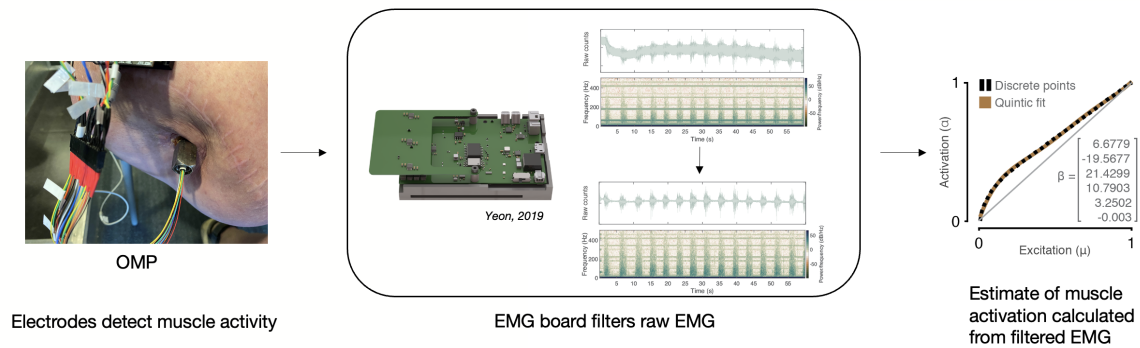
4.2.1 EMG Processing

For subjects with prosthetic sockets, surface EMG were acquired using the techniques and hardware outlined by Yeon et al. [60]. For OMP subjects, distal leads of the intramuscular electrodes were routed to the same EMG processing hardware described by Yeon et al. [60]. For all subjects, EMG were processed to mitigate motion artifacts

using the technique described by Yeon and Herr [61]. EMG were collected from the palpated flexor and extensor muscles in CTL subjects, from the palpated biceps femoris and rectus femoris muscles in AMI subjects, and from the fixed, corresponding bipolar pairs in OMP subjects. Processed EMG were converted into normalized muscle activations using a nonlinear EMG to activation scaling function based on work by Manal et al. [86]. Specifically, a quintic curve was used to transform EMG recorded and normalized by maximum volitional contraction (MVC) into a corresponding value of muscle activation. These two pipelines, along with the nonlinear EMG to activation scaling parameters are shown by Fig. 4-2;



(a) EMG to muscle activation processing pipeline for AMI and CTL subjects (AMI subject shown).



(b) EMG to muscle activation processing pipeline for OMP subjects.

Figure 4-2: EMG to muscle activation processing pipeline.

For OMP subjects, electromagnetic interference (EMI) was observed to be present on the signals read from intramuscular electrodes. These were characterized using a power spectral density analysis and subsequently attenuated by modifying the FIR bandpass filter within the EMG processing steps described by Yeon et al. [60]. The characteristics of this OMP EMI filter are shown in Fig. 4-3.

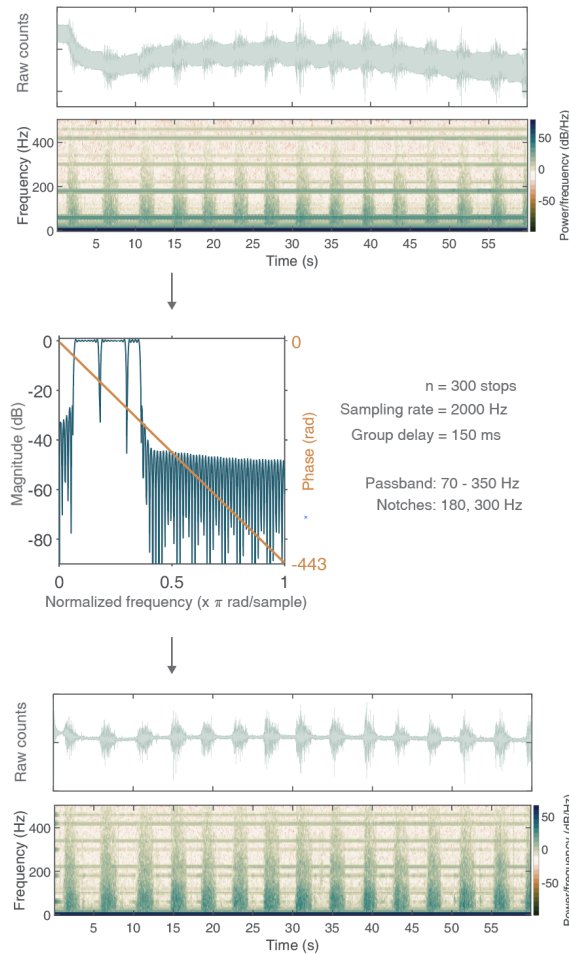


Figure 4-3: OMP noise characteristics and filter configuration.

4.2.2 Torque Computation

A desired torque at the mechatronic knee joint was determined from the summation of contributions from an impedance-based finite state machine (FSM) and a continuous, myoneurally-informed impedance. The basic structure of this summation is shown in Fig. 4-4.

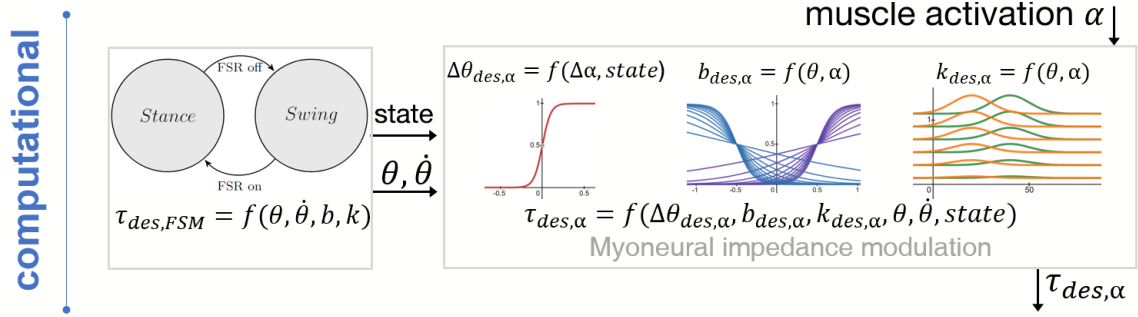


Figure 4-4: Desired knee torque computation.

The FSM alternates between two primary states: stance and swing. Within each state are several unmodulated impedance-based components that individually contribute to torque when their inclusion conditions are satisfied. Additionally, several myoneural impedance modulation components that are informed by state and flexor and extensor activation contribute to the final torque output at the joint. The components may be active in any combination at any time, precluding any mutually exclusive activation conditions. Appendix A details the controller torque calculation loop run at 1 kHz. Importantly, the control structure does not contain features that explicitly classify terrain detection. Rather, unmodulated impedance-based components exist to provide safety and compensate for mechatronic dynamics to achieve biomimetic behaviors based upon joint state only. The same component may be active for different tasks over different terrains.

To compensate for individual variations from subject to subject, k_{max} and b_{max} were scaled according to the following:

$$k_{max} = 1.4 \cdot \frac{mass_{kg}}{RoM_{knee}} \quad (4.1)$$

$$b_{max} = 0.1 \cdot k_{max} \quad (4.2)$$

where RoM_{knee} is in degrees if following the control algorithm outlined in Appendix A. The scaling for k_{max} ensured sufficient torque generation for the most demanding tasks of stair ascent and descent. The scaling for b_{max} ensured stable behavior of the joint across operating conditions, both during stance and swing. For

OMP subjects, k_{max} and b_{max} were scaled according to body mass, but peak torque was clamped to 70 Nm due to abutment loading limits as defined in the associated MIT IRB protocol.

4.2.3 Mechatronics

A single DOF mechatronic knee platform based on the design of Carney et al. [87] was used for all subsequent experiments. The range of motion of the knee was limited by hardware to be between 0 and 90 degrees of flexion. Force sensitive resistors were fixed to the sole of the foot cosmesis at toe, midsole, and heel positions to determine binary ground contact for informing the FSM.

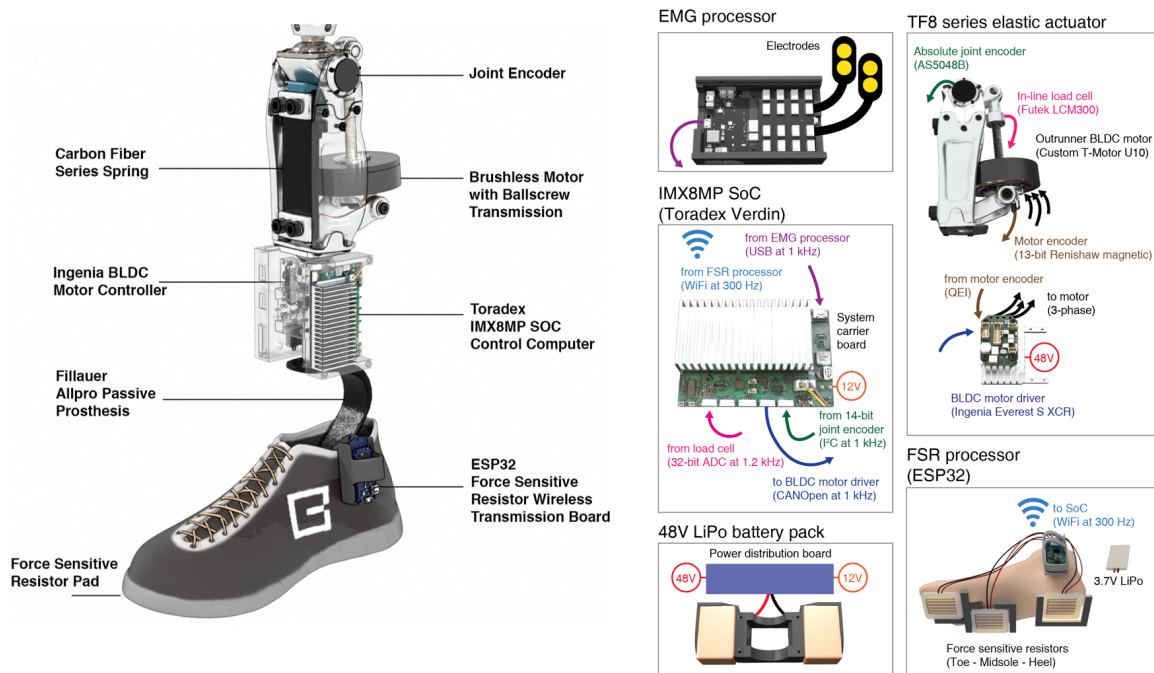


Figure 4-5: Single DOF mechatronic knee with passive ankle prosthesis and complementary sensing peripherals

The open loop torque control bandwidth was determined to be approximately 4.5 Hz by sinusoidal frequency sweep, as shown by the Bode plot in Fig. 4-6. A system ID was performed to fit a second order transfer function to this open loop response. Inversion of the transfer function with an additional low pass filter centered at 20 Hz yielded a realizable feedforward term. The feedforward term was used to tune

the closed loop torque controller outlined in Fig. 4-7, yielding a closed loop torque control bandwidth of approximately 10 Hz.

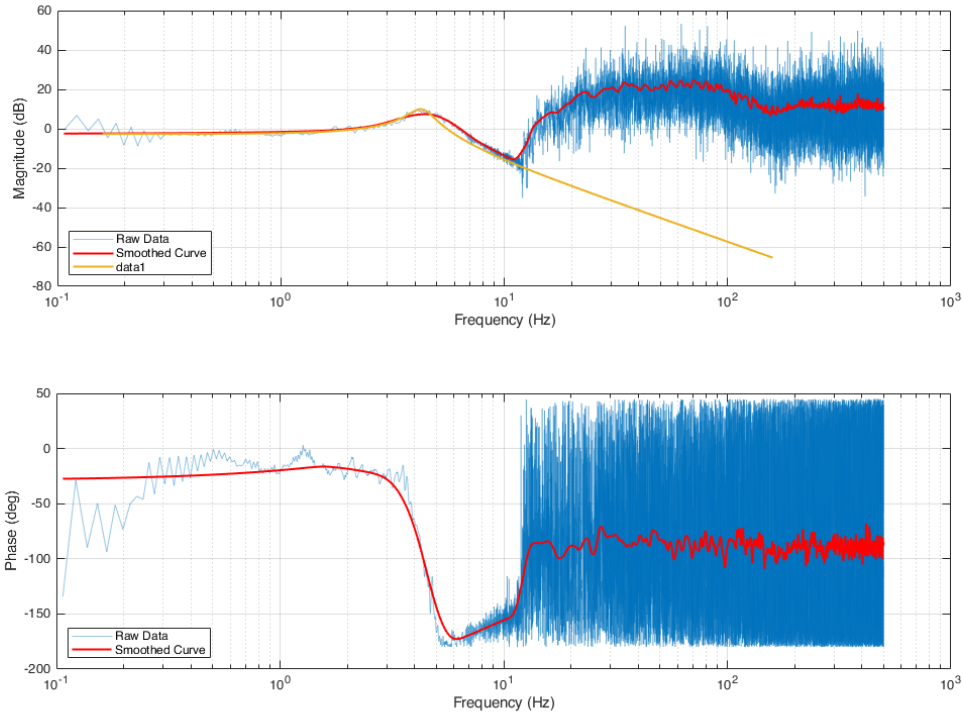


Figure 4-6: Open loop torque control bandwidth for mechatronic knee. Yellow trace represents second order system fitted to experimental data.

The complete implementation of EMG to joint actuation for OMP subjects is represented in Fig. 4-8.

4.2.4 Ultrasound

B-mode ultrasound (US) was recorded at 60 frames per second (MicrUs Pro, Telemed inc.) and used to observe muscle fascicle dynamics of the knee flexor and extensor in all subjects. US data were time-synced with EMG data using a custom script to simultaneously collect both data streams.

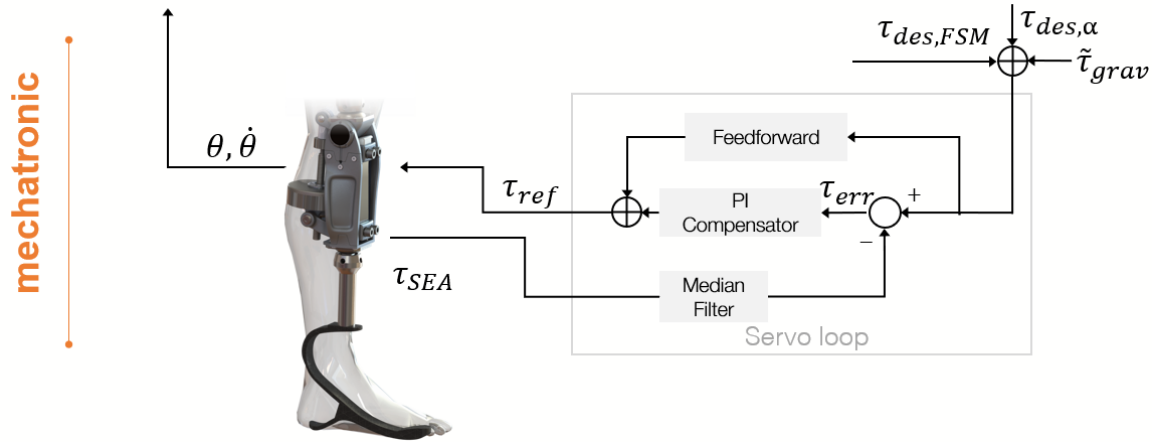


Figure 4-7: Closed loop torque controller for mechatronic knee

4.2.5 Experimental Tasks

Experimental tasks were performed to characterize the influence of the individual and combined augmentative features listed in Table 4.1.

4.2.5.0.1 Rhythmic Bandwidth In the rhythmic bandwidth task, subjects were instructed to flex and extend their phantom knee joint at full perceived range of motion while EMG data were recorded. US data were simultaneously recorded from the extensor muscle to confirm cyclic movements of the appropriate musculature. A click track with tempo accelerating from 90 to 200 beats per minute (BPM) over the course of 1 minute was provided as an audio cue indicating when to move the phantom joint in the opposing direction. Subjects performed cyclic movements until failing to maintain pace with the click track for at least 10 s, at which point the task was stopped. Subjects also cycled the unaffected, contralateral knee in tempo with the click track until failure. Knee angle was measured using a digital goniometer (Biometrics Ltd.).

EMG data were processed into muscle activations and used to generate torque about a virtual knee joint and shank modeled as a point mass rotating around a center with fixed radius. The same myoneural impedance modulation components used to calculate torque applied to the mechatronic knee were used to calculate the torque applied to the virtual knee joint. Subsequent time domain knee kinematics

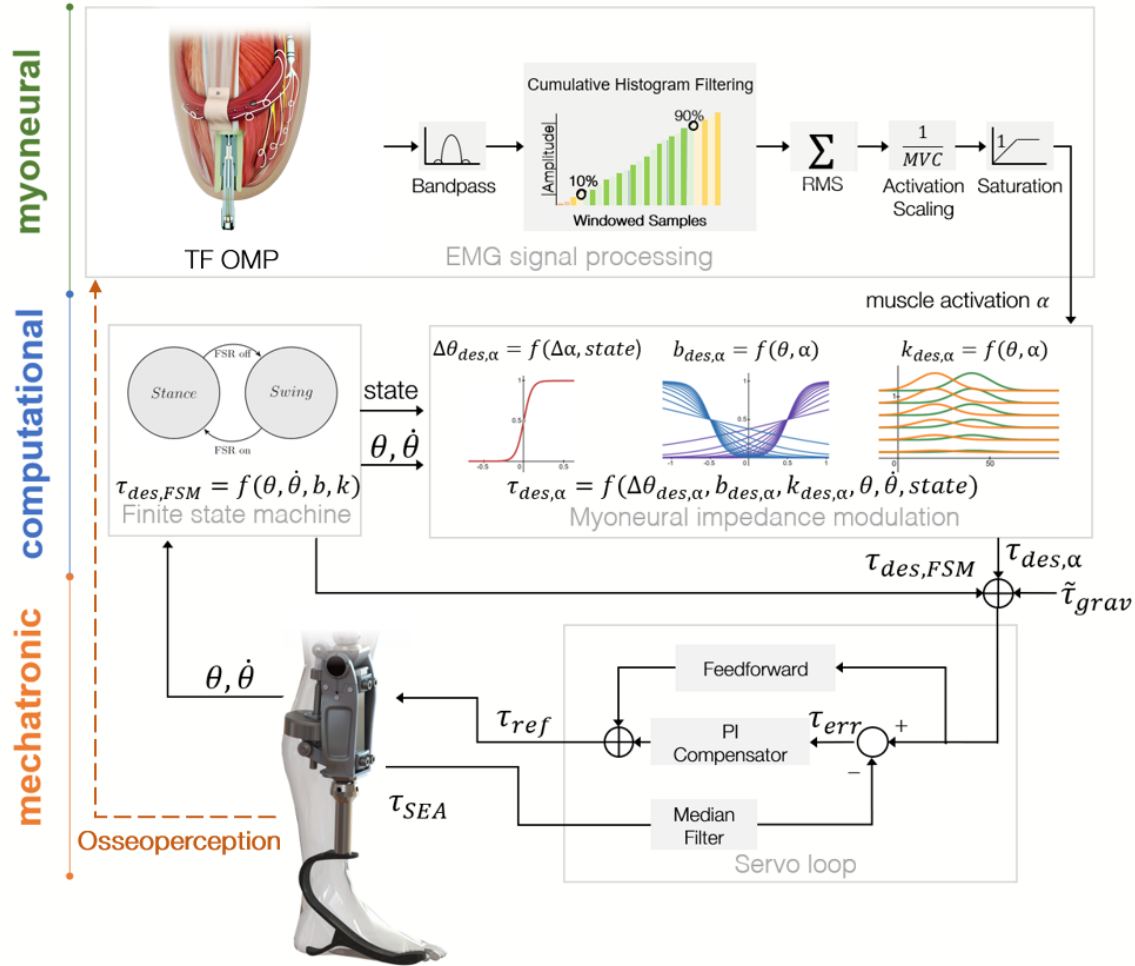


Figure 4-8: Complete control system for OMP subjects

for both virtual and contralateral knees were analyzed in the frequency domain to extract the maximum stable frequency of movement before the trajectory became acyclic due to the subject's inability to match the increased movement speed.

4.2.5.0.2 Freespace Reaching A freespace control task was performed to characterize subjects' abilities to position the knee joint with only visual and proprioceptive feedback. Subjects were seated on an elevated stool with residuum exposed. The neurorobotic knee was mounted on an isolated stand in front of the subject's residuum to approximately occupy the volume of the physiological knee. There was no direct mechanical attachment between residuum and neurorobotic knee in order to prevent the user from using afferent mechanical feedback to assist with the task. Three target

knee positions (low, medium, high extension) were indicated by alignment of three reflective markers placed on the medial aspect of the prosthesis' shoe with a separate reflective marker placed on a stand on the ground in front of the shank's swing radius. Subjects used their fixed visual perspective from their seated position to align the shoe markers with the stand's marker. The quantifiable knee joint target angles on the prosthesis were recorded by the experimenter by backdriving the joint to the target positions confirmed by subjects' verbal feedback.

For each individual reaching trial, a click track at 80 BPM played through noise-cancelling headphones provided verbal instructions to rest for three beats, reach with the neurorobotic knee for three beats, and rest for three beats for a total of eight repetitions. Subjects were instructed on the specific knee extension target at the beginning of each trial. Two trials were performed for each knee extension target. At the beginning of the task, activation scalings for both the extensor and flexor muscles were initially calibrated by MVC and then refined by allowing the subject to practice reaching for the medium knee extension target only. Subjects indicated whether they wanted more or less sensitivity to achieve the movement, corresponding to reducing and increasing the scaling denominator, respectively. After a five minute tuning and training session, subjects began the task.

Separately and subsequently, a blindfolded reaching task was performed to characterize subjects' abilities to generate useful efferent information for neurorobotic knee control with proprioceptive feedback only. In this variant, subjects were blindfolded with the neurorobotic knee's motor disabled. Subjects repeated the reaching task by moving their phantom knee to proprioceptively-ascertained target positions while muscle activations was recorded. As with the condition with visual feedback, a click track was played through noise-cancelling headphones to provide a consistent tempo and instruction.

Performance during the freespace reaching task with visual feedback was determined by the average absolute angular divergence from the target knee extension angle during steady-state (the middle second of the reaching movement instruction). This error signal was averaged per target, per subject. The non-parametric Kruskal-

Wallis test was used to determine any significant differences between performances of populations reaching for each of the three targets. For any significant differences between populations per target, a post-hoc multiple comparison with Tukey-Kramer correction was performed to determine pairwise significant differences. Performance during the freespace reaching task without visual feedback was determined by calculating the Jensen-Shannon Divergence between each subject's extensor activation distributions between all low and medium extensions and then again between all medium and high knee extensions. The Jensen-Shannon Divergence (JSD) provides a scalar value corresponding to the amount of usable information between two given distributions [88]. Statistically significant information differences at the population level between low and medium and also between medium and high knee extension targets was determined using the non-parametric Kruskal-Wallis test. For any significant differences between populations, a post-hoc multiple comparison with Tukey-Kramer correction was performed to determine pairwise significant differences of JSD.

4.2.5.0.3 Static Obstacle Drills Static obstacle drills were performed to characterize subjects' abilities to achieve hybrid freespace positioning movements with discrete ground contact events using the donned neurorobotic knee with efferent myoneural control. Two types of drills were performed with two types of obstacles in a 2x2 factorial design. The first type of drill, so called the over-back drill, required that the subject start from a standing position behind a fixed obstacle and overcome the obstacle with the neurorobotic knee without non-physiological hip abduction. After touching the ground on the other side of the obstacle with the prosthetic foot, the subject was required to return the foot over the obstacle to the original starting position without non-physiological hip abduction. Half a point was awarded for each movement over or back from the obstacle without block contact and without non-physiological hip abduction. The second type of drill, so called the top-tap drill, required that the subject stand behind the fixed obstacle, touch the top of the obstacle with any part of the prosthetic foot, and then touch the ground on the opposite side of the obstacle with any part of the prosthetic foot. The backward movement

involved performing this sequence in reverse. Any contact with the obstacle other than on the top resulted in failure of the movement. Half a point was awarded for each movement over or back from the obstacle with successful top tap. A medium obstacle corresponding to a cinder block with 10 cm height and a large obstacle corresponding to two stacked cinder blocks with a combined height of 20 cm were used in all drills.

For each of the four combination of trial conditions, subjects were provided 30 s to accomplish as many successful obstacle drills as possible. To tune the flexor and extensor activation scaling denominators, confirm understanding of the drills, and allow for practice of the required movements, a three minute training session was provided before the first trial run wherein the subject provided feedback on more or less sensitivity per channel while performing any desired movements with the neurorobotic knee. Trials were administered in order of over-back with medium obstacle, top-tap with medium obstacle, over-back with large obstacle, and top-tap with large obstacle.

Significance testing for differences in performance between populations was performed by aggregating scores from all four trials into an averaged success percentage per subject and proceeding with the non-parametric Kruskal-Wallis test. For any significant differences between populations, a post-hoc multiple comparison with Tukey-Kramer correction was performed to determine pairwise significant differences.

4.2.5.0.4 Sit to Stand A seated sit to stand task was performed to determine each subject's ability to produce useful positive power with constant ground contact. A series of three trials consisting of five sit to stand movements each was recorded per subject. To tune the flexor and extensor activation scaling denominators, confirm understanding of the task, and allow for practice of the required movements, a three minute training session was provided before the first trial run wherein the subject provided feedback on more or less sensitivity while performing sit to stand movements with the neurorobotic knee. The expert experimenter adjusted the muscle activation scaling denominators to each subject's satisfaction.

Performance was scored for each movement using the sitting to standing segment of the Berg Balance Scale [89]. Average performance per trial was calculated by taking the mean of the Berg scores from all five movements. Significance testing for differences in performance between populations was performed by comparing the ultimate score of each population in the third trial and proceeding with the non-parametric Kruskal-Wallis test. For any significant differences between populations, a post-hoc multiple comparison with Tukey-Kramer correction was performed to determine pairwise significant differences.

Additionally, for OMP subjects, ground reaction forces under each foot were recorded using a split belt treadmill (Bertec Corporation).

4.2.5.0.5 Level Ground Walking and Obstacle Avoidance Subjects were instructed perform level-ground walking on a split belt treadmill set to fixed speeds using the neurorobotic knee without efferent myoneural control. These test conditions were designed to acclimate subjects to walking on a powered prosthetic knee. Subjects rated at a K3 activity level by their certified prosthetists were asked to walk at 0.5 and 0.8 m/s, representing their greatest common speed without excessive difficulty. Subjects rated at a K4 activity level by their certified prosthetists were additionally asked to walk at 1.1 m/s, representing their greatest common speed without excessive difficulty. Subjects walked at each speed for at least one minute while the experimenter adjusted the swing phase impulsive flexion torque assistance scalar to compensate for the prosthetic knee’s reflected inertia and produce biomimetic swing kinematics across all tested speeds. After adjustment, subjects walked for at least one minute at each speed while ground reaction forces and on-board prosthesis data was recorded. For all testing on the treadmill, subjects were actively belayed from a chest harness for safety. Gait symmetry was determined by a symmetry index defined as:

$$\text{Symmetry index} = \frac{\text{supportTime}_{\text{unaffected},\text{single}} - \text{supportTime}_{\text{affected},\text{single}}}{2 \cdot \text{supportTime}_{\text{unaffected},\text{single}} + \text{supportTime}_{\text{affected},\text{single}}} \quad (4.3)$$

A symmetry index of 0 indicates perfect single support symmetry.

For the obstacle avoidance task, subjects performed three trials at each of their level ground walking speeds while avoiding foam blocks placed as they were in the practice run. This task was designed to evaluate each subject's ability to efferently control the knee during a cognitively and physically demanding situation, representing the holistic capabilities of an individual with specific augmentative interventions. Subjects were provided efferent myoneural control of the neurorobotic knee. Muscle activation scalings were adjusted to each subject's preference over the course of a three minute practice session to achieve controlled flexion and extension of the knee. Once adjusted, subjects were provided a practice run involving walking on the treadmill at 0.5 m/s for 10 s before 10 foam blocks of 10 cm height were fed onto the affected leg's treadmill belt every 5 s.

Obstacle avoidance performance was assessed based upon the best of three trial runs at each speed. This approach heuristically compensates for the opposing influences of fatigue and training effects that increase over time that may affect individuals at different rates. It also incentivizes experimentation with different strategies by establishing a minimum score after each trial. Performance was scored per block with the overall trial score being the mean of all per block scores according to Table 4.3.

This point structure incentivizes safer maneuvers to get over the block, such as those a subject may choose to perform using a prescribed passive prosthesis, instead of more agile movements in the case they are not confident in their ability to control the knee. In this way, the point structure assesses both physical capabilities and familiarity with the controller. Additionally, the rubric suggests performance with a prescribed, variable damping knee prosthesis may score up to 0.5 points per block, and scores above 0.5 points are only possible with active joint control, either direct or indirect [90].

Significance testing for differences in obstacle performance between populations was performed by comparing the best trial score of K3 and K4 subjects separately and at their max speeds with the non-parametric Kruskal-Wallis test. For any significant differences between populations, a post-hoc multiple comparison with Tukey-Kramer

correction was performed to determine pairwise significant differences.

4.2.5.0.6 Stair Ascent and Descent To determine performance of the efferent myoneural controller in stair ascent and descent, subjects were instructed to ascend and descend a staircase consisting of four steps with a height between steps of 20 cm. Each trial consisted of three ascent/descent cycles and three trials were performed by each subject at a self-selected speed. Muscle activation scalings were adjusted by the examiner as each subject repeatedly attempted to take the first step leading with the neurorobotic knee. This adjustment was performed over three minutes to familiarize subjects with the task.

4.2.5.0.7 Embodiment Questionnaire A prosthetic embodiment questionnaire was administered to each subject before any exposure to the neurorobotic knee to determine a baseline embodiment level for their prescribed knee prosthesis. After four of the experimental tasks above (freespace reaching, obstacle drills, obstacle avoidance, stair ascent and descent), subjects were asked to repeat the questionnaire with respect to their perceived embodiment of the efferently controlled neurorobotic knee. Subjects were not administered the questionnaire after the sit to stand task due to redundant coverage of positive power production during stance of the stairs task. Differences from their baseline prosthesis were recorded and used in subsequent analyses. The questionnaire consisted of 10 questions adapted from the work of Bekrater-Bodmann [91]. Questions were divided to assess each subcategory of embodiment (ownership, body representation, agency) as defined by Segil et al. [1], and as seen in Table 4.4.

4.3 Results

Figure 4-9 shows the frequency domain analysis stemming from the maximum speed phantom knee flexion and extension cycling task. The results demonstrate that subjects with AMI muscular constructs can stably cycle a virtual prosthetic knee joint faster than their contralateral, unaffected knee. In contrast, those with conventional amputation musculature demonstrate no such ability.

Freespace reaching was evaluated in two ways: ability to accurately position the efferently controlled prosthetic knee with visual feedback, and ability to generate distinct EMG information that can be used for subsequent efferent control of a prosthetic knee in a hardware-agnostic manner. The results of these two task conditions are shown in Fig. 4-10. Only OMP subjects demonstrate significantly greater targeting accuracy with visual feedback at a cohort level. These improvements manifested at low and medium knee extension targets when compared to CTL subject performance. In terms of generating distinct information that could be applied toward controlling the position of a prosthetic knee at steady state, OMP subjects again demonstrate significantly greater EMG information between low and medium knee extension compared to the CTL cohort.

OMP subjects were studied for their ability to ambulate on level ground pre- and post-operatively. The top right subfigure of Fig. 4-11 demonstrates typical gait dynamics for OMP1 walking with the powered knee prosthesis controlled only by the FSM without myoneural information. The bottom right subfigure shows that OMP1 improved in terms of gait symmetry with their prescribed device post-operatively, additionally gaining an additional 0.2 m/s to maximum walking speed without handrails. However, OMP2 demonstrated increased asymmetry when walking with their prescribed device post-operatively. OMP2 gained an additional 0.1 m/s to maximum walking speed without handrails, though this was obtained only through use of the powered knee prosthesis with FSM control only.

Results from the static obstacle drill task are shown in Fig. 4-12. OMP subjects demonstrate significantly improved average accuracy across all four drills compared to CTL subjects. Representative knee kinematics and muscle activation trajectories demonstrate a lack of impact artifacts that would negatively affect performance.

OMP subjects perform significantly better than K3 CTL subjects at the maximum tested speed of 0.8 m/s during the obstacle avoidance task. This task tests each subject's physical abilities along with their ability to efferently control the neurorobotic knee simultaneously.

In the sit to stand task, both OMP subjects achieve maximum Berg scores by the

time of the third trial while AMI and CTL cohorts do not. Improvement of OMP and AMI Berg scores over CTL subjects' approach significance. OMP subjects also demonstrate qualitatively improved vertical GRF symmetry when using the efferently controlled neurorobotic knee, as seen in Fig. 4-14iii.

OMP subjects demonstrate limited power production when ascending stairs and damping when descending stairs relative to physiological reference values [92]. Still, OMP subjects gain the ability to ascend step-over-step with efferent control whereas use of passive knee prostheses limits them to step-by-step ascension.

OMP subjects demonstrate significantly improved embodiment scores when using the efferently controlled knee relative to other cohorts under some conditions and within some subcategories, as seen in Fig. 4-16.

Relevant characteristics of all study subjects.

| Subject ID | Amputation type (activity level) | Age (years) | Time since amputation (years) | Biological sex | Height (m) | Weight (kg) | Cause of amputation |
|-------------|----------------------------------|-------------|-------------------------------|----------------|------------|-------------|---------------------------|
| OMP 1 | e-OPRA, AMI (K3) | 64 | 13.7 | Female | 1.63 | 96.6 | Cancer |
| OMP 2 | e-OPRA, AMI (K3) | 61 | 23.0 | Male | 1.78 | 93.4 | Cancer |
| AMI 1 | AMI (K4) | 53 | 2.0 | Male | 1.83 | 72.6 | Trauma |
| AMI 2 | AMI (K4) | 35 | 2.1 | Male | 1.77 | 74.8 | Trauma |
| AMI 3 | AMI (K3) | 55 | 0.5 | Male | 1.83 | 86.2 | Trauma |
| AMI 4 | AMI (K4) | 46 | 3.5 | Male | 1.80 | 77.1 | Distal vascular pathology |
| AMI 5 | AMI (K4) | 59 | 3.8 | Male | 1.78 | 74.8 | Cancer |
| AMI 6 | AMI (K3) | 47 | 0.5 | Male | 1.81 | 97.5 | Trauma |
| CTL 1 | TMR (K4) | 23 | 9.3 | Male | 1.75 | 81.6 | Distal vascular pathology |
| CTL 2 | TMR (K4) | 40 | 6.0 | Male | 1.65 | 70.3 | Trauma |
| CTL 3 | TMR (K3) | 36 | 30.0 | Female | 1.52 | 52.6 | Trauma |
| CTL 4 | TMR (K3) | 59 | 2.0 | Female | 1.58 | 54.4 | Infection |
| CTL 5 | TMR (K4) | 44 | 2.0 | Male | 1.85 | 90.7 | Trauma |
| CTL 6 | TMR (K3) | 56 | 1.5 | Male | 1.65 | 68.9 | Distal vascular pathology |
| CTL 7 | TMR (K4) | 52 | 5.3 | Female | 1.70 | 62.1 | Trauma |
| Mean | | 48.6 | 3.0 | | 1.73 | 76.9 | |
| ±SEM | | ±11.5 | ±8.8 | | ±0.1 | ±14.2 | |

Table 4.2: Subject table

Table 4.3: Obstacle avoidance scoring rubric

| | |
|-------------|--|
| 1 point | obstacle avoidance using efferently controlled knee flexion and extension without unphysiological hip abduction, without handrails |
| 0.75 points | obstacle avoidance using efferently controlled knee flexion and extension without unphysiological hip abduction, with handrails for balance assistance |
| 0.5 points | vaulting over the obstacle without efferently controlled knee flexion and extension, without handrails |
| 0.25 points | obstacle avoidance requiring hip circumduction, without handrails |
| 0 points | contact with the obstacle, vaulting over obstacle with handrails, hip circumduction with handrails |

Test subjects instructed to look at their prosthesis for 60s then answer on a 1-7 point Likert scale:

- I feel as if I were looking at my own leg, rather than at a prosthesis
- The prosthesis belongs to me
- It feels as if I had two legs
- The prosthesis is my leg
- The prosthesis is part of my body
- The posture of the prosthesis corresponds to that of a real leg
- My body feels complete
- The prosthesis is in the location where I would expect my leg to be, if it was not amputated
- The prosthesis is moving in the way I want it to move
- I am in control of the prosthesis

Table 4.4: Embodiment questionnaire provided to assess each subject's embodiment with their prescribed prosthesis. This questionnaire was administered again after freespace reaching, obstacle drills, obstacle avoidance, and stair ascent and descent to compare changes in embodiment when using an efferently controlled knee.

i. Cycling a virtual prosthetic knee at maximum movement frequency

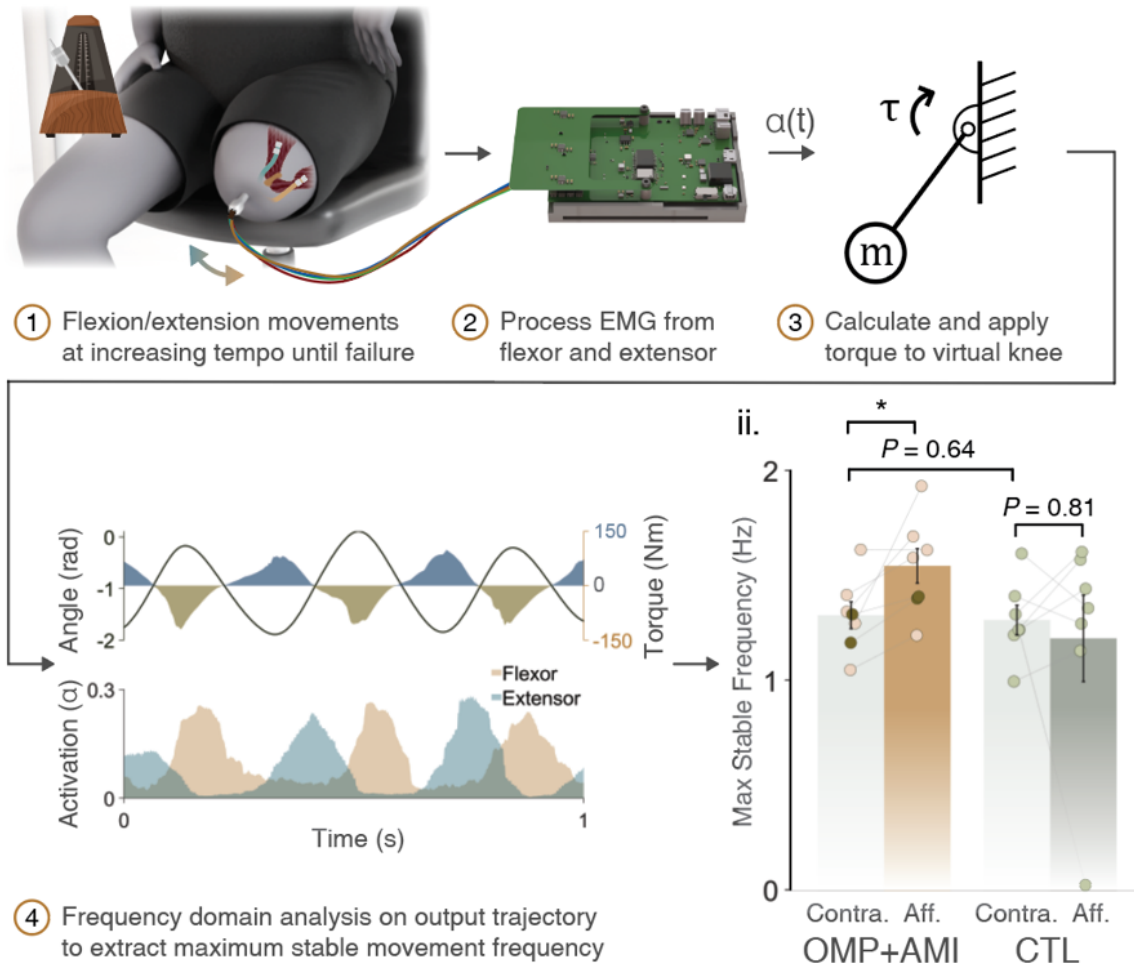


Figure 4-9: Maximum phantom knee cycling bandwidth. Panel (i) shows the processing steps to convert EMG collected during full range of motion movements to kinematic trajectories. Panel (ii) shows that the AMI surgery improves volitional knee movement bandwidth by 15% to supraphysiological levels (Wilcoxon signed rank, $n = 7$, $*P < 0.05$. OMP subjects: brown circles, AMI subjects: pink circles, CTL subjects: gray circles). Meanwhile, conventional amputation demonstrates no significant difference in bandwidth (Wilcoxon signed rank, $n = 7$). Both comparison groups demonstrated similar baseline contralateral bandwidth as measured with a goniometer (Wilcoxon ranked sum, $n = 8$ and 7 for OMP+AMI and CTL, respectively). All bars mean and SEM.

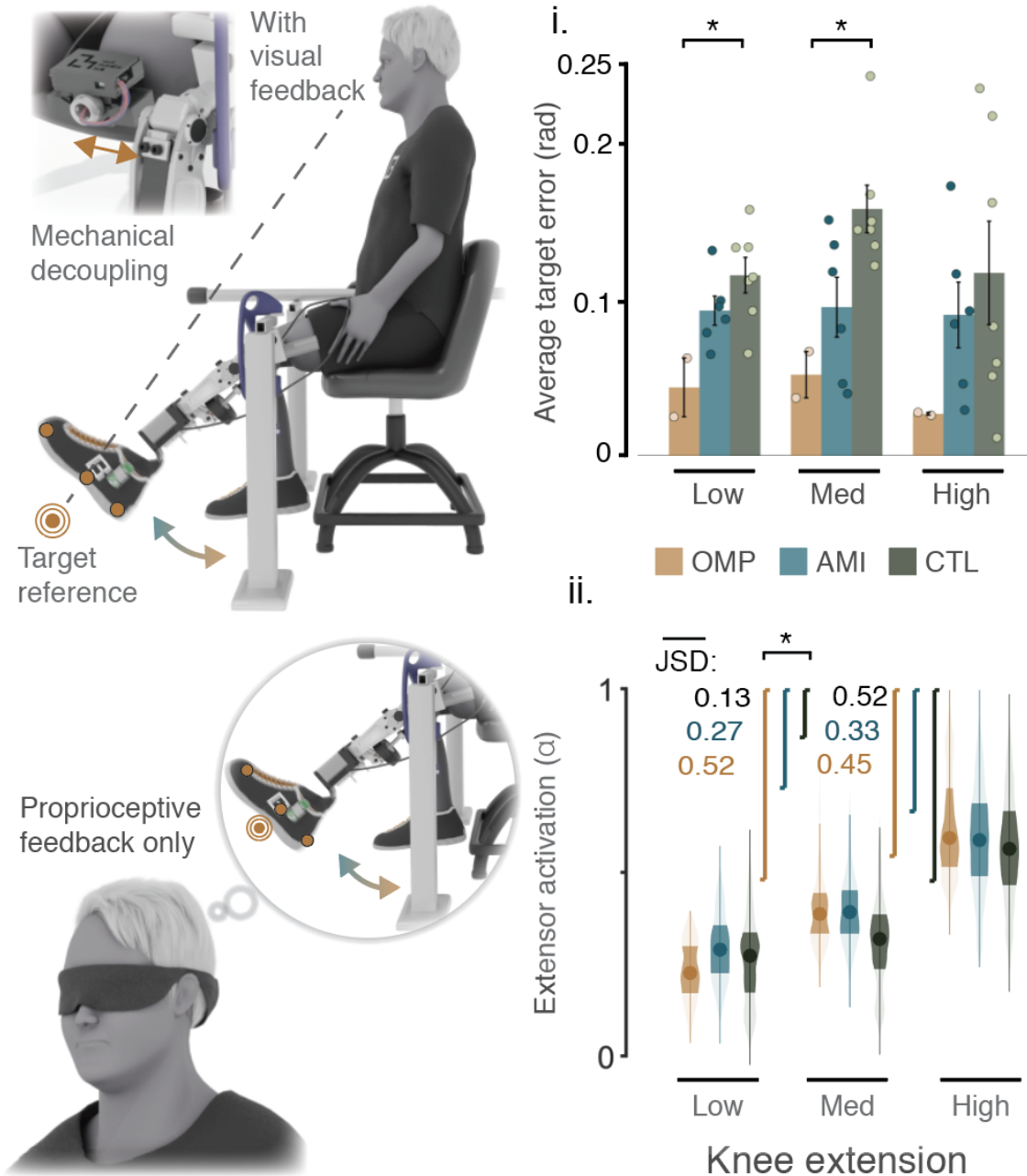


Figure 4-10: Evaluation of volitional free space targeting ability. Panel (i) shows angular targeting error for three levels of prosthetic knee extension with visual feedback allowed. OMP subjects demonstrated significantly less absolute steady-state error compared to CTL subjects at low and medium extension levels (38% and 33% as much error as CTL at low and medium extension, respectively. Kruskal-Wallis with post-hoc multiple comparisons and Tukey-Kramer correction. $n = 16$ movements per target level, per subject. $*P < 0.025$). Panel (ii) shows activation of extensor muscles for three levels of steady-state prosthetic knee extension without visual feedback. OMP subjects generated significantly more information to distinguish between adjacent low and medium extension levels compared to CTL subjects as measured by Jensen-Shannon divergence (JSD) (Kruskal-Wallis with post-hoc multiple comparisons and Tukey-Kramer correction. $n = 16$ movements per target level, per subject. $*P < 0.025$).

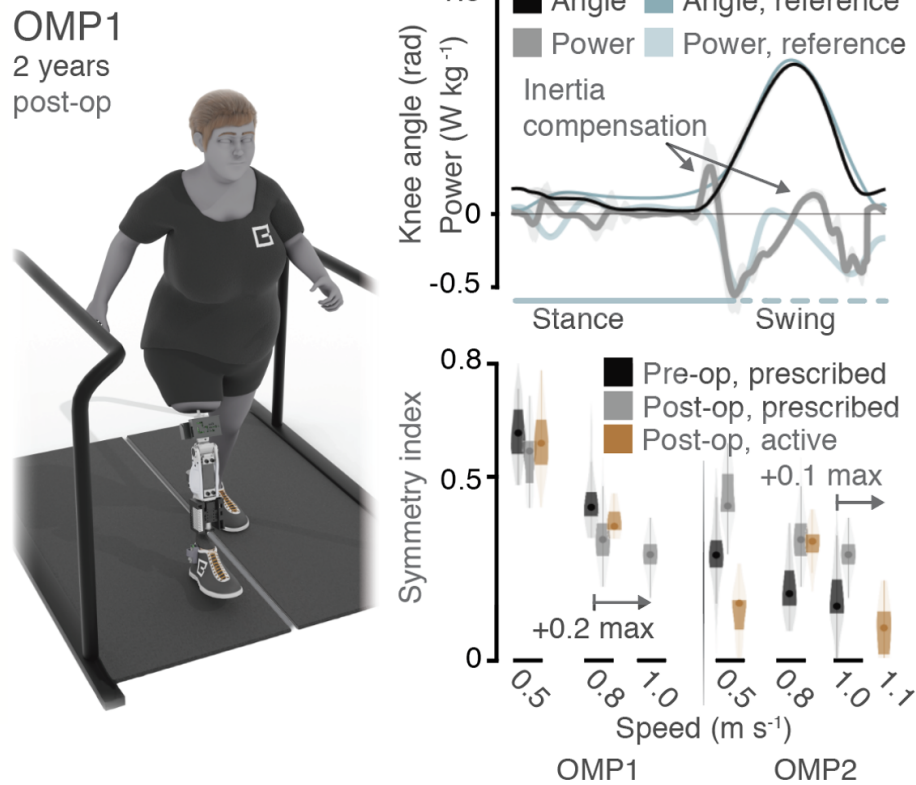


Figure 4-11: OMP level ground walking symmetry. Left panel demonstrates OMP1 completing the level ground walking task. Top right panel shows representative knee dynamics for OMP1. Bottom right panel shows symmetry index determined at different walking speeds for both subjects. A symmetry index closer to 0 indicates more symmetric single support stance time between affected and unaffected sides. Both subjects were able to walk at a faster maximum speed post-operatively, with OMP1 walking faster on their prescribed variable damping knee and OMP2 walking faster with the active powered knee without efferent control.

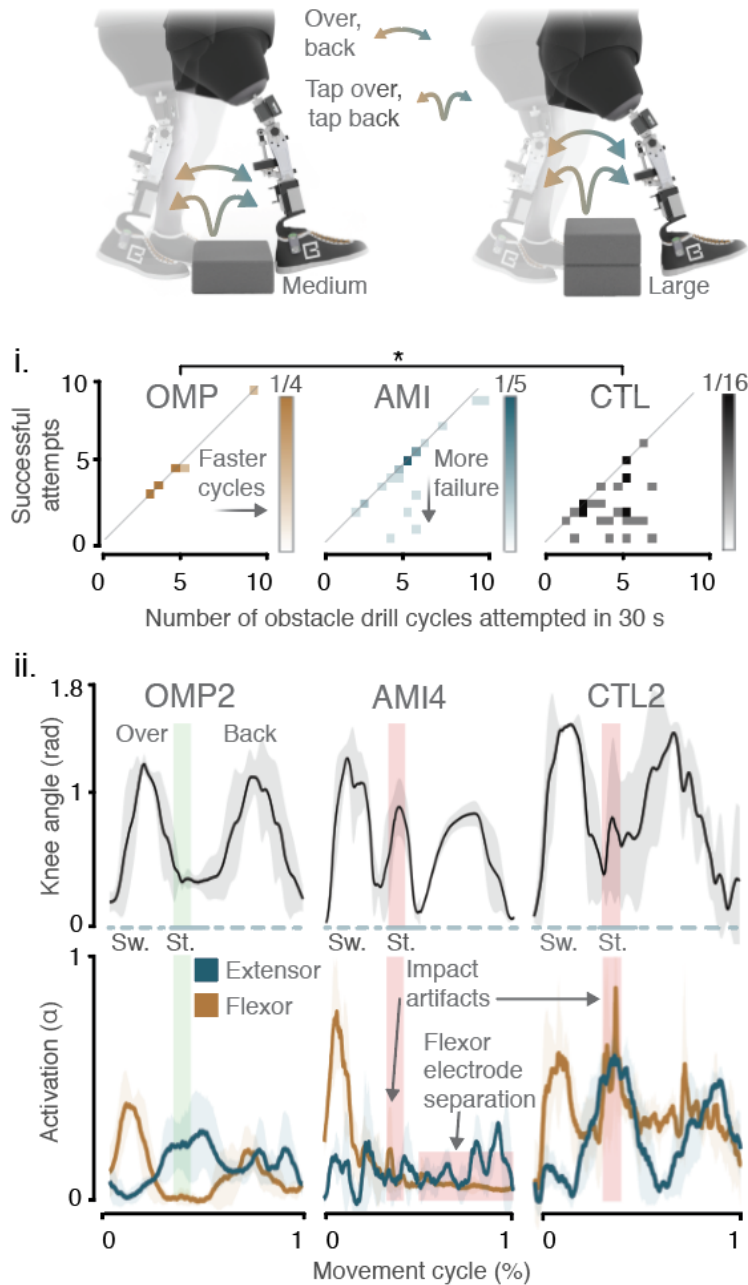


Figure 4-12: Obstacle drill performance. Panel (i) shows that OMP subjects demonstrate significantly better performance than CTL subjects when completing throughout all combinations of obstacle size and drill type. (Average population accuracy of 98.75%, 85.04%, and 60.13%, for OMP, AMI, and CTL, respectively. Average accuracy per subject calculated over all four obstacle drill conditions. Kruskal-Wallis with post-hoc multiple comparisons and Tukey-Kramer correction. * $P < 0.025$). Panel (ii) shows representative knee angle kinematics and muscle activation patterns during the large obstacle over-back drill for one subject from each cohort ($n = 5$ movements each. Shaded area, SD). Vertical green rectangle indicates heel strike window without EMG impact artifacts. Vertical red rectangles indicate heel strike windows with EMG impact artifacts. Horizontal red rectangle indicates spatial separation of the thin electrode on the flexor muscle within a socket and liner that produces an inability to efferently control the neurobotic knee in flexion.

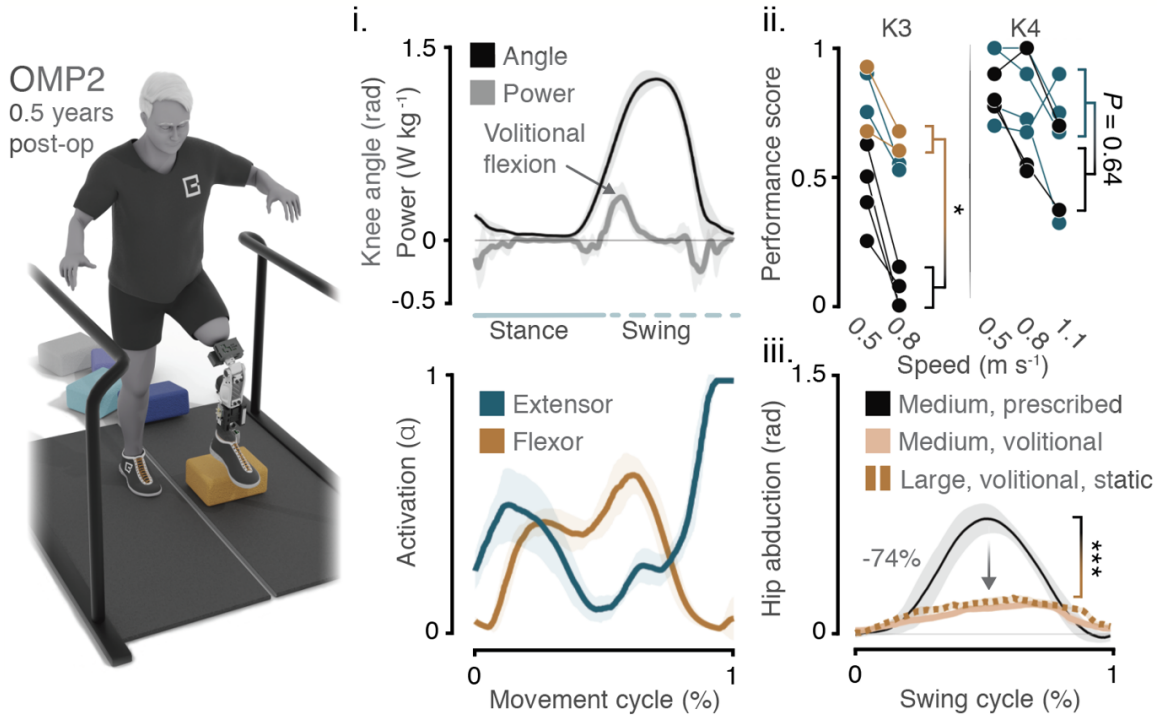


Figure 4-13: Obstacle avoidance task. Panel (i) shows average powered knee dynamics and causal EMG for OMP2 when successfully avoiding obstacles ($n = 8$ movements, shaded regions, SD). Panel (ii) plots best of three scores obtained for the obstacle avoidance trial per treadmill speed per subject. Subjects rated K3 activity level are shown separately from subjects rated K4. K4 subjects performed an additional set of trials at $1.1 \frac{m}{s}$. OMP subjects performed significantly better than K3 CTL subjects at $0.8 \frac{m}{s}$ (0.64 vs. 0.06 mean score, Kruskal-Wallis with post-hoc multiple comparison and Tukey-Kramer correction, $*P < 0.025$). No significant difference in performance was observed for K4 subjects at their fastest tested speed of $1.1 \frac{m}{s}$ (Kruskal-Wallis with post-hoc multiple comparison and Tukey-Kramer correction, $P = 0.64$). Panel (iii) shows that OMP subjects use significantly less peak hip abduction to overcome medium obstacles on the treadmill when utilizing efferent control of a powered knee compared to their prescribed devices (74% reduction), and this advantage remains when utilizing volitional control of a powered knee to overcome larger obstacles in a static setting (73% reduction, Friedman test with post-hoc Wilcoxon signed rank test and Tukey-Kramer correction, $n = 10$ movements each condition, $***P < 0.001$).

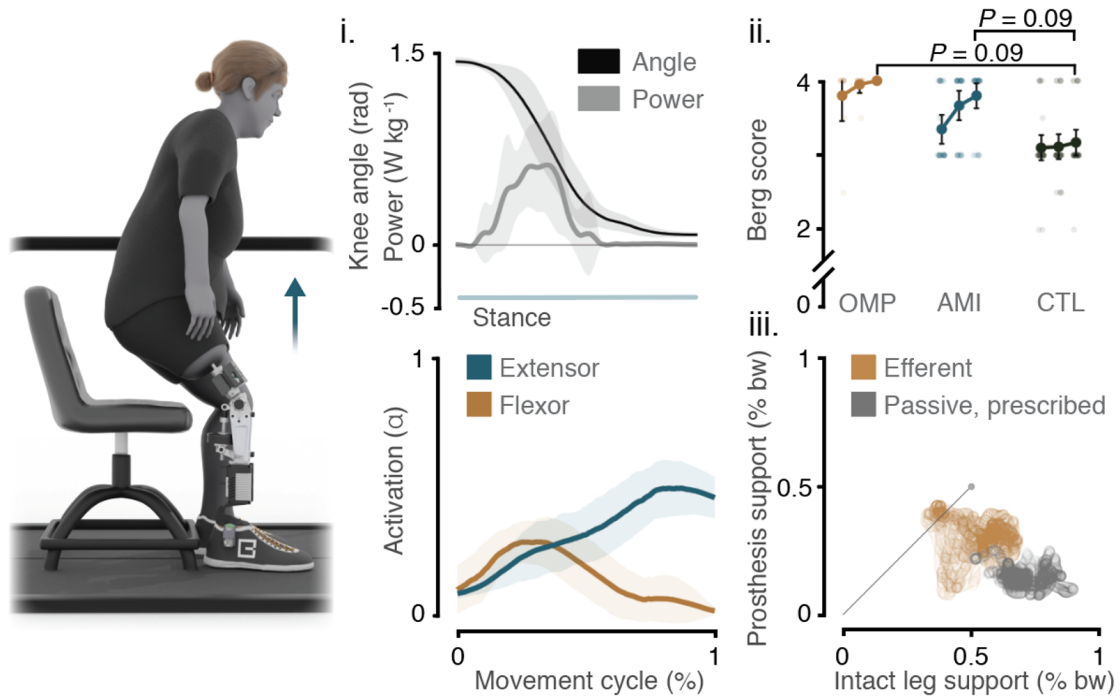


Figure 4-14: Sit to stand task performance. Panel (i) shows representative mean EMG and resultant powered knee dynamics for OMP1 ($n = 15$ movements, shaded regions, SD). Panel (ii) shows sit to stand Berg scores over three successive trials using myoneural control. OMP and AMI subjects demonstrate improvements in ultimate performance over the CTL group that approach significance. (Kruskal-Wallis test with post-hoc multiple comparison and Tukey-Kramer correction. Score per subject averaged from $n = 5$ movements each). Panel (iii) shows the time traces of vertical ground reaction forces between legs for OMP subjects during sit to stand movements ($n = 10$ movements per subject). OMP subjects qualitatively demonstrate improved symmetry when using the powered knee under myoneural control compared to their prescribed passive devices.

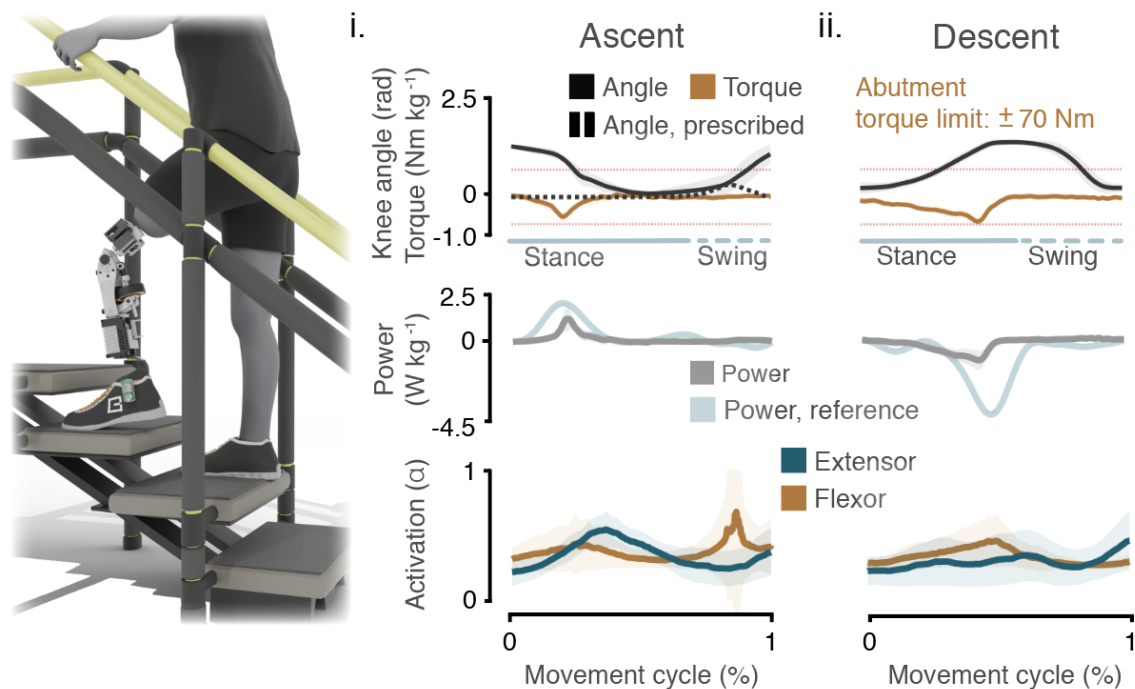


Figure 4-15: Stair ascent and descent. Panel (i) shows stair ascent dynamics and muscle activations for both subjects ($n = 8$ gait cycles each. Shaded regions, SEM). Panel (ii) shows stair descent dynamics and muscle activations for both subjects ($n = 8$ gait cycles each. Shaded regions, SEM). Importantly, the mechanical limits of the eOPRA abutment restrict peak permissible torque to 70 Nm at the knee joint.

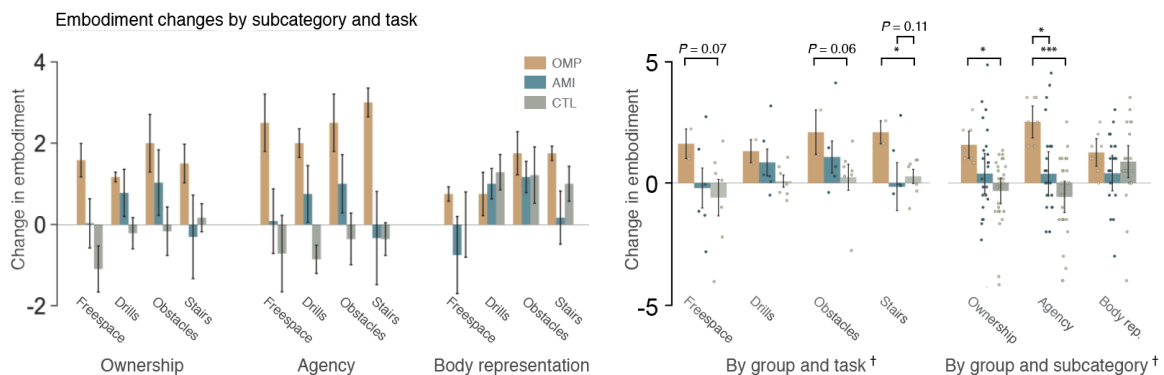


Figure 4-16: Prosthetic embodiment results. Left subfigure shows overall changes in embodiment compared to prescribed device responses by subcategory of embodiment and by task. Right subfigure shows changes in embodiment over prescribed device grouped by significant terms as determined by a sparse multiple linear regression model. Significance testing within each triplet of cohort responses was performed (Kruskal-Wallis test with post-hoc multiple comparison and Tukey-Kramer correction. * $P < 0.025$, *** $P < 0.001$.)

4.4 Discussion

It must be understood if and in which ways an increasing level of surgical invasiveness may improve rehabilitative outcomes over established alternatives in the case of transfemoral amputation. The tasks and tests performed in this section were designed to assess individual and combined interventional aspects for their relative effects on factors which may be relevant to rehabilitation both in the present, and in a future where efferently controlled knee prostheses are commercially available.

Regarding the relative influence of agonist-antagonist musculature in the transfemoral case, it can be observed in Fig. 4-9ii that those with the AMI (whether OMP or AMI cohort proper), demonstrate significantly increased maximum cycling frequency of a virtual prosthetic knee joint using the same myoneural impedance controller implemented on the physical neurorobotic knee. No such improvements are observed in the CTL cohort who do not have intentional agonist-antagonist muscle configurations. This is notable in that there exists a special condition and task wherein amputated musculature offers improvements over intact physiology. The notion is heterodox from the perspective that amputation is understood by most as a disability with no perceived advantages over intact physiology.

Regarding the influence of agonist-antagonist musculature and EMG sensing component combinations to effect changes in prosthetic knee control, it can be seen that extracting EMG from intramuscular electrodes embedded in AMI musculature suggests advantages over extracting EMG from surface electrodes. As observed in Fig. 4-10i, OMP subjects demonstrate significant improvements in knee control with visual feedback at low and medium knee extension levels over CTL subjects. In contrast, AMI subjects who must use surface electrodes do not demonstrate significant improvements over CTL subjects. However, a direct comparison between OMP and AMI subjects does not yield significant differences in freespace reaching performance with visual feedback, in part attributable to the pilot nature of this study on the OMP. When relying on proprioceptive feedback only to generate EMG corresponding to knee movement, it is again observed that OMP subjects generate significantly more

information to discriminate between low and medium knee extension levels compared to CTL subjects. This distinction, seen in Fig. 4-10ii, implies that for a given downstream neurorobotic system, OMP subjects may have an innate advantage toward its control, especially at low levels of activation, due to a greater ability to generate graded control information. A qualitative analysis of average CTL subject JSD between targets suggests that CTL subjects may not be able to distinguish finer levels of knee position, instead producing a binary low or high level of extensor activation.

The sit to stand, static obstacle drill, and obstacle avoidance tasks represent an increasing level of interaction of each subject with the efferently controlled prosthesis. These tasks span from stance-only control, to hybrid free space and stance interactions, and finally to hybrid interactions with a strong emphasis on general physical ability in the obstacle avoidance task. In the sit to stand task, the OMP and AMI cohorts each demonstrate improvements over the CTL cohort that approach significance, as seen in Fig. 4-14ii. Not only do OMP subjects demonstrate a maximum Berg score by the third trial while starting from a higher baseline in the first trial, but CTL subjects demonstrate limited improvement from first to third trial. With all subjects having the same amount of exposure to the task, this difference in performance suggests that OMP subjects are better able to learn and utilize efferent myoneural control toward functional gains, despite their physical disadvantages indicated in Table 4.2.

In the static obstacle drill, OMP subjects demonstrate significantly greater average drill accuracy across all four variants compared to CTL subjects, as seen in Fig. 4-12i. The AMI cohort is overall less accurate than OMP subjects, though the reduced accuracy is not statistically significant. Causal factors for this difference in performance are suggested by the representative knee kinematics and muscle activation trajectories of Fig. 4-12ii. At the moment of ground contact on the other side of the large obstacle during the over-back drill, at least two AMI and CTL subjects demonstrate impact artifacts on the flexor channel that cause failure of the drill cycle. Meanwhile, OMP2's muscle activations and corresponding knee kinematics remain relatively less variable and qualitatively smoother. In this task, it is suggested

that the lack of altered electrode impedance from a socketless interface may provide practical advantages when efferent myoneural control is required during hybrid tasks.

The obstacle avoidance task places an increased demand on a subject's overall physical abilities in addition to their ability to efferently control the neurobotic knee. Importantly, OMP subject obstacle avoidance performance at 0.8 m/s as seen in Fig. 4-13ii is significantly better than K3 CTL performance at the same speed. K3 AMI subjects perform similarly to OMP subjects, but not significantly better than K3 subjects. In this controlled task, it may be that OMP subjects were able to compensate for their disadvantaged physical attributes through increased agility with myoneural control of the knee. By enabling the physiological ability to more easily overcome incoming obstacles without undue hip abduction, seen in Fig. 4-13iii, OMP subjects may be better equipped to maintain balance and stable gait compared to CTL subjects.

One major limitation of the OMP platform relates to the mechanical limits of the titanium abutment in the eOPRA implant system. A restriction of 70 Nm of torque at the knee in both flexion and extension is enforced to prevent damage to both the subject and implant system. This limit manifests most clearly during stair ascent and descent, as seen in Fig. 4-15, as power and damping are limited by peak torque production. OMP subjects do gain the ability to ascend stairs with a step-over-step gait, but require use of handrails to alleviate some of the load at the knee. It is important to note that these mechanical torque limits at the implant also apply to the standard transfemoral OPRA system. Any advantages of the OMP platform over the standard transfemoral OPRA system may be considered to be potential benefits for an individual that is already opting for osseointegration.

Finally, analysis of prosthetic embodiment of an efferently controlled knee relative to a prescribed baseline indicates that OMP subjects demonstrate significantly greater perceived agency compared to both AMI and CTL cohorts. This is indicated by the averaged differences in agency across all surveyed tasks as seen in the right sub-figure of Fig. 4-16. Perhaps unsurprisingly, no significant differences in altered body representation were observed between cohorts. Assuming the three subcategories of

embodiment are appropriately defined, and as the efferently controlled knee used for testing was the same across all subjects, changes to body representation changes should also be the same across cohorts. Further afferent information to the subject from the prosthesis may be required to gain corresponding increases to ownership and body representation.

Chapter 5

Conclusion

In this dissertation, an invasive osseointegrated mechanoneural knee prosthesis was characterized in a pilot study of two individuals with unilateral transfemoral amputation. Evidence is provided that the revisional transfemoral AMI likely retains the ability to restore neuromechanics in a manner similar to the acute AMI implementation. Further, it is suggested that neurophysiology of the motor cortex and supplementary motor area recovers as a result of peripheral intervention to provide the revisional transfemoral AMI. When the revisional transfemoral AMI is implemented alongside osseointegrated femoral implants and intramuscular electrodes, all interventions demonstrate successful function without obvious interference between components. Finally, in a comparison of functional task performance and subjective embodiment of OMP subjects, AMI subjects, and CTL subjects, OMP subjects are demonstrated capable of significant improvements in terms of efferent myoneural control and prosthetic agency over CTL subjects while these same improvements are not seen in those with AMI only. Such testing also establishes the existence of a hybrid intrinsic and efferent myoneural control architecture that produces unprecedented agility at the knee joint.

The results suggest that an increase in invasiveness at the transfemoral level can yield improvements in tasks and factors that have close association with rehabilitation following transfemoral amputation. Further study is warranted with a larger population of OMP subjects to more strongly assess these advantages at a population

level.

Appendices

Appendix A

Knee Torque Control

Implementation

```
1 void ControlLogic::calcKneeControl(float commandTorqueKnee, float agAct, float antAct
  , float maxK, float maxB) {
2
3 //agonist = BF, antagonist = RF
4
5 enum {
6     STANCE,
7     SWING
8 };
9
10 static float ascendDescendTransitionAngle = m_helper->c_pushOffAngle();
11 static int16_t preswingTimeout = m_helper->c_stanceTorqueThresh_counter();
12 static float swingAngleThresh = m_helper->c_swingAngleThresh();
13 static float swingTorqueThresh = m_helper->c_stanceTorqueThresh();
14 static float swingAngleSafetyThresh = m_helper->c_swingAngleSafetyThresh();
15 static float swingStanceThresh = m_helper->c_swingStanceThresh();
16
17 static float plantarTorqueThresh = m_helper->c_plantarTorqueThresh();
18 static float swingVelSafetyThresh = m_helper->c_swingVelSafetyThresh();
19 //k, b, theta
20 static float stanceOneParams [3] = {m_helper->c_stanceOneParams_K(),
21                                     m_helper->c_stanceOneParams_B(),
22                                     m_helper->c_stanceOneParams_TH()};
23 static float stanceTwoParams [3] = {m_helper->c_stanceTwoParams_K(),
24                                     m_helper->c_stanceTwoParams_B(),
25                                     m_helper->c_stanceTwoParams_TH()};
26 static float swingParams [3] = {m_helper->c_swingParams_K(),
```

```

27         m_helper->c_swingParams_B(),
28         m_helper->c_swingParams_TH()};
29     static float standParams[3] = {m_helper->c_standParams_K(),
30         m_helper->c_standParams_B(),
31         m_helper->c_standParams_TH()};
32     static float transitionTime = m_helper->c_transitionTime();
33
34     float agTorque = 0;
35     float antTorque = 0;
36     float muscleTorque = 0;
37     float impTorque = 0;
38     float restoreTorque = 0;
39     float commandTorque = 0;
40     float gravityTorque = 0;
41     float climbStiff = 0; //stiffness gain for cocontraction
42     static int state = STANCE;
43     static int prev_state = STANCE;
44     static bool flex_now = false;
45     float gravComponent = m_helper->getFilteredGravityComponent();
46     static size_t cnt = 0;
47     static size_t cnt_state = 0;
48
49     /* CALCULATE CONTRIBUTION FROM NEURAL CONTROL */
50     static float lockThetaDeg = 0;
51     static float lockDeltaAct = 0.0;
52     static bool lockOn = 0;
53     const float lowAngleLimit0g = 5;
54     static float lowAngleLimit = lowAngleLimit0g; //-5
55     static float highAngleLimit = 90;
56     static float angleRange = highAngleLimit-lowAngleLimit;
57     const float agActMax = 1.0;
58     const float antActMax = 1.0;
59     const float actLockThresh = 0.04;
60     const float cutoffPercent = 0.02; //sets the limit of the entry point for the
        inverse logistic function (to prevent super saturation)
61     const float logisticExp = -10; //logistic function exponent that sets deltaAct
        magnitude between lowAngleLimit + angleRange*f(deltaAct)
62     const float stanceFlexLimit = 20;
63     static bool m_isLimitExtension = false;
64     static bool armLimitExtension = false;
65     const float extendLimitAngleThreshold = 60;
66     const float extendLimitActThreshold = 0.6;
67     float deltaAct = 0;
68     float deltaTheta = 0;
69     static float oldDeltaAct = 0;

```



```

70 float desiredMuscleTheta = 0;
71 static bool enableStiffnessControl = false;
72 static bool swingAssist = false;
73 static bool descendFlag = false;
74 float antActAngleScale = 0;
75 float antActGravScale = 0;
76
77 /* NEURAL CONTROL CONTRIBUTION */
78 if (m_helper->_neuralControlEnabled()) {
79
80     //nonlinear activation scaling
81     agAct = 6.6779*powf(agAct,5) - 19.5677*powf(agAct,4) + 21.4299*powf(agAct,3) -
10.7903*powf(agAct,2) + 3.2602*agAct - 0.0030;
82     antAct = 6.6779*powf(antAct,5) - 19.5677*powf(antAct,4) + 21.4299*powf(antAct,3)
- 10.7903*powf(antAct,2) + 3.2602*antAct - 0.0030;
83
84     //limit output after nonlinear activation scaling
85     agAct = fmin(agActMax, fmax(0.01, agAct - 0.03));
86     antAct = fmin(antActMax, fmax(0.01, antAct - 0.03));
87
88     if (m_measuredJointAngleDeg[0] < 15) {
89         armLimitExtension = true;
90         m_isLimitExtension = false;
91     }
92
93     //add muscle torque contribution with significant activation
94     if (agAct > actLockThresh || antAct > actLockThresh) {
95
96         //if we overflex, then assist with stair climbing
97         if (!m_isLimitExtension && m_measuredJointAngleDeg[0] >
extendLimitAngleThreshold && fabs(gravComponent-0.15) < 0.05 &&
98             !m_isHeelContact && !m_isToeContact && !swingAssist && armLimitExtension) {
99             m_isLimitExtension = true;
100             armLimitExtension = false;
101             std::cout << "LIMITING EXTENSION" << std::endl;
102         } else if (m_isLimitExtension && (m_jointVelValDeg[0] < -200 &&
m_measuredJointAngleDeg[0] < 45 || m_isHeelContact || m_isToeContact)) {
103             m_isLimitExtension = false;
104             armLimitExtension = false;
105             std::cout << "Released limited extension rule 1: contact or extension
velocity under 45 degrees" << std::endl;
106         } else if (m_isLimitExtension && (antAct < 0.15 && agAct < 0.15) && fabs(
gravComponent-0.2) > 0.25) {
107             m_isLimitExtension = false;
108             armLimitExtension = false;

```

```

109     std::cout << "Released limited extension rule 2: relaxed and flexed" << std::
endl;
110   } else if (m_isLimitExtension && antAct > 0.4 && fabs(gravComponent-0.2) >
0.25) {
111     m_isLimitExtension = false;
112     armLimitExtension = false;
113     std::cout << "Released limited extension rule 3: extension while flexed" <<
std::endl;
114   }
115
116     //if knee is statically flexed and close to vertical, reduce extension
activation to account for hip flexed posture increasing knee extensor activation
without corresponding intent to do so
117     if (fabs(m_jointVelValDeg[0]) < 60 && (!m_isHeelContact && !m_isToeContact)
|| (m_jointVelValDeg[0] > -5 && (m_isHeelContact || m_isToeContact))) {
118         antActAngleScale = 1/(1 + exp(-30*((highAngleLimit-
m_measuredJointAngleDeg[0])/highAngleLimit - 0.35))); // sigmoidal reduce antAct
to 0 beyond ~50 degrees flex
119         antActGravScale = fmin(1,2000*powf((gravComponent-0.15),4)); //quartic
function
120         antAct = antAct*fmax(antActAngleScale,antActGravScale); //screen for both
correct knee and hip angle for stairs
121     }
122
123     oldDeltaAct = deltaAct; //store the sign of the deltaAct
124
125     if (!m_isHeelContact && !m_isToeContact) {
126         deltaAct = agAct - antAct; //positive is flexion, hence agAct is amount to be
subtracted from
127     } else {
128         //allow for descent but both sensors must be on the ground and time in stance
more than 500 ms (avoid impact jitter)
129         if (m_measuredJointAngleDeg[0] < stanceFlexLimit && m_isHeelContact &&
m_isToeContact && cnt_state > 600) {
130             deltaAct = -fmax(agAct, antAct);
131         } else {
132             deltaAct = -fmax(agAct, antAct); //if foot on ground, both muscles act to
extend knee
133         }
134     }
135
136     //if the sign of deltaAct switches, then turn lockOn off to get a new reference
lock angle
137     if (oldDeltaAct * deltaAct < 0) {
138         lockOn = false;

```

```

139     }
140
141     //note the theta upon entry into activated muscle state
142     if (!lockOn) {
143         lockThetaDeg = fmin(fmax(m_measuredJointAngleDeg[0]-lowAngleLimit,
144             cutoffPercent*angleRange),(1-cutoffPercent)*angleRange); //bound lockThetaDeg so
145             log() works
146         //inverse logistic function to convert lockThetaDeg to equivalent lock delta
147             activation
148         lockDeltaAct = log(angleRange/lockThetaDeg-1)/logisticExp;
149         lockOn = true;
150     }
151
152     //if limiting extension, then set the desired muscle theta to max flexion
153     if (m_isLimitExtension) {
154         //limit the amount of extension for free space control
155         lowAngleLimit = 50;
156         angleRange = highAngleLimit - lowAngleLimit;
157
158         lockThetaDeg = fmin(fmax(highAngleLimit-lowAngleLimit,cutoffPercent*
159             angleRange),(1-cutoffPercent)*angleRange); //bound lockThetaDeg so log() works
160         //inverse logistic function to convert lockThetaDeg to equivalent lock delta
161             activation
162         lockDeltaAct = log(angleRange/lockThetaDeg-1)/logisticExp;
163     } else {
164         lowAngleLimit = lowAngleLimit0g;
165         angleRange = highAngleLimit - lowAngleLimit;
166     }
167
168     deltaTheta = angleRange * 1/(1+exp(logisticExp*(lockDeltaAct+deltaAct))); //
169     amount to set the desired angle at above lowAngleLimit
170
171     desiredMuscleTheta = lowAngleLimit + deltaTheta;
172
173     //allow for knee flexion during stance
174     if ((m_isHeelContact || m_isToeContact) && m_measuredJointAngleDeg[0] <
175         stanceFlexLimit) {
176         descendFlag = true;
177         //if stanceFlexLimit exceeded, then set lockDeltaAct to limit to minimize
178             sudden changes
179     } else if ((m_isHeelContact || m_isToeContact) && descendFlag &&
180         m_measuredJointAngleDeg[0] >= stanceFlexLimit) {
181         desiredMuscleTheta = stanceFlexLimit;
182     }
183
184

```

```

175     //only damping during stance
176
177     float dampGain = 1.0;
178     const float kFloor = 0.2;
179     const float u = 45;
180     const float sigma = -10;
181     const float gain = 6.5;
182
183     if (m_jointVelValDeg[0] < 0 && m_measuredJointAngleDeg[0] < angleRange/2) {
184         dampGain = 1 + 1.3/(1+exp(-10*(-((m_measuredJointAngleDeg[0]-angleRange/2) /
angleRange/2)+0.25)))));
185     } else if (m_jointVelValDeg[0] > 0 && m_measuredJointAngleDeg[0] >= angleRange
/2) {
186         dampGain = 1 + 2/(1+exp(-10*((m_measuredJointAngleDeg[0]-angleRange/2) /
angleRange/2)-0.25)))));
187     } else {
188         dampGain = 1;
189     }
190
191     if (!m_isHeelContact && !m_isToeContact && !swingAssist) {
192         // if flexing quickly, keep linear stiffness response
193         if (m_jointVelValDeg[0] > 50) {
194             muscleTorque = calcImpedance(kFloor+(maxK - kFloor)*fmax(agAct,antAct),
dampGain*maxB*fmax(agAct,antAct), desiredMuscleTheta, m_helper);
195             // if flexing slowly, use sigmoidal stiffness boost. If extending quickly,
use linear stiffness
196         } else if (m_jointVelValDeg[0] <= 50 || m_jointVelValDeg[0] < -50) {
197             muscleTorque = calcImpedance(kFloor+( (0.5/(1+exp(-0.2*(
m_measuredJointAngleDeg[0]-60))) + 1)*maxK - kFloor)*fmax(agAct,antAct), dampGain
*maxB*fmax(agAct,antAct), desiredMuscleTheta, m_helper);
198             // if extending slowly, use sigmoidal stiffness boost
199         } else {
200             muscleTorque = calcImpedance(kFloor+( (0.5/(1+exp(-0.2*(-
m_measuredJointAngleDeg[0]+5))) + 1)*maxK - kFloor)*fmax(agAct,antAct), dampGain*
maxB*fmax(agAct,antAct), desiredMuscleTheta, m_helper);
201         }
202
203     } else if (m_isHeelContact || m_isToeContact) {
204         //stair descent
205         if (descendFlag) {
206             if (m_measuredJointAngleDeg[0] < stanceFlexLimit) {
207                 muscleTorque = calcImpedance(kFloor+(1.0*maxK-kFloor)*fmin(agAct,antAct),
dampGain*maxB*fmax(agAct,antAct), desiredMuscleTheta, m_helper);
208             } else if (m_jointVelValDeg[0] > 0 && m_measuredJointAngleDeg[0] >
stanceFlexLimit) {

```

```

209     muscleTorque = calcImpedance(0.0*maxK*fmax(agAct,antAct), 0.1 + dampGain*
maxB*fmax(agAct,antAct), desiredMuscleTheta, m_helper);
210     }
211     //torque booster for power ascent
212     } else if (m_jointVelValDeg[0] < 20) {
213         muscleTorque = calcImpedance(kFloor + (2.3*maxK*(gain/powf(2*M_PI*sigma*
sigma,0.5)*exp(-( powf(m_measuredJointAngleDeg[0]-u,2)/(2*sigma*sigma))) + 1 ) -
kFloor)*fmin(agAct+antAct,1), dampGain*maxB*fmax(agAct,antAct),
desiredMuscleTheta, m_helper);
214         //standard stance control
215     } else {
216         muscleTorque = calcImpedance(kFloor+(1.3*maxK-kFloor)*fmax(agAct,antAct),
dampGain*maxB*fmax(agAct,antAct), desiredMuscleTheta, m_helper);
217     }
218     }
219
220     //disable muscle flex when ascending or descending - safety catch
221     if ((m_isHeelContact || m_isToeContact) && m_measuredJointAngleDeg[0] >=
stanceFlexLimit) {
222         if (muscleTorque > 0) {
223             muscleTorque = 0;
224         }
225     }
226
227     } else {
228         lockOn = false;
229         muscleTorque = 0;
230     }
231
232     //turn off descendFlag
233     if (m_measuredJointAngleDeg[0] > 55 && m_jointVelValDeg[0] < -30 || (!
m_isHeelContact && !m_isToeContact)) {
234         descendFlag = false;
235     }
236
237     }
238
239     /* CALCULATE CONTRIBUTION FROM GRAVITY */
240     static float gravComponentPrev = 0;
241
242     //trust accelerometer only at low velocities and omit swing states
243     if (fabs(m_jointVelValRad[0]) < 2.0 && !m_isLimitExtension) {
244         if (gravComponent != gravComponentPrev && (agAct < 0.2 && antAct < 0.2)) {
245             gravityTorque = calcGravityTorque(gravComponent, m_jointVelValRad[0])*(1.01-
fmax(agAct,antAct));

```

```

246     }
247     //gravity compensation term at high velocities (off for now)
248 } else {
249     gravityTorque = 0;
250 }
251
252 /* CALCULATE CONTRIBUTION FROM FSM */
253
254 //ratcheting setpoint
255 static float entryTheta = 90;
256 const float thetaThresh = 20; //deviation beyond which to reset spring
257 static float heelToeCounter = 0;
258 const float heelToeMinCount = 100;
259 const float stanceTwoTimeLimit = 900.;
260 static bool heelToeAchieved = false;
261 static bool disableStanceTwo = false;
262 static const float reasonableStanceTime = 1400;
263 static float timeSinceHeelToe = 0;
264 static float prevTimeInStance = 10000;
265 static float timeInPrevSwing = 10000; //swing is roughly 40% of entire gait cycle
266 float prevSwingDivisor = 1.7;
267 float stanceTwoKScalar = 1;
268
269 switch (state) {
270     case STANCE:
271
272         //set entryTheta to maximum knee extension observed
273         if (m_measuredJointAngleDeg[0] < entryTheta) {
274             entryTheta = fmax(m_measuredJointAngleDeg[0], 5.0);
275         }
276
277         //start counting time with both heel and toe on and detect if midstance
278         //achieved
279         if (m_isHeelContact && m_isToeContact && m_measuredJointAngleDeg[0] <
280             stanceTwoParams[2]) {
281             heelToeCounter++;
282             if (heelToeCounter >= heelToeMinCount) {
283                 heelToeAchieved = true;
284             }
285             //if we're climbing stairs and joint is over bent, disable preswing
286         } else if (m_isHeelContact && m_measuredJointAngleDeg[0] < stanceTwoParams[2]
287             && cnt_state < reasonableStanceTime) {
288             heelToeCounter++;
289         } else if (m_isToeContact && heelToeCounter > heelToeMinCount) {
290             heelToeAchieved = true;

```

```

288     } else if (m_measuredJointAngleDeg[0] >= stanceTwoParams[2]) {
289         disableStanceTwo = true;
290         //reset counter to account for transients at impact, otherwise keep
heelToeCounter value
291     } else if (!heelToeAchieved && cnt_state > stanceTwoTimeLimit) {
292         heelToeCounter = 0;
293     }
294
295     //start counting time since midstance
296     if (heelToeAchieved) {
297         timeSinceHeelToe++;
298     }
299
300     //only provide impedance damping and stiffness if there's ground contact and
knee flexing
301     if (m_jointVelValDeg[0] > -5) {
302         //if preswing detected, apply stance two params
303         if (!disableStanceTwo && heelToeAchieved && timeSinceHeelToe >
timeInPrevSwing/prevSwingDivisor &&
304             timeSinceHeelToe < stanceTwoTimeLimit && cnt_state < reasonableStanceTime
&& //&& antAct < 0.5
305             swingAssist) { //only allow stanceTwo if swingAssist persisted after
previous step
306             if (timeInPrevSwing > 200) {
307                 stanceTwoKScalar = fmin(1.5, fmax(0.8, transitionTime/timeInPrevSwing));
308                 impTorque += calcImpedance(stanceTwoKScalar*stanceTwoParams[0],
stanceTwoParams[1], stanceTwoParams[2], m_helper);
309             } else {
310                 stanceTwoKScalar = 0; //if stutter or short step, no stanceTwo flexion
torque
311                 impTorque += calcImpedance(stanceOneParams[0], stanceOneParams[1],
stanceOneParams[2], m_helper);
312             }
313
314             // else provide flexion damping
315         } else {
316             //prevent flexion if close to full extension heel strike
317             if (m_measuredJointAngleDeg[0] < thetaThresh && cnt_state < 100) {
318                 impTorque += calcImpedance(stanceOneParams[0], stanceOneParams[1],
stanceOneParams[2], m_helper);
319                 //if we happen to be in the air for a brief moment near full extension (
short step), then extend leg to catch
320             } else if (m_measuredJointAngleDeg[0] < thetaThresh && !m_isHeelContact &&
!m_isToeContact) {
321                 impTorque += calcImpedance(stanceOneParams[0], stanceOneParams[1],

```

```

stanceOneParams[2], m_helper);
322     //general stronger damping when close to full extension otherwise
323     } else if (m_measuredJointAngleDeg[0] < entryTheta + thetaThresh) {
324         impTorque += calcImpedance(0, 0.7*stanceOneParams[1], stanceOneParams[2],
m_helper);
325         //half damping for extreme deviations (sitting)
326     } else {
327         impTorque += calcImpedance(0, 0.3*stanceOneParams[1], stanceOneParams[2],
m_helper);
328     }
329 }
330 //only provide a limited amount of extension depending on deviation from
entryTheta
331 } else {
332     if (m_measuredJointAngleDeg[0] < entryTheta + thetaThresh) {
333         impTorque += calcImpedance(stanceOneParams[0], stanceOneParams[1]*0.2,
entryTheta, m_helper);
334         //slide entryTheta if extension velocity, but currently overflexed
335     } else if (m_measuredJointAngleDeg[0] > entryTheta + thetaThresh) {
336         entryTheta = m_measuredJointAngleDeg[0] - thetaThresh;
337     }
338 }
339
340 //transition to swing
341 if (!m_isHeelContact && !m_isToeContact && cnt_state > 400) {
342     state = SWING;
343     prev_state = STANCE;
344     entryTheta = 90;
345     heelToeAchieved = false;
346     disableStanceTwo = false;
347     swingAssist = false;
348     prevTimeInStance = cnt_state;
349     cnt_state = 0;
350
351     if (m_jointVelValDeg[0] > 5 && m_measuredJointAngleDeg[0] < swingParams[2]) {
352         impTorque = calcImpedance(swingParams[0], swingParams[1], swingParams[2],
m_helper);
353     } else {
354         impTorque = 0;
355     }
356
357 }
358
359 cnt_state++;
360

```



```

361     break;
362
363     case SWING:
364         static const int assistTime = 70;
365         static const int extendTime = 800;
366         static int assistDuration = 0;
367         static int assistDurationLimit = 60;
368         static const float extendTransAngle = 50;
369         static int holdCnt = 0;
370
371         //assist with motor impedance if we're flexing upon entry
372         static float swingKgain = fmin(1.3, fmax(0.8, swingStanceThresh/
prevTimeInStance));
373
374         if (cnt_state < assistTime && assistDuration < assistDurationLimit &&
m_measuredJointAngleDeg[0] < swingParams[2]) {
375             if (m_measuredJointAngleDeg[0] < swingParams[2]) {
376                 impTorque += fmax(0, calcImpedance(swingKgain*swingParams[0], 0, swingParams
[2], m_helper));
377                 assistDuration++;
378             } else {
379                 assistDuration = assistDurationLimit;
380             }
381             swingAssist = true;
382             //else assume we are descending from step and got to swing phase
383         } else if (cnt_state < assistTime && m_measuredJointAngleDeg[0] >= swingParams
[2] && assistDuration == 0) {
384             swingAssist = true;
385             assistDuration = assistDurationLimit;
386         }
387
388         //turn off swing assist if flexion desired if detected flex intent upon
transition into swing
389         if (swingAssist && agAct > extendLimitActThreshold && m_helper->
_neuralControlEnabled() && (cnt_state < 30 || m_targetJointAngleDeg[0] < 15)) {
390             swingAssist = false;
391             assistDuration = assistDurationLimit;
392             //if detected flex beyond some nominal amount of flexion
393         } else if (swingAssist && m_measuredJointAngleDeg[0] > extendTransAngle - 20 &&
(agAct > extendLimitActThreshold && m_helper->_neuralControlEnabled())) {
394             holdCnt++;
395             if (holdCnt > 5) {
396                 swingAssist = false;
397                 assistDuration = assistDurationLimit;
398             }

```

```

399     } else if (swingAssist && m_measuredJointAngleDeg[0] > extendTransAngle - 30 &&
(agAct > extendLimitActThreshold+0.1 && antAct < extendLimitActThreshold-0.3 &&
m_helper->_neuralControlEnabled())) {
400         swingAssist = false;
401         assistDuration = assistDurationLimit;
402     } else {
403         holdCnt = 0;
404     }
405
406     //knee extension assistance if taking a step
407     if (swingAssist && cnt_state < extendTime && (cnt_state >= assistTime ||
assistDuration == assistDurationLimit) ) {
408         if (m_measuredJointAngleDeg[0] > extendTransAngle) {
409             impTorque += fmax(plantarTorqueThresh - 0.60*(m_measuredJointAngleDeg[0]-
extendTransAngle), -60);
410         } else if (m_measuredJointAngleDeg[0] <= extendTransAngle &&
m_measuredJointAngleDeg[0] > 30 && m_jointVelValDeg[0] < -5) {
411             impTorque += calcImpedance(standParams[0], standParams[1]*0.6, standParams
[2], m_helper);
412         } else if (m_measuredJointAngleDeg[0] <= 30 && m_jointVelValDeg[0] < 0) {
413             impTorque += calcImpedance(standParams[0], standParams[1], standParams[2],
m_helper);
414         } else if (m_jointVelValDeg[0] < -5) {
415             impTorque += -5;
416         }
417     }
418     #endif
419
420     //compensate for knee dynamics during swing extension to catch next stance
phase
421     if (cnt_state >= extendTime || !swingAssist) {
422         if (m_measuredJointAngleDeg[0] > 55 && m_jointVelValDeg[0] > 50 && ((agAct <
0.5 && m_helper->_neuralControlEnabled()) || !m_helper->_neuralControlEnabled())
) {
423             impTorque += calcImpedance(0, 0.08, 0, m_helper);
424         } else if ((!m_isLimitExtension && m_helper->_neuralControlEnabled()) &&
m_measuredJointAngleDeg[0] < 20 && m_jointVelValDeg[0] > -20 && m_jointVelValDeg
[0] < 50 && ((agAct < extendLimitActThreshold && antAct < extendLimitActThreshold
&& m_helper->_neuralControlEnabled()) || !m_helper->_neuralControlEnabled()) ) {
425             impTorque += calcImpedance(standParams[0], 0.2*standParams[1], standParams
[2], m_helper);
426         } else if ((!m_isLimitExtension && m_helper->_neuralControlEnabled()) &&
m_measuredJointAngleDeg[0] < 15 && m_jointVelValDeg[0] <= -50 && ((antAct < 0.2
&& agAct < 0.2 && m_helper->_neuralControlEnabled()) || !m_helper->
_neuralControlEnabled()) ) {

```

```

427     impTorque += calcImpedance(standParams[0], 0.5*standParams[1], standParams
[2], m_helper);
428     }
429
430     swingAssist = false; //we timed out of swing extension
431     }
432
433     if ((m_isHeelContact || m_isToeContact) && cnt_state > 200) {
434         state = STANCE;
435         prev_state = SWING;
436         if (swingAssist) { //only update this value if we don't activate volitional
control
437             timeInPrevSwing = cnt_state;
438         }
439         cnt_state = 0;
440         entryTheta = m_measuredJointAngleDeg[0];
441         lockOn = false;
442         assistDuration = 0;
443         holdCnt = 0;
444         heelToeCounter = 0; //reset stance variables
445         timeSinceHeelToe = 0; //reset stance variables
446     }
447
448
449     cnt_state++;
450
451     break;
452
453     default:
454         break;
455 }
456
457 commandTorque = muscleTorque + impTorque + gravityTorque;
458 cnt++;
459
460 m_state->updateValue(state);
461 m_system->getAllGenVariables()[0]->updateValue(desiredMuscleTheta); //update state
462 m_system->getAllGenVariables()[1]->updateValue(agAct);
463 m_system->getAllGenVariables()[2]->updateValue(antAct);
464 m_system->getAllGenVariables()[3]->updateValue(muscleTorque); //update muscleTorque
465
466 commandTorqueKnee->updateValue(commandTorque);
467 }

```


Bibliography

- [1] Jacob L. Segil, Leah Marie Roldan, and Emily L. Graczyk. Measuring embodiment: A review of methods for prosthetic devices. *Frontiers in Neurorobotics*, 16, December 2022. Publisher: Frontiers.
- [2] Tony Shu, Guillermo Herrera-Arcos, Cameron R. Taylor, and Hugh M. Herr. Mechanoneural interfaces for bionic integration. *Nature Reviews Bioengineering*, pages 1–18, February 2024. Publisher: Nature Publishing Group.
- [3] Max Ortiz-Catalan, Rickard Brånemark, Bo Håkansson, and Jean Delbeke. On the viability of implantable electrodes for the natural control of artificial limbs: Review and discussion. *BioMedical Engineering OnLine*, 11:33, June 2012.
- [4] Rachel Gehlhar, Maegan Tucker, Aaron J. Young, and Aaron D. Ames. A Review of Current State-of-the-Art Control Methods for Lower-Limb Powered Prostheses. *Annual Reviews in Control*, 55:142–164, 2023.
- [5] N. Hogan. Adaptive control of mechanical impedance by coactivation of antagonist muscles. *IEEE Transactions on Automatic Control*, 29(8):681–690, August 1984.
- [6] Hyungeun Song, Erica A. Israel, Samantha Gutierrez-Arango, Ashley C. Teng, Shriya S. Srinivasan, Lisa E. Freed, and Hugh M. Herr. Agonist-antagonist muscle strain in the residual limb preserves motor control and perception after amputation. *Communications Medicine*, 2(1):97, August 2022.
- [7] Jordan G. Tropf and Benjamin K. Potter. Osseointegration for amputees: Current state of direct skeletal attachment of prostheses. *Orthoplastic Surgery*, 12:20–28, June 2023.
- [8] Max Ortiz-Catalan, Bo Håkansson, and Rickard Brånemark. An osseointegrated human-machine gateway for long-term sensory feedback and motor control of artificial limbs. *Sci. Transl. Med.*, 6(257):257re6., October 2014. Publisher: American Association for the Advancement of Science. _eprint: 25298322.
- [9] Jan Zbinden, Paolo Sassu, Enzo Mastinu, Eric J. Earley, Maria Munoz-Novoa, Rickard Brånemark, and Max Ortiz-Catalan. Improved control of a prosthetic limb by surgically creating electro-neuromuscular constructs with implanted electrodes. *Science Translational Medicine*, 15(704):eabq3665, July 2023. Publisher: American Association for the Advancement of Science.

- [10] Max Ortiz-Catalan, Jan Zbinden, Jason Millenaar, Daniele D’Accolti, Marco Controzzi, Francesco Clemente, Leonardo Cappello, Eric J. Earley, Enzo Mastinu, Justyna Kolankowska, Maria Munoz-Novoa, Stewe Jönsson, Christian Cipriani, Paolo Sassu, and Rickard Brånemark. A highly integrated bionic hand with neural control and feedback for use in daily life. *Science Robotics*, 8(83):eadf7360, October 2023. Publisher: American Association for the Advancement of Science.
- [11] C.R. Taylor, S.S. Srinivasan, S.H. Yeon, M.K. O’Donnell, T.J. Roberts, and H.M. Herr. Magnetomicrometry. *Science robotics*, 6(57):eabg0656, August 2021. Issue: 57.
- [12] Francis McGlone and Charles Spence. The cutaneous senses: touch, temperature, pain/itch, and pleasure. *Neuroscience and Biobehavioral Reviews*, 34(2):145–147, February 2010.
- [13] Uwe Proske and Simon C. Gandevia. The proprioceptive senses: their roles in signaling body shape, body position and movement, and muscle force. *Physiological Reviews*, 92(4):1651–1697, October 2012. Publisher: American Physiological Society.
- [14] Anne-Sophie Augurelle, Allan M. Smith, Thierry Lejeune, and Jean-Louis Thonnard. Importance of cutaneous feedback in maintaining a secure grip during manipulation of hand-held objects. *Journal of Neurophysiology*, 89(2):665–671, February 2003. Publisher: American Physiological Society.
- [15] Alice G. Witney, Alan Wing, Jean-Louis Thonnard, and Allan M. Smith. The cutaneous contribution to adaptive precision grip. *Trends in Neurosciences*, 27(10):637–643, October 2004.
- [16] Xavier Libouton, Olivier Barbier, Yorick Berger, Leon Plaghki, and Jean-Louis Thonnard. Tactile roughness discrimination of the finger pad relies primarily on vibration sensitive afferents not necessarily located in the hand. *Behavioural Brain Research*, 229(1):273–279, April 2012.
- [17] Jeffrey Weiler, Paul L. Gribble, and J. Andrew Pruszynski. Spinal stretch reflexes support efficient control of reaching. *Journal of Neurophysiology*, 125(4):1339–1347, April 2021. Publisher: American Physiological Society.
- [18] Kenneth O. Johnson, Takashi Yoshioka, and Francisco Vega-Bermudez. Tactile functions of mechanoreceptive afferents innervating the hand. *Journal of Clinical Neurophysiology*, 17(6):539, November 2000.
- [19] Jeffrey M. Yau, Sung Soo Kim, Pramodsingh H. Thakur, and Sliman J. Bensmaïa. Feeling form: the neural basis of haptic shape perception. *Journal of Neurophysiology*, 115(2):631–642, February 2016. Publisher: American Physiological Society.

- [20] Ayman M. Ebied, Graham J. Kemp, and Simon P. Frostick. The role of cutaneous sensation in the motor function of the hand. *Journal of Orthopaedic Research*, 22(4):862–866, 2004. eprint: <https://onlinelibrary.wiley.com/doi/pdf/10.1016/j.orthres.2003.12.005>.
- [21] Julien Voisin, Yves Lamarre, and C. Elaine Chapman. Haptic discrimination of object shape in humans: contribution of cutaneous and proprioceptive inputs. *Experimental Brain Research*, 145(2):251–260, July 2002.
- [22] Peter F. Meyer, Lars I. E. Oddsson, and Carlo J. De Luca. The role of plantar cutaneous sensation in unperturbed stance. *Experimental Brain Research*, 156(4):505–512, June 2004.
- [23] Eric Eils, Susann Behrens, Oliver Mers, Lothar Thorwesten, Klaus Völker, and Dieter Rosenbaum. Reduced plantar sensation causes a cautious walking pattern. *Gait & Posture*, 20(1):54–60, August 2004.
- [24] Angela Höhne, Sufyan Ali, Christian Stark, and Gert-Peter Brüggemann. Reduced plantar cutaneous sensation modifies gait dynamics, lower-limb kinematics and muscle activity during walking. *European Journal of Applied Physiology*, 112(11):3829–3838, November 2012.
- [25] Frederic Viseux, Antoine Lemaire, Franck Barbier, Pascal Charpentier, Sebastien Leteneur, and Philippe Villeneuve. How can the stimulation of plantar cutaneous receptors improve postural control? Review and clinical commentary. *Neurophysiologie Clinique*, 49(3):263–268, June 2019.
- [26] Volker Dietz. Proprioception and locomotor disorders. *Nature Reviews Neuroscience*, 3(10):781–790, October 2002. Number: 10 Publisher: Nature Publishing Group.
- [27] E. Paul Zehr and Richard B. Stein. What functions do reflexes serve during human locomotion? *Progress in Neurobiology*, 58(2):185–205, June 1999.
- [28] Hugh M. Herr, Tyler R. Clites, Shriya Srinivasan, Simon G. Talbot, Gregory A. Dumanian, Paul S. Cederna, and Matthew J. Carty. Reinventing extremity amputation in the era of functional limb restoration. *Annals of Surgery*, 273(2):269–279, February 2021.
- [29] Xavier Navarro, Enrique Verdú, and Miquel Butí. Comparison of Regenerative and Reinnervating Capabilities of Different Functional Types of Nerve Fibers. *Experimental Neurology*, 129(2):217–224, October 1994.
- [30] Tessa Gordon. Peripheral nerve regeneration and muscle reinnervation. *International Journal of Molecular Sciences*, 21(22):8652, November 2020.
- [31] T. M. Brushart. Preferential motor reinnervation: a sequential double-labeling study. *Restorative Neurology and Neuroscience*, 1(3):281–287, January 1990.

- [32] T. M. Brushart. Motor axons preferentially reinnervate motor pathways. *Journal of Neuroscience*, 13(6):2730–2738, June 1993. Publisher: Society for Neuroscience Section: Articles.
- [33] Thomas M. Brushart, Jonathan Gerber, Philip Kessens, You-Gang Chen, and Richard M. Royall. Contributions of pathway and neuron to preferential motor reinnervation. *The Journal of Neuroscience*, 18(21):8674–8681, November 1998.
- [34] Sara Bolívar and Esther Udina. Preferential regeneration and collateral dynamics of motor and sensory neurons after nerve injury in mice. *Experimental Neurology*, 358:114227, December 2022.
- [35] Wale Sulaiman and Tessa Gordon. Neurobiology of peripheral nerve injury, regeneration, and functional recovery: from bench top research to bedside application. *The Ochsner Journal*, 13(1):100–108, 2013.
- [36] Tyler R. Clites, Matthew J. Carty, Jessica B. Ullauri, Matthew E. Carney, Luke M. Mooney, Jean-François Duval, Shriya S. Srinivasan, and Hugh M. Herr. Proprioception from a neurally controlled lower-extremity prosthesis. *Science Translational Medicine*, 10(443):eaap8373, May 2018.
- [37] Tyler R. Clites, Hugh M. Herr, Shriya S. Srinivasan, Anthony N. Zorzos, and Matthew J. Carty. The Ewing amputation: the first human implementation of the agonist-antagonist myoneural interface. *Plastic and Reconstructive Surgery – Global Open*, 6(11):e1997, November 2018. Publisher: Wolters Kluwer.
- [38] Hugh M. Herr, Ronald R. Riso, Katherine W. Song, Richard J. Casler Jr, and Matthew J. Carty. Peripheral Neural Interface Via Nerve Regeneration to Distal Tissues, June 2015.
- [39] Tyler R. Clites, Matthew J. Carty, Shriya Srinivasan, Anthony N. Zorzos, and Hugh M. Herr. A murine model of a novel surgical architecture for proprioceptive muscle feedback and its potential application to control of advanced limb prostheses. *Journal of Neural Engineering*, 14(3), March 2017. Publisher: Institute of Physics Publishing.
- [40] Hugh M. Herr, Tyler Clites, Benjamin MAIMON, Anthony Zorzos, Matthew J. CARTY, and Jean-Francois DUVAL. Method and system for providing proprioceptive feedback and functionality mitigating limb pathology, July 2017.
- [41] Tyler R. Clites, Matthew J. Carty, Shriya S. Srinivasan, Simon G. Talbot, Rickard Brånemark, and Hugh M. Herr. Caprine Models of the Agonist-Antagonist Myoneural Interface Implemented at the Above- and Below-Knee Amputation Levels. *Plastic and Reconstructive Surgery*, 144(2):218e, August 2019.
- [42] Waleed A. Farahat and Hugh M. Herr. Optimal workloop energetics of muscle-actuated systems: an impedance matching view. *PLOS Computational Biology*, 6(6):e1000795, June 2010. Publisher: Public Library of Science.

- [43] Tony Shu, Christopher Shallal, Ethan Chun, Aashini Shah, Angel Bu, Daniel Levine, Seong Ho Yeon, Matthew Carney, Hyungeun Song, Tsung-Han Hsieh, and Hugh M. Herr. Modulation of prosthetic ankle plantarflexion through direct myoelectric control of a subject-optimized neuromuscular model. *IEEE Robotics and Automation Letters*, 7(3):7620–7627, July 2022. Conference Name: IEEE Robotics and Automation Letters.
- [44] Shriya S. Srinivasan, Greta Tuckute, Jasmine Zou, Samantha Gutierrez-Arango, Hyungeun Song, Robert L. Barry, and Hugh M. Herr. Agonist-antagonist myoneural interface amputation preserves proprioceptive sensorimotor neurophysiology in lower limbs. *Science translational medicine*, 12(573):eabc5926, December 2020.
- [45] Shriya S. Srinivasan, Samantha Gutierrez-Arango, Ashley Chia-En Teng, Erica Israel, Hyungeun Song, Zachary Keith Bailey, Matthew J. Carty, Lisa E. Freed, and Hugh M. Herr. Neural interfacing architecture enables enhanced motor control and residual limb functionality postamputation. *Proc. Natl. Acad. Sci. U.S.A.*, 118(9):e2019555118., March 2021. Publisher: the Author(sPNAS. eprint: 33593940.
- [46] Hugh Herr and Matthew J. Carty. The agonist-antagonist myoneural interface. *Techniques in Orthopaedics (Rockville, Md.)*, 36(4):337–344, May 2021.
- [47] Paul D. Marasco, Jacqueline S. Hebert, Jonathon W. Sensinger, Dylan T. Beckler, Zachary C. Thumser, Ahmed W. Shehata, Heather E. Williams, and Kathleen R. Wilson. Neurorobotic fusion of prosthetic touch, kinesthesia, and movement in bionic upper limbs promotes intrinsic brain behaviors. *Science Robotics*, 6(58):eabf3368, September 2021.
- [48] Robert J. Rudy, Paul A. Levi, Fred J. Bonacci, Arnold S. Weisgold, and Daniel Engler-Hamm. Intraosseous anchorage of dental prostheses: an early 20th century contribution. *Compendium of Continuing Education in Dentistry (Jamesburg, N.J.: 1995)*, 29(4):220–222, 224, 226–228 passim, May 2008.
- [49] Per-Ingvar Branemark. Osseointegration and its experimental background. *The Journal of Prosthetic Dentistry*, 50(3):399–410, September 1983.
- [50] Kerstin Hagberg, Elisabeth Hansson, and Rickard Brånemark. Outcome of Percutaneous Osseointegrated Prostheses for Patients With Unilateral Transfemoral Amputation at Two-Year Follow-Up. *Archives of Physical Medicine and Rehabilitation*, 95(11):2120–2127, November 2014.
- [51] Eva Häggström, CPO, Kerstin Hagberg, PT, PhD, Björn Rydevik, MD, PhD, Rickard Brånemark, and MD, PhD. Vibrotactile evaluation: Osseointegrated versus socket-suspended transfemoral prostheses. *Journal of Rehabilitation Research and Development*, 50(10):1423–1434, 2013.

- [52] Kevin Carroll and Joan E. Edelstein. *Prosthetics and Patient Management: A Comprehensive Clinical Approach*. SLACK Incorporated, 2006.
- [53] Kerstin Hagberg, Rickard Brånemark, Björn Gunterberg, and Björn Rydevik. Osseointegrated trans-femoral amputation prostheses: Prospective results of general and condition-specific quality of life in 18 patients at 2-year follow-up. *Prosthetics and Orthotics International*, 32(1):29, March 2008.
- [54] J. Sullivan, M. Uden, K. P. Robinson, and S. Sooriakumaran. Rehabilitation of the transfemoral amputee with an osseointegrated prosthesis: The United Kingdom experience. *Prosthetics and Orthotics International*, 27(2):114–120, August 2003. Publisher: SAGE Publications Ltd STM.
- [55] Rickard P. Brånemark, Kerstin Hagberg, Katarzyna Kulbacka-Ortiz, Örjan Berlin, and Björn Rydevik. Osseointegrated Percutaneous Prosthetic System for the Treatment of Patients With Transfemoral Amputation: A Prospective Five-year Follow-up of Patient-reported Outcomes and Complications. *The Journal of the American Academy of Orthopaedic Surgeons*, 27(16):e743–e751, August 2019.
- [56] P. K. Tomaszewski, N. Verdonschot, S. K. Bulstra, and G. J. Verkerke. A Comparative Finite-Element Analysis of Bone Failure and Load Transfer of Osseointegrated Prostheses Fixations. *Annals of Biomedical Engineering*, 38(7):2418–2427, July 2010.
- [57] Frank Sup, Amit Bohara, and Michael Goldfarb. Design and Control of a Powered Transfemoral Prosthesis. *The International Journal of Robotics Research*, 27(2):263–273, February 2008. Publisher: SAGE Publications Ltd STM.
- [58] Ryan W. Sinnet, Huihua Zhao, and Aaron D. Ames. Simulating prosthetic devices with human-inspired hybrid control. In *2011 IEEE/RSJ International Conference on Intelligent Robots and Systems*, pages 1723–1730, September 2011. ISSN: 2153-0866.
- [59] Rachel Gehlhar and Aaron D. Ames. Emulating Human Kinematic Behavior on Lower-Limb Prostheses via Multi-Contact Models and Force-Based Nonlinear Control. In *2023 IEEE International Conference on Robotics and Automation (ICRA)*, pages 10429–10435, London, United Kingdom, May 2023. IEEE.
- [60] Seong Yeon, Tony Shu, Hyungeun Song, Tsung-Han Hsieh, Junqing Qiao, Emily Rogers-Bradley, Samantha Gutierrez-Arango, Erica Israel, Lisa Freed, and Hugh Herr. Acquisition of Surface EMG Using Flexible and Low-Profile Electrodes for Lower Extremity Neuroprosthetic Control. *IEEE Transactions on Medical Robotics and Bionics*, 3:563–572, August 2021.
- [61] Seong Ho Yeon and Hugh M. Herr. Rejecting Impulse Artifacts from Surface EMG Signals using Real-time Cumulative Histogram Filtering. In *2021 43rd*

Annual International Conference of the IEEE Engineering in Medicine & Biology Society (EMBC), pages 6235–6241, November 2021. ISSN: 2694-0604.

- [62] Nikolaï Aleksandrovich Bernshteïn. *The Co-ordination and Regulation of Movements*. Pergamon Press, Oxford, 1st edition, 1967. Google-Books-ID: F9dqAAAAMAAJ.
- [63] Mark L. Latash, Mindy F. Levin, John P. Scholz, and Gregor Schöner. Motor control theories and their applications. *Medicina (Kaunas, Lithuania)*, 46(6):382–392, 2010.
- [64] Jonathon S. Schofield, Marcus A. Battraw, Adam S. R. Parker, Patrick M. Pilarski, Jonathon W. Sensinger, and Paul D. Marasco. Embodied cooperation to promote forgiving interactions with autonomous machines. *Frontiers in Neuro-robotics*, 15, 2021.
- [65] Jan Zbinden, Eva Lendaro, and Max Ortiz-Catalan. Prosthetic embodiment: systematic review on definitions, measures, and experimental paradigms. *Journal of Neuroengineering and Rehabilitation*, 19(1):37, March 2022.
- [66] Antal Haans, Wijnand A. IJsselsteijn, and Yvonne A. W. de Kort. The effect of similarities in skin texture and hand shape on perceived ownership of a fake limb. *Body Image*, 5(4):389–394, December 2008.
- [67] Birgitta Rosén, H. Henrik Ehrsson, Christian Antfolk, Christian Cipriani, Fredrik Sebelius, and Göran Lundborg. Referral of sensation to an advanced humanoid robotic hand prosthesis. *Scandinavian Journal of Plastic and Reconstructive Surgery and Hand Surgery*, 43(5):260–266, 2009.
- [68] Harry Farmer, Ana Tajadura-Jiménez, and Manos Tsakiris. Beyond the colour of my skin: how skin colour affects the sense of body-ownership. *Consciousness and Cognition*, 21(3):1242–1256, September 2012.
- [69] Jan Zbinden, Eva Lendaro, and Max Ortiz-Catalan. A multi-dimensional framework for prosthetic embodiment: a perspective for translational research. *Journal of NeuroEngineering and Rehabilitation*, 19(1):122, November 2022.
- [70] Tamar R. Makin, Nicholas P. Holmes, and H. Henrik Ehrsson. On the other hand: Dummy hands and peripersonal space. *Behavioural Brain Research*, 191(1):1–10, August 2008.
- [71] Andreas Kalckert and H. Ehrsson. Moving a rubber hand that feels like your own: a dissociation of ownership and agency. *Frontiers in Human Neuroscience*, 6, 2012.
- [72] C. Farrer, G. Valentin, and J. M. Hupé. The time windows of the sense of agency. *Consciousness and Cognition*, 22(4):1431–1441, December 2013.

- [73] Amit Regev Krugwasser, Eiran V. Harel, and Roy Salomon. The boundaries of the self: The sense of agency across different sensorimotor aspects. *Journal of Vision*, 19(4):14, April 2019.
- [74] S. Antusch, R. Custers, H. Marien, and H. Aarts. Studying the sense of agency in the absence of motor movement: an investigation into temporal binding of tactile sensations and auditory effects. *Experimental Brain Research*, 239(6):1795–1806, June 2021.
- [75] Noam Karsh, Baruch Eitam, Ilya Mark, and E. Tory Higgins. Bootstrapping agency: How control-relevant information affects motivation. *Journal of Experimental Psychology: General*, 145:1333–1350, 2016. Place: US Publisher: American Psychological Association.
- [76] Shaun Gallagher and Jonathan Cole. Body image and body schema in a deaf-ferented subject. *The Journal of Mind and Behavior*, 16(4):369–389, 1995. Publisher: Institute of Mind and Behavior, Inc.
- [77] Matthew R. Longo. Types of body representation. In *Perceptual and Emotional Embodiment*. Routledge, 2015. Num Pages: 18.
- [78] Lucilla Cardinali, Francesca Frassinetti, Claudio Brozzoli, Christian Urquizar, Alice C. Roy, and Alessandro Farnè. Tool-use induces morphological updating of the body schema. *Current Biology*, 19(12):R478–R479, June 2009.
- [79] Helena De Preester and Manos Tsakiris. Body-extension versus body-incorporation: Is there a need for a body-model? *Phenomenology and the Cognitive Sciences*, 8(3):307–319, September 2009.
- [80] Dominic James Farris and Glen A. Lichtwark. UltraTrack: Software for semi-automated tracking of muscle fascicles in sequences of B-mode ultrasound images. *Computer Methods and Programs in Biomedicine*, 128:111–118, May 2016.
- [81] E. Formento, K. Minassian, F. Wagner, JB. Mignardot, C. G. Le Goff, A. Rowald, J. Bloch, S. Micera, M. Capogrosso, and G. Courtine. Electrical spinal cord stimulation must preserve proprioception to enable locomotion in humans with spinal cord injury. *Nature neuroscience*, 21(12):1728–1741, December 2018.
- [82] Tamar R. Makin, Jan Scholz, Nicola Filippini, David Henderson Slater, Irene Tracey, and Heidi Johansen-Berg. Phantom pain is associated with preserved structure and function in the former hand area. *Nature Communications*, 4(1):1570, March 2013. Publisher: Nature Publishing Group.
- [83] José P. Marques, Tobias Kober, Gunnar Krueger, Wietske van der Zwaag, Pierre-François Van de Moortele, and Rolf Gruetter. MP2RAGE, a self bias-field corrected sequence for improved segmentation and T1-mapping at high field. *NeuroImage*, 49(2):1271–1281, January 2010.

- [84] Junqing Qiao. *EMG methods for prosthesis ankle-subtalar free-space control*. Thesis, Massachusetts Institute of Technology, February 2023. Accepted: 2023-08-30T16:00:46Z.
- [85] Corey Sullivan, Tony Shu, Rachael Chiao, Lori Berger, Kendall Clites, Marco Ferrone, Richard O’Donnel, Rickard Brånemark, Hugh Herr, and Matthew Carty. Transfemoral Amputation Incorporating eOPRA and Agonist-Antagonist Myoneural Interface (AMI) Design: Surgical Technique and Perioperative Care, October 2023. Journal Abbreviation: Plastic and Reconstructive Surgery - Global Open Publication Title: Plastic and Reconstructive Surgery - Global Open Volume: 11.
- [86] Kurt Manal and Thomas S Buchanan. A one-parameter neural activation to muscle activation model: estimating isometric joint moments from electromyograms. *Journal of Biomechanics*, 36(8):1197–1202, August 2003.
- [87] Matthew E. Carney, Tony Shu, Roman Stolyarov, Jean-François Duval, and Hugh M. Herr. Design and Preliminary Results of a Reaction Force Series Elastic Actuator for Bionic Knee and Ankle Prostheses. *IEEE Transactions on Medical Robotics and Bionics*, 3(3):542–553, August 2021. Conference Name: IEEE Transactions on Medical Robotics and Bionics.
- [88] Hoang-Vu Nguyen and Jilles Vreeken. Non-parametric Jensen-Shannon Divergence. In Annalisa Appice, Pedro Pereira Rodrigues, Vítor Santos Costa, João Gama, Alípio Jorge, and Carlos Soares, editors, *Machine Learning and Knowledge Discovery in Databases*, pages 173–189, Cham, 2015. Springer International Publishing.
- [89] Natalia Miranda-Cantellops and Timothy K. Tiu. Berg Balance Testing. In *StatPearls*. StatPearls Publishing, Treasure Island (FL), 2024.
- [90] Joel Mendez, Sarah Hood, Andy Gunnell, and Tommaso Lenzi. Indirect Volitional Swing Control Allows for Level-ground Walking and Crossing over Obstacles with a Powered Knee and Ankle Prosthesis. *Science robotics*, 5(44):eaba6635, July 2020.
- [91] Robin Bekrater-Bodmann. Perceptual correlates of successful body-prosthesis interaction in lower limb amputees: psychometric characterisation and development of the Prosthesis Embodiment Scale. *Scientific Reports*, 10(1):14203, August 2020.
- [92] Martin Grimmer, Robert Riener, Conor James Walsh, and André Seyfarth. Mobility related physical and functional losses due to aging and disease - a motivation for lower limb exoskeletons. *Journal of NeuroEngineering and Rehabilitation*, 16(1):2, January 2019.